AD-A162 085 KINETICS OF IODINE MONOFLUORIDE EXCITATION BY ENERGETIC 1/2
NITROGEN(U) PHYSICAL SCIENCES INC ANDOVER MA
L G PIPER ET AL. OCT 85 PSI-851/TR-460 AFWL-TR-84-156
UNCLASSIFIED F29601-83-C-0051 F/G 7/4 NL

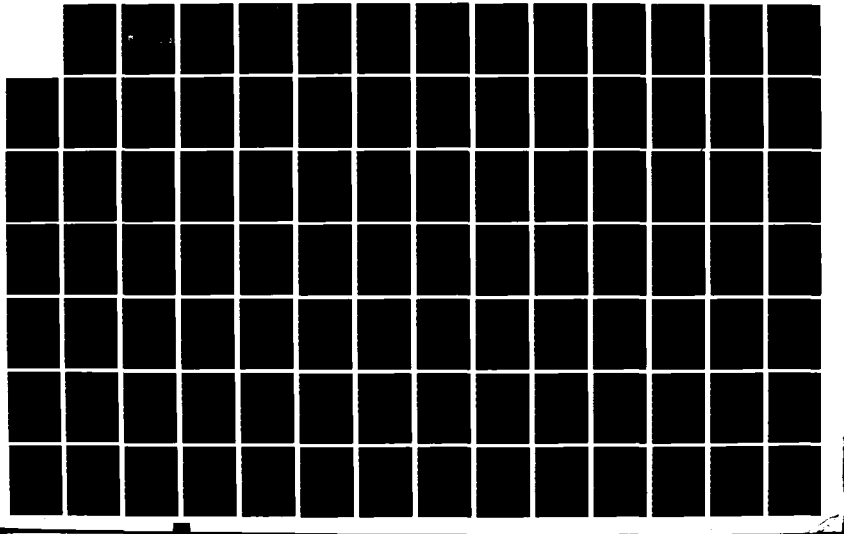

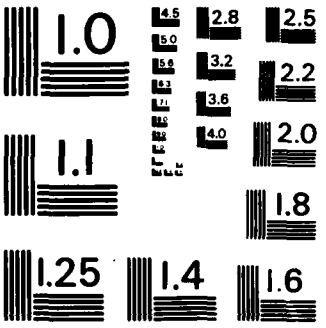

MICROCOPY RESOLUTION TEST CHART

NATIONAL BUREAU OF STANDARDS - 1963 - A

AFWL-TR-
84-156

(2)

AD-A162 085

KINETICS OF IODINE MONOFLUORIDE EXCITATION BY ENERGETIC NITROGEN

Lawrence G. Piper, et al

Physical Sciences Inc
Research Park
Andover, MA 01810

October 1985

Final Report

DTIC
ELECTE
DEC 0 5 1985
S D
D

Approved for public release; distribution unlimited.

AIR FORCE WEAPONS LABORATORY
Air Force Systems Command
Kirtland Air Force Base, NM 87117-6008

DTIC FILE COPY

85 12 3 133

This final report was prepared by Physical Sciences Inc, Andover, Massachusetts, under Contract F29601 -83-C-0051, Job Order 33260339 with the Air Force Weapons Laboratory, Kirtland Air Force Base, New Mexico. Capt Paul J. Wolf (ARDD) was the Laboratory Project Officer-in-Charge.

When Government drawings, specifications, or other data are used for any purpose other than in connection with a definitely Government-related procurement, the United States Government incurs no responsibility or any obligation whatsoever. The fact that the Government may have formulated or in any way supplied the said drawings, specifications, or other data, is not to be regarded by implication, or otherwise in any manner construed, as licensing the holder, or any other person or corporation; or as conveying any rights or permission to manufacture, use, or sell any patented invention that may in any way be related thereto.

This report has been authored by a contractor of the United States Government. Accordingly, the United States Government retains a nonexclusive, royalty-free license to publish or reproduce the material contained herein, or allow others to do so, for the United States Government purposes.

This report has been reviewed by the Public Affairs Office and is releasable to the National Technical Information Services (NTIS). At NTIS, it will be available to the general public, including foreign nations.

If your address has changed, if you wish to be removed from our mailing list, or if your organization no longer employs the addressee, please notify AFWL/ARDD, Kirtland AFB, NM 87117-6008 to help us maintain a current mailing list.

This technical report has been reviewed and is approved for publication.

Paul J. Wolf

PAUL J. WOLF
Captain, USAF
Project Officer

FOR THE COMMANDER

Gerald A. Hasen

GERALD A. HASEN
Major, USAF
Actg Ch, Short Wavelength Laser Br

Harro Ackermann

HARRO ACKERMANN
Lt Col, USAF
Ch, Laser Science & Technology Ofc

DO NOT RETURN COPIES OF THIS REPORT UNLESS CONTRACTUAL OBLIGATIONS OR NOTICE ON A SPECIFIC DOCUMENT REQUIRES THAT IT BE RETURNED.

UNCLASSIFIED

SECURITY CLASSIFICATION OF THIS PAGE

AD-A163 025

REPORT DOCUMENTATION PAGE

1a. REPORT SECURITY CLASSIFICATION UNCLASSIFIED	1b. RESTRICTIVE MARKINGS
2a. SECURITY CLASSIFICATION AUTHORITY	3. DISTRIBUTION/AVAILABILITY OF REPORT Approved for public release; distribution unlimited.
2b. DECLASSIFICATION/DOWNGRADING SCHEDULE	
4. PERFORMING ORGANIZATION REPORT NUMBER(S) PSI-051/TR-460	5. MONITORING ORGANIZATION REPORT NUMBER(S) AFWL-TR-84-156
6a. NAME OF PERFORMING ORGANIZATION Physical Sciences Inc 6b. OFFICE SYMBOL (If applicable) 8K901	7a. NAME OF MONITORING ORGANIZATION Air Force Weapons Laboratory
6c. ADDRESS (City, State and ZIP Code) P.O. Box 3100, Research Park Andover, MA 01810	7b. ADDRESS (City, State and ZIP Code) Kirtland AFB, NM 87117-6008
8a. NAME OF FUNDING/SPONSORING ORGANIZATION 8b. OFFICE SYMBOL (If applicable)	9. PROCUREMENT INSTRUMENT IDENTIFICATION NUMBER F29601 -83-C-0051
8c. ADDRESS (City, State and ZIP Code)	10. SOURCE OF FUNDING NOS. PROGRAM ELEMENT NO. 62601F; PROJECT NO. 3326; TASK NO. 03; WORK UNIT NO. 39
11. TITLE (Include Security Classification) KINETICS OF IODINE MONOFLUORIDE EXCITATION BY ENERGETIC NITROGEN	
12. PERSONAL AUTHOR(S) Piper, L.G.; Marinelli, W.J.; Green, B.D.; Rawlins, W.T.; Murphy, H.C.; Lewis, P.F.; (over)	
13a. TYPE OF REPORT Final 13b. TIME COVERED FROM 16Jun83 TO 16Aug84	14. DATE OF REPORT (Yr., Mo., Day) 1985 October 15. PAGE COUNT 116
16. SUPPLEMENTARY NOTATION	

17. COSATI CODES		
FIELD	GROUP	SUB. GR.
07	04	

18. SUBJECT TERMS (Continue on reverse if necessary and identify by block number)
Iodine monofluoride, Energy transfer, Excited nitrogen, Electronic quenching, Photon yields, Vibrational relaxation, Electronic excitation, R-centroid (over)

19. ABSTRACT (Continue on reverse if necessary and identify by block number)

The excitation of the IF($B^3\pi_{0^+}$) state was studied in reactions of $N_2(A\ ^3\Sigma^+)$ and the effluents of microwave discharges through Ar/N_2 mixture with IF($X^1\Sigma^+$). The experiments were conducted in a fast-flow discharge reactor. $N_2(A)$ was formed by energy transfer from $Ar(^3P_{0,2})$ to N_2 with Ar metastables having been produced in a low power, hollow-rathode, d.c. discharge. The IF was formed in a reaction between F and CF_3I. Several diagnostics were employed to make spectral observations between 200 nm and 700 nm. The production and loss of IF was also examined in the flow system using laser induced fluorescence for measuring IF number densities.

The energy transfer reaction between IF(X) and $N_2(A)$ was extremely rapid ($k = 2.0 \times 10^{-10}$ cm^3 $molecule^{-1}S^{-1}$) and 40% of the $N_2(A)$ quenching collisions result in IF(B) Formation. The results indicate that differences in IF excitation between $N_2(A)$ v' = 1 and v' = 0 are small ($k_{v'=2}/k_{v'=1} \leq 1.2$). IF(B) vibrational distributions were characterized under (over)

20. DISTRIBUTION/AVAILABILITY OF ABSTRACT UNCLASSIFIED/UNLIMITED ☒ SAME AS RPT. ☐ DTIC USERS ☐	21. ABSTRACT SECURITY CLASSIFICATION UNCLASSIFIED
22a. NAME OF RESPONSIBLE INDIVIDUAL Capt Paul J. Wolf	22b. TELEPHONE NUMBER (Include Area Code) (505) 844-1871 22c. OFFICE SYMBOL ARDD

DD FORM 1473, 83 APR EDITION OF 1 JAN 73 IS OBSOLETE.

UNCLASSIFIED

SECURITY CLASSIFICATION OF THIS PAGE

12. PERSONAL AUTHORS (Contd)

and Donahue, M.E.

18. SUBJECT TERMS (Contd)

Transition probabilities
Flow reactor

19. ABSTRACT (Contd)

several conditions and IF(B,v') vibrational relaxation rate coefficients were determined. $N_2(A)$ quenching rate coefficients by CF_3I, CF_4, NF_3, and SF_6 were measured.

Active nitrogen, created in microwave discharges in Ar/N_2 mixtures, also excited IF(B) strongly when ground-state IF mixed with it. A 2000 K Boltzmann distribution characterized, roughly, the vibrational distribution from this reaction. The primary species in the active nitrogen responsible for the IF(B) excitation appeared not to be $N_2(A)$, but perhaps $N_2(X,v >> 0)$.

SUMMARY

We have studied the excitation of the $IF(B^3\Pi_0^+)$ state in energy transfer reactions of $N_2(A^3\Sigma_u^+)$ and the effluents of microwave discharges through argon/nitrogen mixtures with $IF(X^1\Sigma^+)$. These studies were carried out in a discharge-flow reactor in which the $N_2(A)$ was made by energy transfer from $Ar(^3P_{0,2})$ to N_2, the argon metastables having been produced in low-power, hollow-cathode, d.c. discharge. The IF was made in a side arm of the flow reactor in the reaction between F and CF_3I. The major species diagnostic in these experiments was spectral observations between 200 and 700 nm. Air afterglow measurements at 580 nm in the presence of known quantities of O and NO calibrated our system for absolute photon emission-rate measurements. Relative vibrational-level populations of the various emitters in the reactor were determined by least-squares fits of synthetic spectra to the experimentally measured spectra.

We studied the production and loss of IF_x in our flow system using a laser-induced fluorescence diagnostic for measuring IF number densities. We related the production of F-atoms to the residence time of CF_4 in the microwave discharge and found a yield of about 0.3 F-atoms per CF_4 molecule under typical operating conditions. We identified flow conditions that produce complete reaction of CF_3I in the injector and showed that a negligible amount of IF is destroyed in the injector under these conditions. Some loss of IF in the main flow tube was found at low flow velocities; however, this loss appeared to be negligible at higher velocities and permitted us to operate in a regime where IF number densities were directly related to the amount of CF_3I flowing into the injector. We also found that operation of the injector using excess CF_3I resulted in the deposition of an optically opaque thin film on the reactor walls. This required us to operate in excess F-atoms and eliminated the need to measure absolute F-atom number densities.

Our experiments show that the energy-transfer reaction between $N_2(A^3\Sigma_u^+)$ and $IF(X^1\Sigma^+)$ is extremely rapid (k_{total} = 2.0×10^{-10} cm^3 $molecule^{-1}s^{-1}$) and that 40% of the quenching collisions result in IF(B) photons. The reaction populates IF(B) vibrational levels up through v'=9 and produces v'=0-6 with about equal probability. The vibrational distribution relaxes rapidly,

however, in collisions with the reactor bath gas even at pressures of a few torr. The vibrational relaxation rate coefficients for levels 3-6 of IF(B) are about $3 \times 10^{-12} cm^3$ $molecule^{-1} s^{-1}$, with levels 1 and 2 being a little slower. Our results indicate that any differences in IF excitation between $N_2(A)$ $v'=1$ and $v'=0$ are small ($k_{v'=1}/k_{v'=0} \leq 1.2$). Electronic quenching of the IF(B) at higher reactor pressures did not appear to be significant. In addition to measuring the kinetics of the reaction between $N_2(A)$ and IF, we also measured quenching-rate coefficients of $N_2(A)$, by CF_3I, CF_4, NF_3, and SF_6.

Active nitrogen, created in microwave discharges in Ar/N_2 mixtures, also excited IF(B) strongly when ground-state IF mixed with it. A 2000 K Boltzmann distribution characterized, roughly, the vibrational distribution from this reaction. The primary species in the active nitrogen responsible for the IF(B) excitation appeared not to be $N_2(A)$, but perhaps $N_2(X, v>>0)$.

CONTENTS

Accesion For
NTIS CRA&I ☒
DTIC TAB ☐
Unannounced ☐
Justification .....
By .....
Di.t ib.:tion/
Availability Codes
Di.t | Avail and/or Special
A-1

QUALITY INSPECTED 3

LIST OF ILLUSTRATIONS

LIST OF ILLUSTRATIONS

LIST OF ILLUSTRATIONS

LIST OF TABLES

1. INTRODUCTION*

Iodine monofluoride (IF) and other interhalogens have been the subject of considerable interest in recent years because their compressed electronic energy manifold and intense radiative transitions cause these molecules to exhibit visible lasing action. For example, the "blue-green" emission, $D'(^3\Pi_2) \rightarrow A'(^3\Pi_2)$, of IF has been studied extensively for application in short-wavelength, gas-discharge chemical lasers (Ref. 1).

Recently, interest has also focussed on the $B(^3\Pi_{0+}) \rightarrow X(^1\Sigma^+)$ bands of the interhalogens. In an elegant series of papers, Clyne and coworkers studied the radiative and collisional properties of IF and BrF (Refs. 2-7). Clyne et al. showed that these species were highly suitable for forming an electronic transition laser operating on the B → X transition because the upper states have short radiative and long quenching lifetimes (Refs. 2-7). In parallel with this work, Davis and Hanko, using a pulsed dye laser to excite ground-state IF formed in an I_2/F_2 flame, demonstrated optically pumped lasing on the IF(B → X) transition (Ref. 8). Optimal chemical (kinetic) means for pumping the IF(B) state remain to be determined.

More than a decade ago, Clyne et al. studied the three-body recombination of I with F, and noted extensive enhancement of the IF(B → X) emission upon adding $O_2(^1\Delta, ^1\Sigma)$ to the reacting mixture (Ref. 9). Recently, Davis and coworkers demonstrated and examined the enhancement of IF(B) emission from the I_2/F_2 system upon introducing $O_2(^1\Delta)$ and $O_2(^1\Sigma)$ (Ref. 10). In these experiments, $O_2(^1\Delta)$ rather than $O_2(^1\Sigma)$ appeared to be responsible for the IF(B) enhancement. In the absence of O_2*, IF(B(v)) distributions were relatively cold, extending only to about v = 4 - 5. Adding O_2* greatly enhanced the B → X emission intensity, with up to ten vibrational quanta excited in the B state. Subsequent work by Davis and coworkers shows even stronger IF(B) excitation when the effluents of microwave discharges in He/N_2 mixtures interact with the I_2/F_2 mixing zone of their reactor (Ref. 11). They did not identify the species in their active nitrogen that was responsible for the IF excitation.

*The inclusion of names of any specific commercial product, commodity, or service in this publication is for information purposes only and does not imply endorsement by the Air Force.

The present study examined the feasibility of enhancing IF(B → X) chemiluminescence by energy-transfer processes between a number of nitrogen-containing metastable species and ground-state IF. Candidate metastables included $N_2(A\ ^3\Sigma_u^+)$, $N_2(X, v)$, $NH(a\ ^1\Delta, b\ ^1\Sigma^+)$, $NCl(a\ ^1\Delta, b\ ^1\Sigma^+)$ and $N(^2D, ^2P)$, all of which can be produced by chemical means (Refs. 12-16). Preliminary results on $N_2(A)$ and active nitrogen were so exciting that the program focussed on these systems.

Our experiments show that the energy-transfer reaction between $N_2(A\ ^3\Sigma_u^+)$ and $IF(X\ ^1\Sigma^+)$ is extremely rapid ($k_{total} = 2.0 \times 10^{-10}$ cm^3 molecule^{-1}s^{-1}) and that 40% of the quenching collisions result in IF(B) photons. The reaction populates IF(B) vibrational levels up through v' = 9 and produces v' = 0 - 6 with about equal probability. The vibrational distribution relaxes rapidly, however, in collisions with the reactor bath gas even at pressures of a few torr.† The vibrational relaxation rate coefficients for levels 3-6 are about 3×10^{-12} cm^3 molecule^{-1} s^{-1}. Although we did not study it explicitly, electronic quenching of IF(B) in our reactor must have been much slower because we observed strong IF(B) excitation by $N_2(A$ at pressures up to 10 torr.

Active nitrogen--created in microwave discharges in Ar/N_2 mixtures--also excited IF(B) strongly when ground-state IF mixed with it. A 2000 K Boltzmann distribution characterizes roughly the vibrational distribution from this reaction. The primary species in the active nitrogen responsible for the IF(B) excitation appeared not to be $N_2(A)$, but perhaps $N_2(X, v >> 0)$.

---

† 1 torr - 133.3 Pa

2. EXPERIMENTAL

2.1 Apparatus

The apparatus consisted of a 50.8 mm flow tube, pumped by a Leybold-Heraeus Roots blower/forepump combination which produced linear velocities up to 5×10^3 cm s^{-1} at pressures of one torr. The flow-tube design was modular (see Fig. 1), with separate source, reaction, and detection sections which clamp together with O-ring joints. The details of the flow system were described in several publications (Refs. 17-21). The detection region was a rectangular stainless-steel block bored out internally to a 50.8 mm circular cross section and coated with Teflon® (Dupont Poly TFE #852-201) to retard surface recombination of atoms (Refs. 22-24). Use of a black primer prior to the Teflon® coating significantly reduced scattered light inside the block. The block contained two sets of viewing positions which consisted of four circular ports each on the four faces of the block. These circular ports accommodated vacuum-ultraviolet (VUV) resonance lamps, VUV and visible monochromator interfaces, laser delivery side-arms and a spatially filtered photomultiplier/interference filter combination.

The upstream observation position (Fig. 2) was fitted with two microwave-discharge resonance lamps placed normal to each other, with a VUV monochromator diametrically opposite one of the resonance lamps. The lamp which was viewed by the monochromator was used in absorption studies, while the lamp normal to the monochromator's optical axis was used to excite resonance fluorescence of atomic species in the flow reactor. The lamps and the monochromator were separated from the flow tube by 25 mm diameter MgF_2 windows which have a short-wavelength cutoff of 115 nm.

The downstream observation position contained baffled side arms to allow entry and exit of a laser beam, and at right angles to these a filtered photomultiplier and a UV/visible monochromator interface. The filtered photomultiplier was for detecting LIF fluorescence, while the monochromator was used in the bulk of these studies to detect fluorescence between 180 and 850 nm. A suprasil lens collected light from the center of the flow tube and focused it

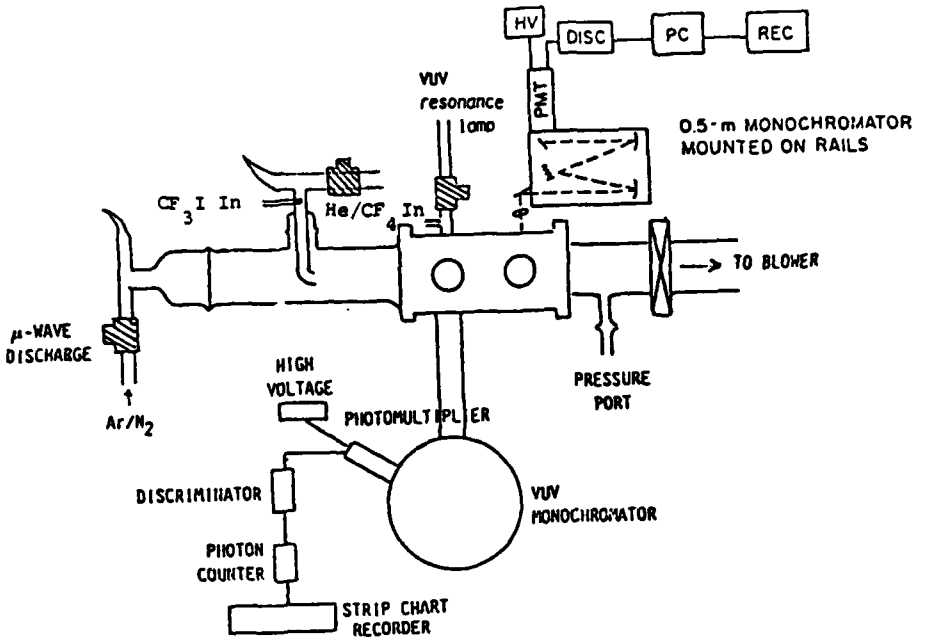

Fig. 1a. Flow-tube apparatus for studying $N_2(v)$ and N^* (^2D, ^2P) with IF.

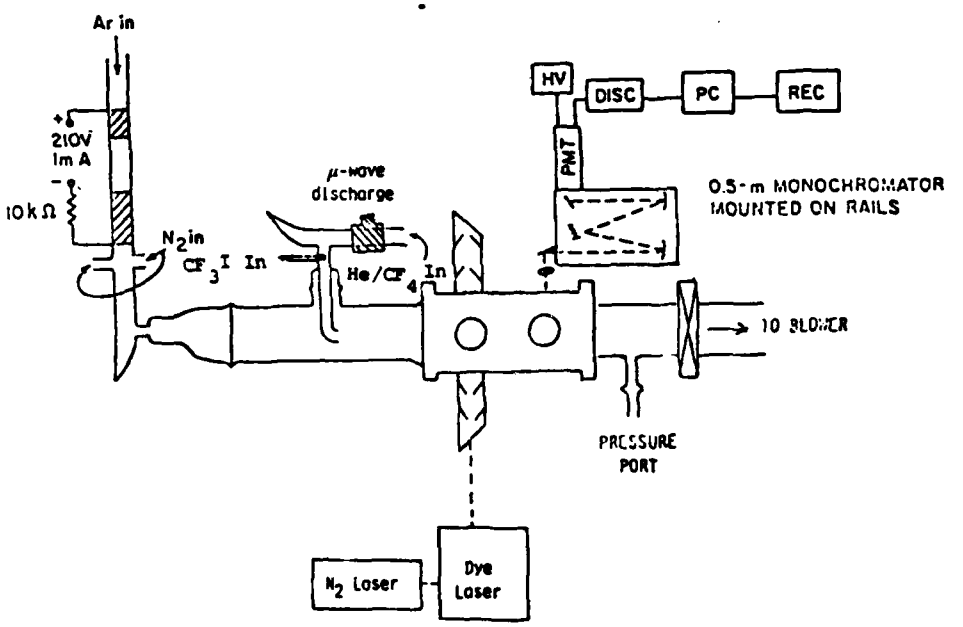

Fig. 1b. Flow-tube apparatus for studying $N_2(A)$ with IF.

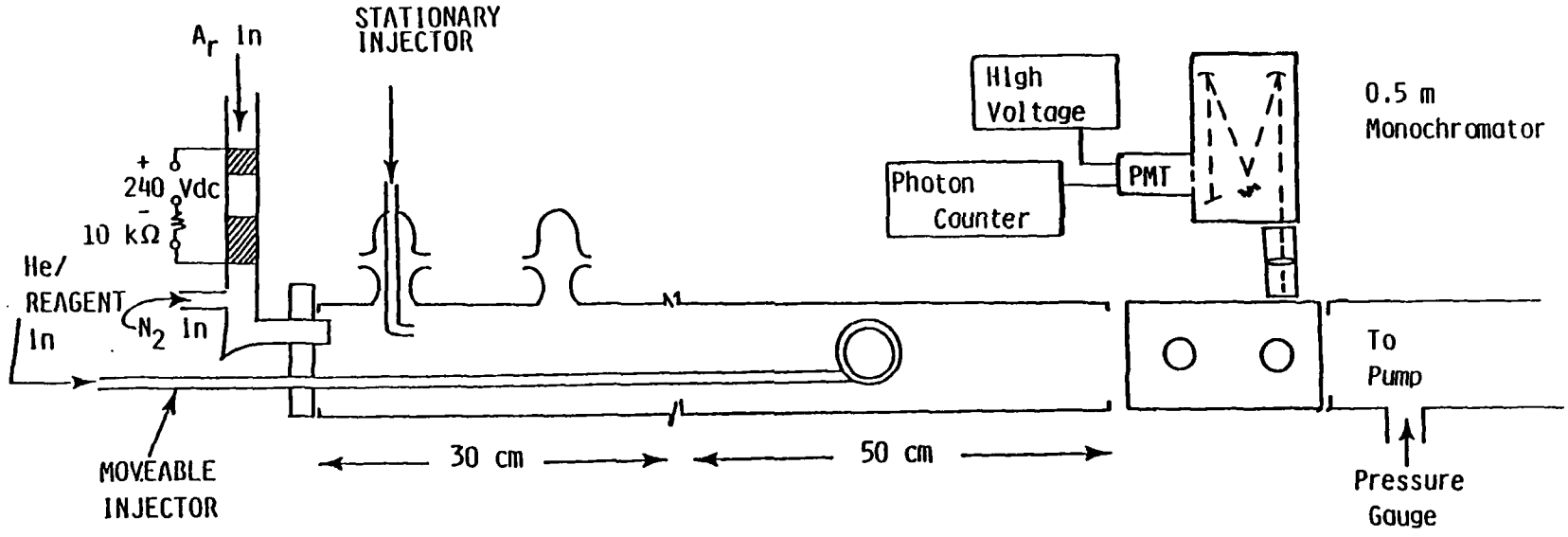

Fig. 1c. Flow tube apparatus configured for $N_2(A)$ decay kinetics measurements.

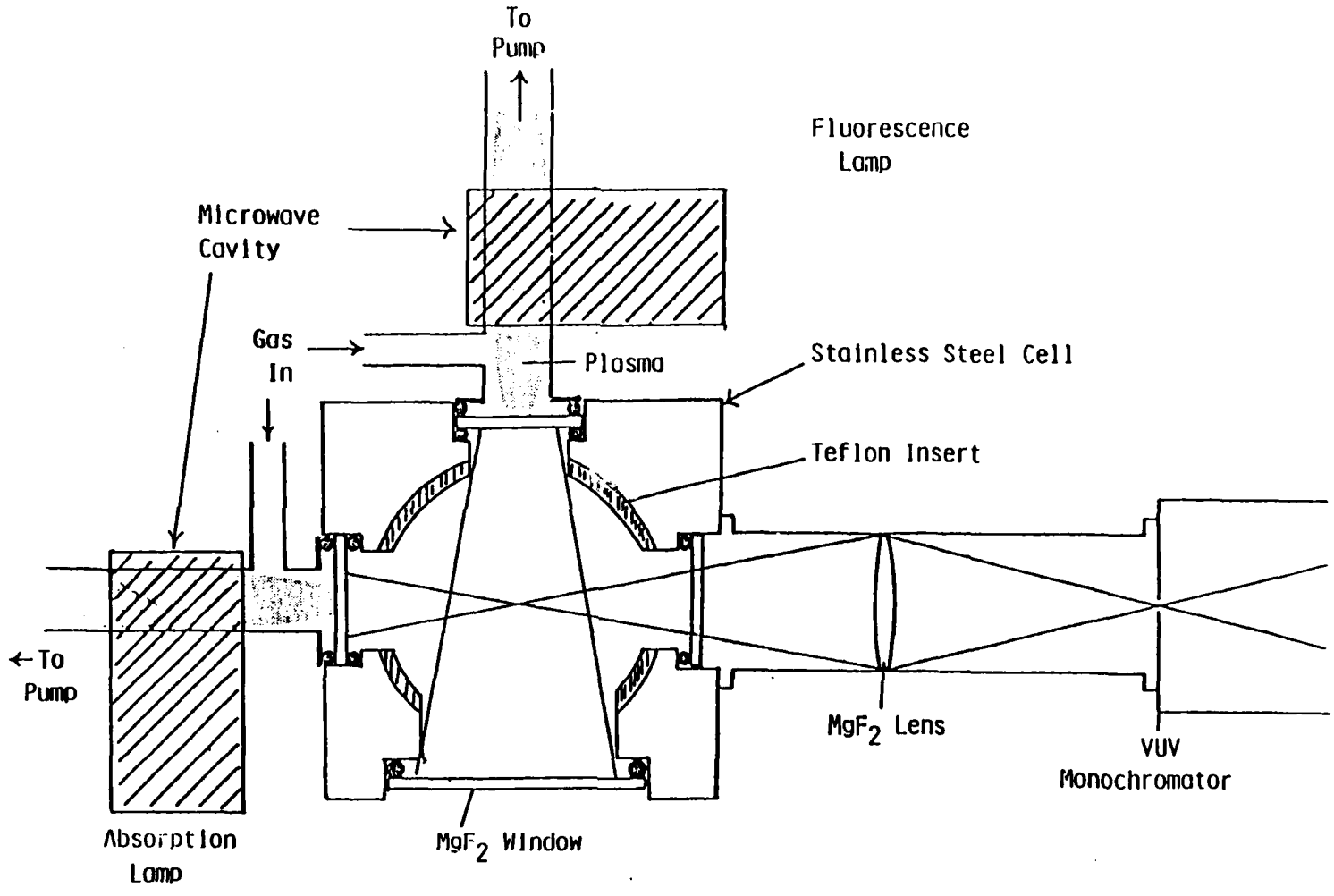

Fig. 2 Cross sectional view of the absorption/fluorescence cell showing the placement of the lamps. The direction of the flow in the reactor is perpendicular to the figure.

on the entrance slit of the monochromator (0.5 m Minuteman instrument outfitted with a 1200 groove mm^{-1} grating blazed at 250 nm). A thermoelectrically-cooled photomultiplier tube (PMT) detected photons with the aid of an SSR 1105 photon-counting rate meter and strip-chart recorder. Initial experiments used an EMI 9659QA PMT (S-20 response), but near the end of the work this was replaced by an HTV R943-02 PMT (GaAs photocathode). This change resulted in significant improvements in red sensitivity, particularly beyond 650 nm.

The spectral system was calibrated for relative response as a function of wavelength using a standard quartz-halogen or D_2 lamp. Absolute response calibrations were made in situ by observing the air afterglow under carefully controlled conditions (see below).

The metastable nitrogen molecules, $N_2(A^3\Sigma_u^+)$, were produced in the reaction between metastable $Ar(^3P_{0,2})$ and molecular nitrogen (Ref. 25). This transfer excited $N_2(C^3\Pi_u)$ which quickly cascades radiatively to the metastable $A^3\Sigma_u^+$ state via the $B(^3\Pi_g)$ state (Ref. 26). A hollow-cathode discharge source was built to produce the argon metastables. While most experimenters used tantalum for the electrodes (Refs. 25,27), we found a 0.127 mm thick aluminum shim made an excellent electrode material. The shim was rolled into a cylinder whose diameter was the same as the inside diameter of the glass tubing through which the gas flowed (13 mm). The cathode (the downstream electrode) is 40 mm long, the anode 15 mm long, and the two electrodes were separated by 45 mm. The discharge was operated in the dc mode with the anode biased at +240 V. A load resistor of 10 kΩ gave the discharge stability and limited the current. The current in the present experiments was about 3 mA. The argon and nitrogen were purified by flowing the gases through traps filled with 5Å molecular sieve. Since the experiments involved metastable nitrogen, it was not necessary to remove the nitrogen impurity from the argon carrier. The argon metastables produced in the discharge were detected by the appearance of the characteristic reddish-violet flame which is obtained upon the addition of nitrogen downstream from the discharge. The concentrations of N_2 at the point of addition, $\sim 10^{15}$ cm^{-3}, resulted in a flame length of about 2 cm. This length was governed by diffusional mixing of the two streams of gas, because, at these nitrogen concentrations, the collisional quenching times for nitrogen on argon were on the order of tens of microseconds (Ref. 28).

A typical spectrum of the Vegard-Kaplan bands emanating from the flow tube is shown in Fig. 3. The spectrum shows that the first three vibrational levels of $N_2(A)$ are populated in our system with relative populations of approximately 100:50:10 for v'=0,1, and 2, respectively. This is in contrast to the relative populations reported by Stedman and Setser of 100:95:10 for the same three levels, respectively (Refs. 24,25). We performed some experiments which showed that the ratio $[N_2(A)]_{v=1}/[N_2(A)]_{v=0}$ increased under conditions of higher total pressure and higher mole fractions of nitrogen in the flow, and when the nitrogen inlet was separated from the Ar metastable discharge by a Wood's horn light trap. (These general conditions obtained in the work of Stedman and Setser, and, for the most part, did not in the present experiments.) In particular, the intervention of a light trap between the hollow-cathode discharge and the nitrogen injection point enhanced the ratio $[N_2(A)_{v=1}/[N_2(A)]_{v=0}$ by more than a factor of two.

Several runs were made to measure the IF(B) excitation by active nitrogen. The active nitrogen was prepared by microwave discharging (70 W) a mixture of nitrogen in argon. We diagnosed the discharge effluent spectroscopically in the region 130-850 nm. Prominant radiators observed 20 ms downstream of the discharge included the Lyman-Birge-Hopfield ($a^1\Pi_u$-$X^1\Sigma_g^+$), Vegard-Kaplan ($A^3\Sigma_u^+$-$X^1\Sigma_g^+$), second-positive ($C^3\Pi_u$-$B^3\Pi_g$) and first-positive ($B^3\Pi_g$-$A^3\Sigma_u^+$) systems of N_2, the NO γ-bands ($A^2\Sigma^+$-$X^2\Pi$) and N(^2P-^2D, λ = 346.6 nm). Under some conditions when CF_3I or discharged CF_4 was added to the reactor, the CN blue ($B^2\Sigma^+$-$X^2\Sigma^+$) and red ($A^2\Pi$-$X^2\Sigma^+$) systems appeared.

The reagents for producing IF entered the flow tube through hook-shaped injectors whose outlet orifices are coaxial with the main flow tube. For some studies, reagents entered through a 25.4 mm diameter loop injector seated on the end of a 6.2 mm diameter tube which slides along the bottom of the flow tube, parallel to its axis, thus allowing a variety of reaction distances for accurate kinetic studies. The hook injectors facilitated introduction of unstable species produced in a secondary discharge. These injectors had relatively large diameters (10 mm) and were Teflon® coated to inhibit wall recombination of these unstable species. IF was produced in one of these injectors by the reaction between CF_3I and F atoms. Fluorine atoms were

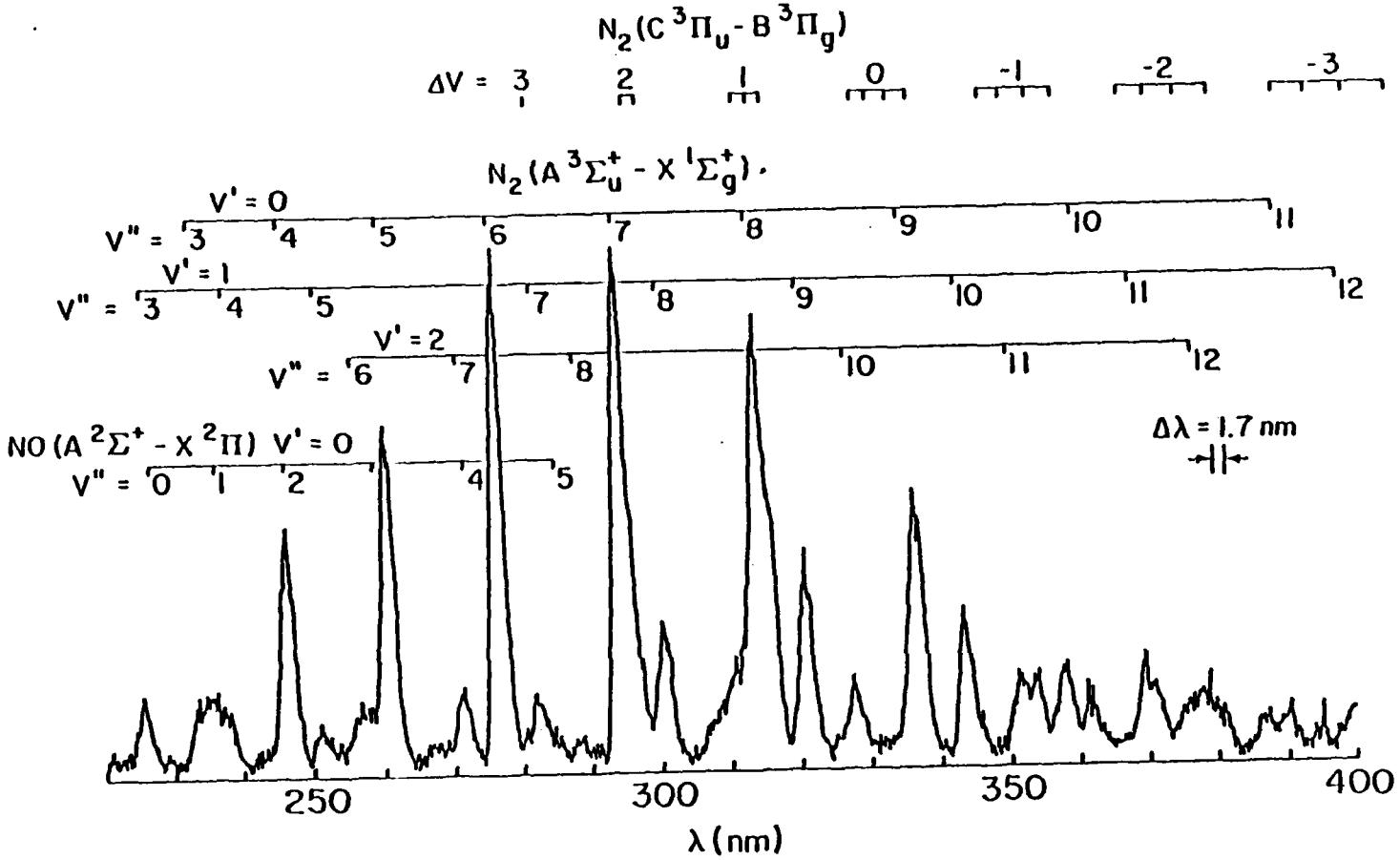

Fig. 3 Vegard-Kaplan emission in flow reactor 9 ms downstream from the discharge.

produced in a microwave discharge of He/CF_4 mixtures further upstream in the injector. We'll discuss the characterization of this IF source in more detail below.

Mass-flow meters or rotameters monitored the flow rates of most gases. All flow meters were calibrated by measuring rates of increase of pressure with time into 6.5 or 12 ℓ flasks, using appropriate differential pressure transducers (Validyne DP-15) which themselves have been calibrated with silicon oil or mercury manometers. Typical flow rates for argon, nitrogen, and helium through the injector were 2000-5000, 100-500 and 200-500 $\mu mol\ s^{-1}$, respectively, while CF_4 and CF_3I flow rates ranged between 0 and 1 $\mu mol\ s^{-1}$, respectively. Total pressures, as measured by a Baratron® capacitance manometer, ranged from 0.4 to 9 torr, and flow velocities varied from 500 to 5000 $cm\ s^{-1}$.

Tetrafluoromethane (CF_4) was obtained 99.5% pure from Matheson, and, due to the small amount employed, was used without further purification. Trifluoroiodomethane (CF_3I) was obtained 99% pure from PCR Research Chemicals. The major impurity, I_2, was removed by distilling CF_3I from a trap at -115°C followed by storage in a dark bulb.

During the latter part of the contract, a laboratory computer system enhanced our data acquisition and analysis capabilities. The system comprises an IBM PC with 512 K of RAM, two 360 K diskette drives, a monochrome monitor, and a 160 cps dot-matrix printer with graphics capability. Data acquisition is accomplished using an I/O system manufactured by Data Translation (DT2801A), which features 16 channels of A/D input, two channels of D/A output, two 8-bit digital I/O ports, software programmable gain, single-ended or differential input, and data acquisition rates as fast as 14 kHz.

A software package written by Laboratory Technologies Inc. ("Real-time Laboratory Notebook") interfaced the computer to the D/A board and organized data in a form compatible for analysis using the "Lotus 123" business spreadsheet software.

2.2 Iodine Monofluoride Production and Destruction in the Flow Reactor

Because IF is known to be somewhat unstable with respect to wall reactions, we performed experiments to characterize IF production and loss in our flow system. These experiments used a laser-induced fluorescence system to measure IF concentrations under a variety of injector and main flow tube conditions. The goal of these experiments was to determine the optimum conditions for IF production, and to determine the extent to which IF was destroyed in the flow tube in the absence of any pumping agents or their co-products. The knowledge of this latter quantity was important in determining absolute IF excitation efficiencies and in choosing the simplest and most effective way of measuring IF number densities. In the following sections, we describe these experiments, their results and conclusions, and their implications for the research.

2.2.1 Background

In our experiments the reaction of F-atoms with CF_3I produced IF. Bozzelli and Kaufman determined the rate coefficient for this reaction to be $(1.2 \pm 0.6) \times 10^{-10}$ cm^3 $molecule^{-1}$ s^{-1} (Ref. 30). Stein, Wanner, and Walther showed that the IF produced in this reaction had both a relatively "cold" and statistical internal energy distribution, and that most of the exoergicity of the reaction was channelled into internal excitation of the CF_3 radical (Ref. 31).

Fluorine atoms were produced in a microwave discharge using CF_4 diluted in He. This discharge was conducted in an alumina tube which was connected to a Teflon®-coated Pyrex® injector equipped with a Wood's horn light trap. The CF_4/He mixture was made by mixing a small flow of a stock 10% CF_4/He mixture with a larger flow of pure He in a preparation line prior to entering the discharge tube. The typical composition of the final mixture covered a range from 0.04 - 0.6%.

The F-atoms produced in the discharge were swept into a small mixing region by the He carrier gas. A dilute mixture of CF_3I in He entered this region via a side arm, and the two gas streams mixed and flowed for a distance of 10.5 cm down an 8 mm inside diameter, Teflon®-coated Pyrex® tube which injected the gas mixture on the main flow tube center line. The CF_3I/He mixture was made in a similar manner to the CF_4 mixture using a stock of 3% CF_3I in He.

Our experiments were generally conducted with F-atoms in excess over CF_3I. In the absence of any loss mechanisms for IF this method of operation was preferred, because the amount of IF produced was related directly to the amount of CF_3I introduced. In addition, we discovered that operating the flow system using excess CF_3I over F-atoms resulted in the deposition of an opaque material on the inside of the flow reactor which severely decreases our ability to observe IF emission. This will be discussed in more detail in a later section.

An important consideration in designing and operating the IF injector is to allow sufficient residence time in the injector for all of the CF_3I to react with F-atoms. The fraction of unreacted CF_3I leaving the injector is given by the expression

$$\frac{[CF_3I]}{[CF_3I]_o} = e^{-k_F[F](\ell/v_I)} . \qquad (1)$$

In this expression, k_F is the rate coefficient for the reaction of F-atoms with CF_3I, [F] is the number density of F-atoms in the injector, ℓ is the length of the injector tube (10.5 cm), and v_I is the linear flow velocity in the injector. The concentration of F-atoms in the injector is given by

$$[F] = \frac{\alpha\, f_{CF_4}}{f_I} \frac{N_o P_I}{RT} \qquad (2)$$

and the linear flow velocity is obtained using

$$v_I = 10^{-6} \frac{f_I RT}{P_I A_I} . \qquad (3)$$

In these expressions, f_{CF_4} and f_I are the CF_4 and total flow rates (μmol s^{-1}) entering the injector respectively, α is the fractional yield of F-atoms per CF_4 molecule, P_I is the pressure in the injector, N_o is Avagadro's constant, and A_I is the cross sectional area of the injector tube. Using these relations, expression (1) becomes

$$\frac{[CF_3I]}{[CF_3I]_o} = e^{-\alpha 10^6 N_o k_F \frac{f_{CF_4}}{f_I^2} \cdot \ell A_I \left(\frac{P_I}{RT}\right)^2} \quad . \tag{4}$$

For fast flow in the injector, the viscous pressure drop along the tube may be substantial and P_I will vary down the tube length. The magnitude of this pressure drop is given by the Poiseuille equation (Ref. 32)

$$P_1^2 - P_2^2 = \frac{16F\ell\eta RT}{\pi r^4} \quad . \tag{5}$$

In this expression, P_1 and P_2 are the upstream and downstream pressures in dyne cm^{-2}, F is the molar flow rate in mol s^{-1}, ℓ is the tube length in cm, η is the He carrier gas viscosity in Poise, r is the tube radius in cm, R is the ideal gas constant, and T is the gas temperature in Kelvins.

If the pressure drop down the length of the tube is small, as in our injector, then the Poiseuille equation may be simplified to give ΔP as

$$\Delta P = 6.00 \times 10^{-9} \frac{\eta f_I RT\ell}{P_o \pi r^4} \quad . \tag{6}$$

In this expression, ΔP is the pressure drop in torr, f_I is the injector flow rate in μmol s^{-1}, and P_o is the injector outlet pressure in torr. The average injector pressure, $\overline{P_I}$, is at the midpoint of the injector tube and is given by the expression

$$\overline{P_I} = P_o + \frac{\Delta P}{2} = P_o + 6.00 \times 10^{-9} \frac{\eta f_I RT}{P_o \pi r^4} \cdot \frac{\ell}{2} \quad . \tag{7}$$

This value of $\overline{P_I}$ is a lower limit since there is an additional pressure drop due to a bend in the injector tube at the flow tube center line. The fractional consumption of CF_3I in the injector was determined by substituting $\overline{P_I}$, calculated using expression (7), for P_I in expression (4).

2.2.2 LIF Detection of IF

A Molectron DL200 dye laser pumped by a Molectron UV14 (400 kW) nitrogen laser was the cornerstone of the laser-induced fluorescence system for detecting IF. A 100 cm focal length lens coupled almost 50% of the laser output energy into the fluorescence viewing region (~ 130 μJ at 470 nm). The beam was collimated as it passed through the tube, which significantly reduced the scattered laser light. The LIF signal was monitored by a spatially and spectrally filtered PMT (HTV/R955) connected to a boxcar integrator (PARC 160) via a 1 kΩ load resistor. A 520 nm long pass filter on the PMT blocked the 469.7 nm probe light, which pumped the 6-0 band, while passing more than 50% of the total emission from that level. An energy meter (Laser-Precision) monitored the dye laser energy at the output of the flow tube detection cell.

2.2.3 Fluorine Atom Generation

Our initial experiments explored the optimum conditions for generating F atoms. A schematic diagram of the injector and flow system are shown in Fig. 4. In these experiments, the main flow tube pressure was held at 1 torr with a linear flow velocity of approximately 4500 cm s^{-1} and a transit time of 4 ms from the injector to the detector. This flow velocity was maintained by flowing Ar or an Ar/N_2 mixture through a port upstream of the IF injector. The flow of He carrier gas for the CF_3I and the flow of the 10% CF_4/He mixture for the discharge were kept constant. Three different flow rates were tested for the He which carries the CF_4 mixture into the discharge. At each flow rate, the variation in the IF fluorescence signal was determined with the amount of CF_3I added downstream of the F-atom discharge.

The results of these experiments are shown in Fig. 5 where the energy-normalized LIF signal is plotted against the CF_3I concentration that would be found in the flow tube if it were not consumed by F-atoms. All three flow rates through the discharge show a linear dependence of the LIF signal on CF_3I added at low CF_3I flow rates. This is characteristic of a regime where F-atoms are in excess. At higher CF_3I number densities each of the curves rolls off to an asymptotic value. This is due to a transition from a regime

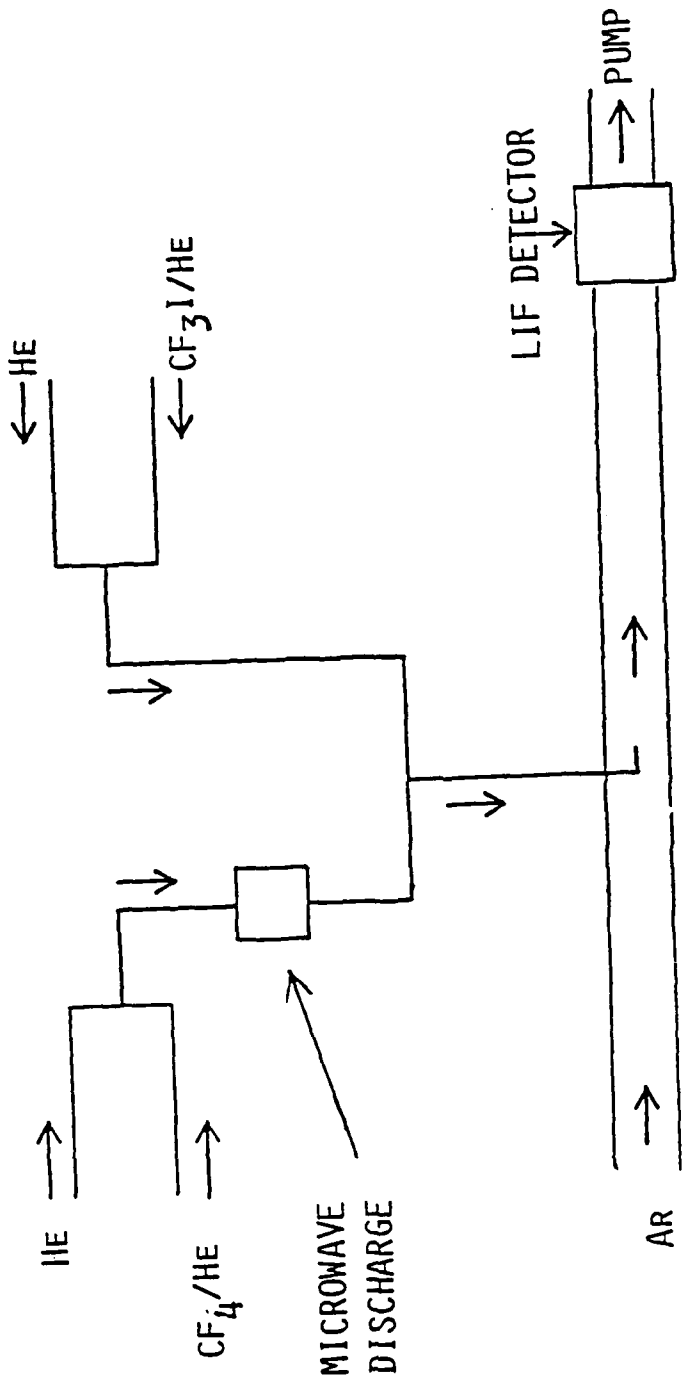

Fig. 4 Schematic diagram of flow system.

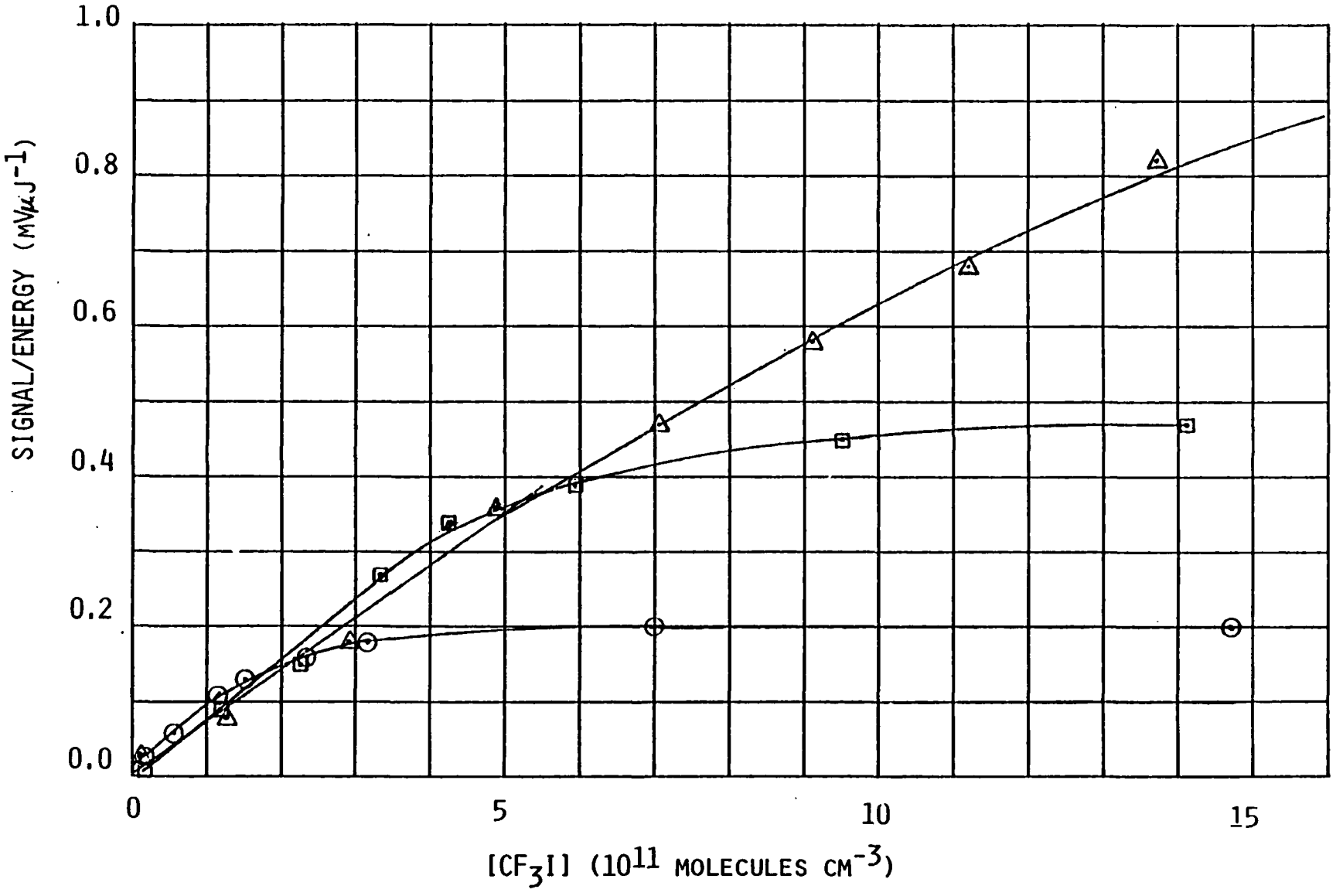

Fig. 5 LIF signal as a function of added CF_3I for three discharge flow rates: △, 407 μmole s^{-1}; ⊡, 105 μmole s^{-1}; ⊙, 52 μmole s^{-1}.

having excess F-atoms to one having excess CF_3I. The CF_3I number density in the injector at which each curve reaches its asymptote is equal to the initial F-atom number density entering the injector. These experiments show that large flow rates through the F-atom discharge, corresponding to smaller residence times in the discharge region, result in larger initial F-atom number densities. This is most likely due to diminished F-atom recombination, probably occurring in the alumina discharge tube and in the short section of tubing between the discharge and the tee where CF_3I is added to the flow.

A second set of experiments were done to measure α, the effective yield of F-atoms from the CF_4/He discharge. In these experiments, the flow tube pressure and flow velocity were fixed at 1 torr and 4500 cm s^{-1}, and the He flows carrying the CF_3I and CF_4 into the injector were fixed at the conditions corresponding to the intermediate flow depicted in Fig. 5. We determined α by observing how the concentration of CF_3I in the injector at the roll over point, demonstrated in Fig. 5, varied as a function of the flow of CF_4 into the discharge. This CF_3I concentration is equivalent to the F-atom concentration in the injector, and the derivative of this function at any CF_4 concentration gives us the effective F-atom yield. These experiments are difficult to do because, each time one enters a regime with excess CF_3I, a deposit quickly builds up on the optical surfaces and degrades the detection sensitivity.

The results of these experiments are shown in Fig. 6. They show a linear variation in the effective F-atom concentration with CF_4 flow over the range studied. The slope of this line gives an F-atom yield of 0.3 per CF_4 molecule for the flow conditions employed. Our earlier experiments showed that lower He carrier flow rates through the discharge decreases this F-atom yield.

The desire to optimize the F-atom number density from the discharge must be tempered by the need to have complete reaction of CF_3I in the injector. Expression (4) shows that the log of the fractional consumption of CF_3I

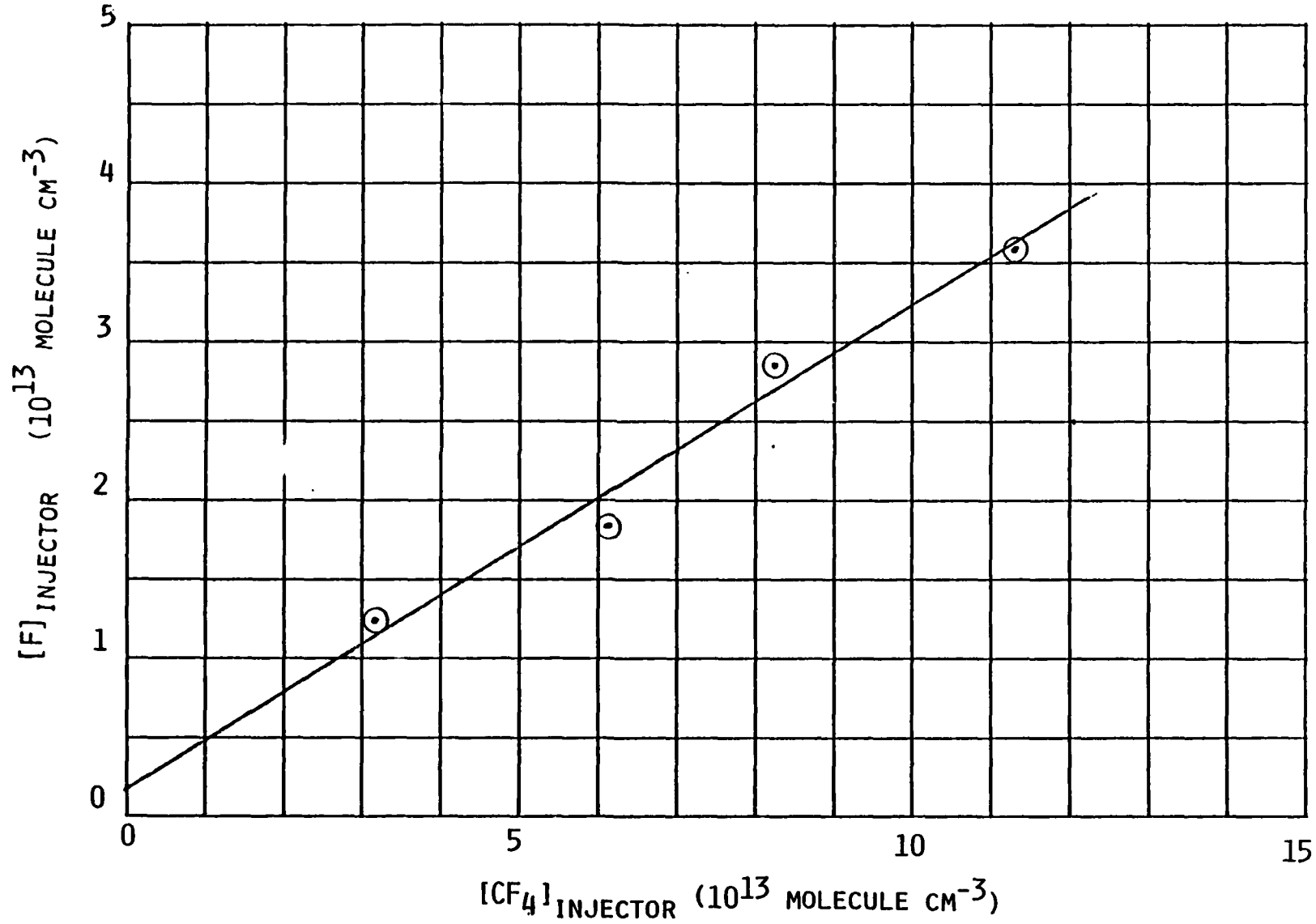

Fig. 6 Injector F-atom concentration as a function of CF4 added to the discharge. The slope of the line, α, is 0.30.

is proportional to $-1/f_I^2$; therefore it is important to minimize the total flow rate through the injector. Using expression (4) for a 1 torr flow tube pressure, a flow rate through the injector less than approximately 100 μmole s^{-1} is required to completely consume the CF_3I. This restricts us to operating on the curve corresponding to the smallest flow in Fig. 2, unless we increase the amount of CF_4 in the discharge.

2.2.4 Injector Losses

A third series of experiments tested for any homogeneous or heterogeneous loss of IF in the injector. This was done by varying the residence time of IF in the injector. If the formation of IF in the injector was rapid and the loss mechanism was first order, the fractional loss of IF in the injector would be given by the equation

$$\frac{[IF]_I}{[IF]_o} = e^{-k_L \left(\frac{\ell}{v_I}\right)} \quad . \tag{8}$$

In this expression k_L is the first order rate coefficient, ℓ is the length of the injector mixing region, and v_I is the linear flow velocity in the mixing region. The linear flow velocity is given by expression (3) where f_I, the total flow rate through the injector, is approximately equal to the combined flows of the He carriers for the CF_4 and CF_3I, f_D and f_M. Expression (8) can now be rewritten as

$$\frac{[IF]_I}{[IF]_o} = e^{-k_L A_I \ell P_I / (f_D + f_M) RT.} \tag{9}$$

The IF exiting the injector is diluted by the bulk flow in the main flow tube, its concentration measured at the detector is given by

$$[IF]_M = [IF]_I \cdot \frac{f_D + f_M}{f_T} \cdot \frac{P_o}{\bar{P}_I} \tag{10}$$

where f_T is the total flow rate in the main flow tube. This expression is only valid if there is no loss of IF in the main flow tube. The initial

concentration of IF formed in the injector when excess F-atoms are present, $[IF]_o$, is approximately given by the expression

$$[IF]_o = \frac{f_{CF_3I}}{f_D + f_M} \cdot \frac{N_o \bar{P}_I}{RT} \quad . \tag{11}$$

In this expression f_{CF_3I} is the flow rate of CF_3I. Combining expressions (9), (10), and (11) gives

$$[IF]_M = \frac{f_{CF_3I}}{f_T} \cdot \frac{P_o N_o}{RT} \, e^{-\left\{\frac{k_L \ell A_I \bar{P}_I}{(f_D+f_M)RT}\right\}} \quad . \tag{12}$$

The energy-normalized signal from the LIF detector for IF, S_E, is related to the IF number density by the expression

$$S_E = \beta \, [IF]_M \tag{13}$$

where β is a calibration constant. Substituting (12) into (13) gives

$$S_E = \beta \, \frac{f_{CF_3I}}{f_T} \cdot \frac{P_o N_o}{RT} \, e^{-\left\{\frac{k_L \ell A_I \overline{P_I}}{(f_D+f_M)RT}\right\}} \quad . \tag{14}$$

Expression (14) shows that excess F-atoms and constant f_T, f_D, and f_M, the LIF signal will be a linear function of the quantity $(f_{CF_3I} P_o N_o / f_T RT)$ with slope β. If k_L is significant, varying either f_D or f_M will modify the apparent value of β. Greater values of f_D or f_M would give larger values of β, and plotting $\ell n \beta$ vs. $A_I \ell P_I/(f_D + f_M)RT$ would give a line with a slope of k_L.

We measured the apparent value of β for 3 values of $f_D + f_M$ at 1 torr total pressure and constant flow velocity in the flow tube. To vary this quantity we changed f_M, the He carrier for CF_3I in the injector, since varying f_D, the carrier for CF_4 through the discharge, effects the F-atom yield. In Fig. 7, S_E is plotted vs. $f_{CF_3I} \, P_o N_o / f_T RT$ for these 3 different injector flow rates. The quantity $f_{CF_3I} \, P_o N_o / f_T RT$ is actually the concentration of CF_3I

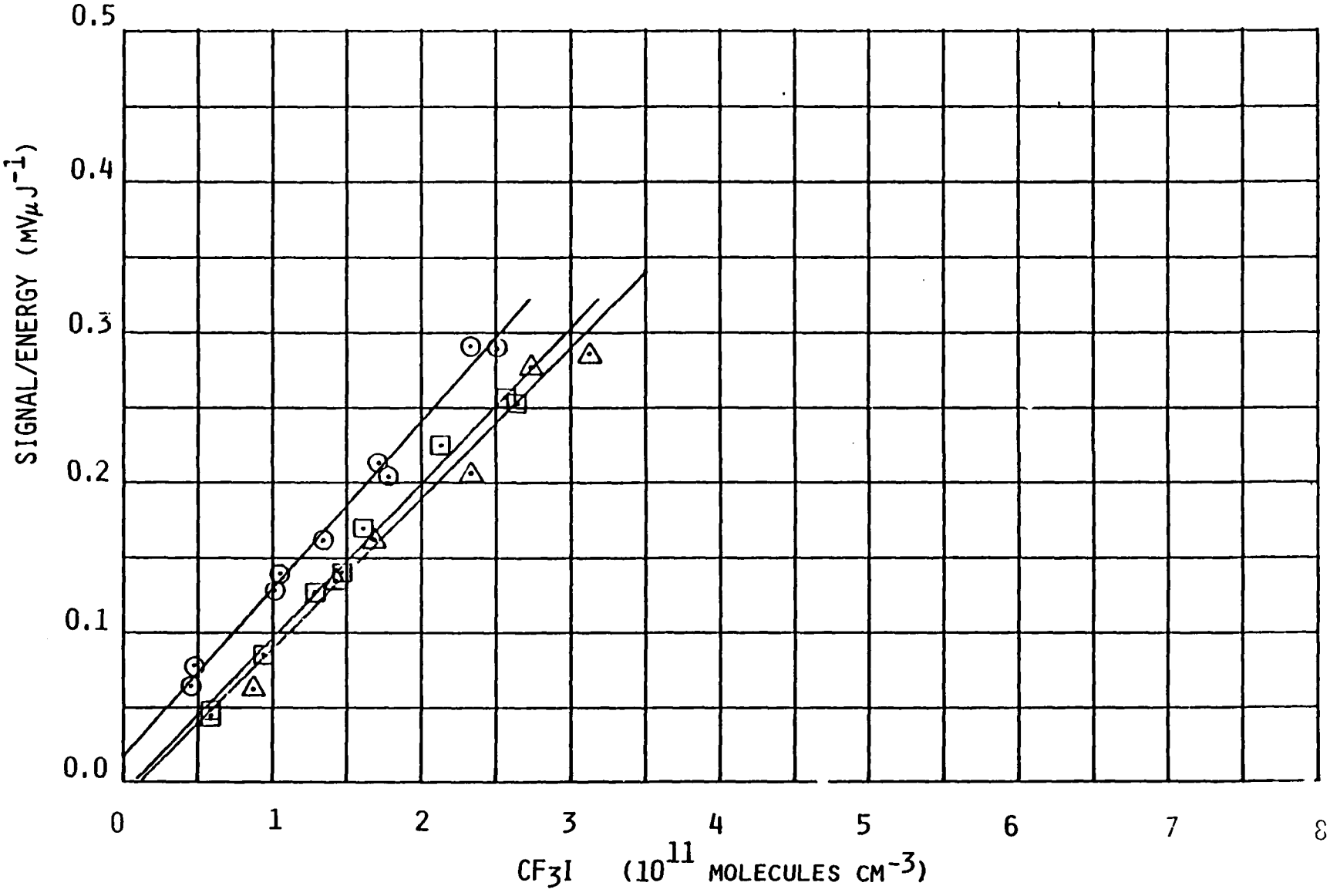

Fig. 7. LIF signal as a function of added CF_3I for 3 total injector flow rates: ⊙, 102 μmole s^{-1}; ⊡, 155 μmole s^{-1}; △, 207 μmole s^{-1}.

which would be found in the main flow tube if it were not removed by reaction with F-atoms, and the abscissa is labeled as such. If k_L is insignificant, there are no constant losses due to impurities in the CF_4 or CF_3I, and there are no losses in the main flow tube, then the apparent value for β is a true calibration constant relating the IF number density at the detector to the LIF signal. This is true because CF_3I would be directly converted to IF with no losses. For almost a factor of two variation in the injector residence time, we measure values of β of 1.00, 1.03, and 1.11 x 10^{-12} $mV_{\mu}J^{-1}$ $molecule^{-1}$ cm^3 for residence times of 1.7, 2.4, and 3.1 ms, respectively, in the injector. When these values are corrected for incomplete consumption of CF_3I(< 12%) at shorter residence times, the values become 1.14, 1.07, and 1.11 x 10^{-12} $mV_{\mu}J^{-1}$ $molecule^{-1}$ cm^3. Within experimental error there is no variation β over this range, and it appears that losses in the injector are insignificant.

2.2.5 Flow Tube Losses

Experiments to determine the extent of losses in the main flow tube were similar in concept to those done for the injector. At constant pressure the rate of diffusion of IF to the tube walls, where most of the losses should occur, is constant. If the time that IF is in contact with the tube walls is varied by changing the linear flow velocity in the tube at constant pressure, injection rate, and injector position, then any losses of IF on the walls will result in a variation in the apparent value of β. Expression (15) relates the LIF signal to the wall loss rate in the flow tube:

$$S_E = \beta \frac{f_{CF_3I}}{f_T} \frac{P_o N_o}{RT} e^{-k_w \left(\frac{L}{v_T}\right)} . \qquad (15)$$

In this expression L is the distance from the injector outlet to the LIF detector, v_T is the linear flow velocity in the flow tube, and k_w is the first order wall-loss rate coefficient.

In Fig. 8 we show a plot of S_E vs. the effective $[CF_3I]$ in the flow tube for several values of (L/v_T), the transit time from the injector to the detector. We have varied (L/v_T) from about 4-20 ms by varying f_T, the bulk

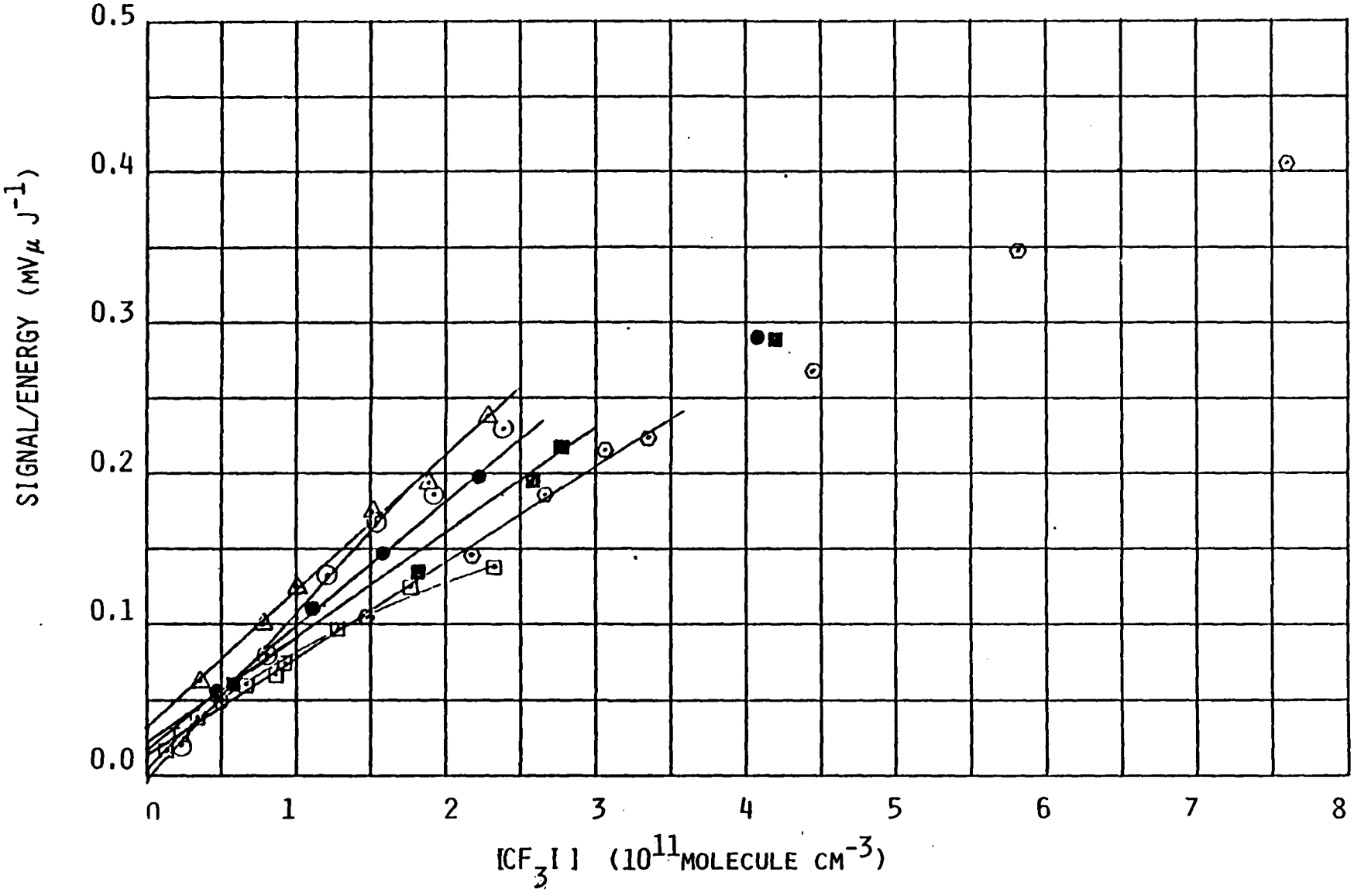

Fig. 8 LIF signal as a function of added CF_3I for 5 different values of (L/v_T) in the main flow tube: ⊡, 4.2 ms; ⊙, 5.7 ms; △, 7.4 ms; ●, 8.9 ms; ■, 11.9 ms, ⊙, 19.1 ms.

rate through the tube, while also varying the pumping speed to maintain constant pressure. All these plots have a regime of linear increase in S_E with $[CF_3I]$, but the roll off region moves to higher $[CF_3I]$ as the transit time is increased. This is because there is less dilution of the IF leaving the injector as f_T is decreased to give longer transit times. This moves the roll off region to higher number densities in the main flow tube. It is clear from Fig. 8 that β is not invariant with transit time at 1 torr total pressure.

If the wall loss mechanism is first order in IF, then plotting $\ell n\ \beta$ vs. (L/v_T) should give a straight line with slope $-k_w$. This plot is shown in Fig. 9. While the data do not clearly define a straight line, it is clear that there is some loss of IF at longer transit times. At shorter transit times, the loss of IF is negligible so that we can operate safely in this flow regime.

2.2.6 Solid Deposition in Excess CF_3I

Experiments by Appelman and Clyne, investigating the reaction of F-atoms with I_2 and $IC\ell$, showed that excess F-atoms in their systems promoted the formation of IF_5 via heterogeneous reactions (Ref. 29). Their flow tube system had uncoated silica walls. Given these results, we originally designed our experiments to operate in a regime with excess CF_3I. As a result, much of our early effort was directed toward the need to measure absolute F-atom number densities. Early in our LIF studies to measure IF, we found that operation in excess CF_3I resulted in the rapid formation of a smokey-gray substance on all of the exposed surfaces of the flow tube, including our optical viewing ports. This severely degraded our detection sensitivity. The film is very similar in appearence to thin films of I_2 and washes off with methanol. In excess F-atoms, there is no evidence for the formation of any solids in our system similar to those reported by Appelman and Clyne (Ref. 29).

This deposition problem requires that we operate in excess F-atoms. As shown above, there appears to be no serious problem in the injector due to operation in this mode; however, there does seem to be some loss of IF in the

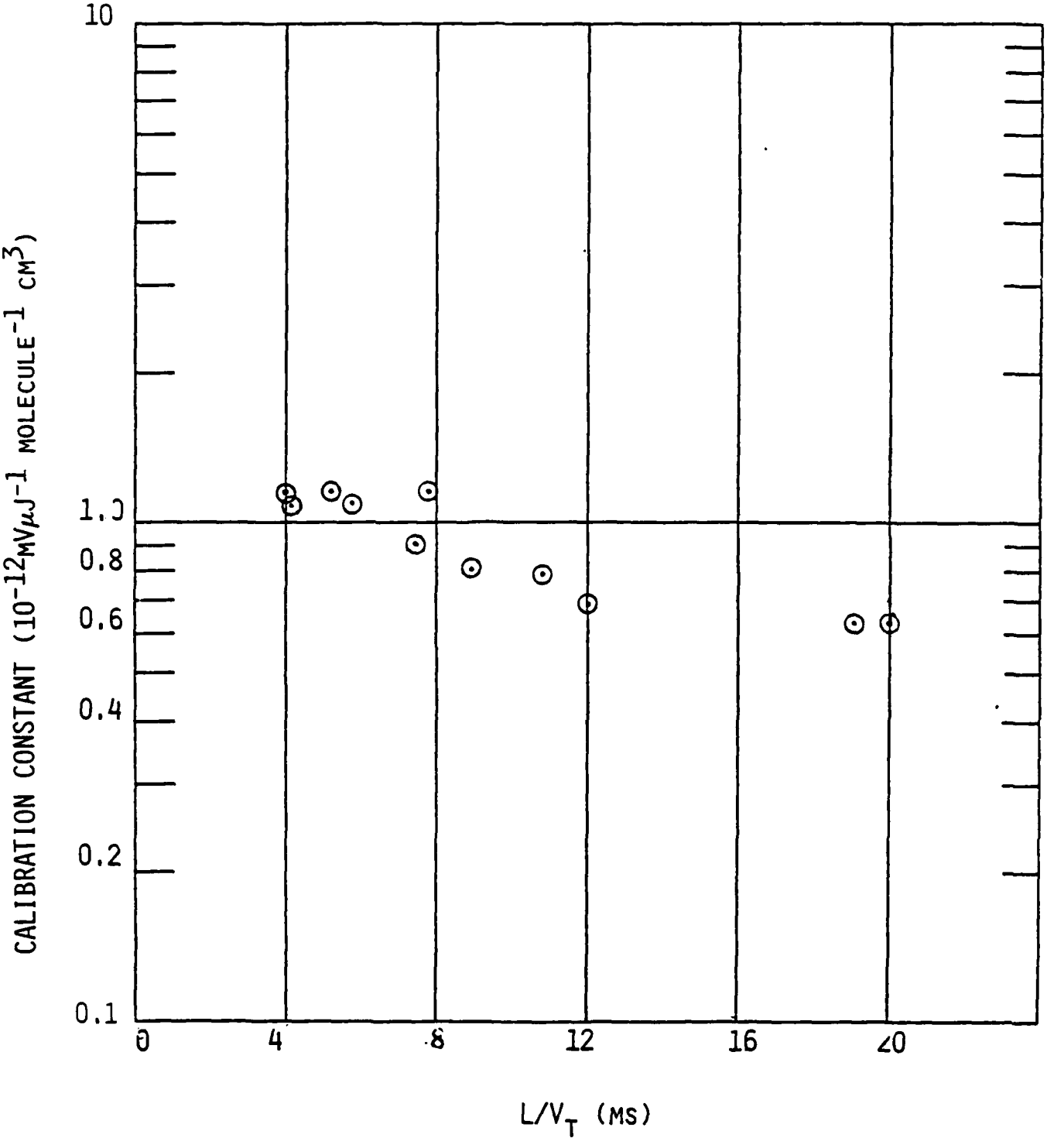

Fig. 9 Semi-log plot of β versus (L/v_T).

main flow tube. This may be a result of having some surfaces in the main flow tube, such as optical viewing ports, which are not Teflon®-coated and may catalyze the rapid destruction of IF.

2.2.7 Summary of IF Production and Loss Studies

We studied the production and loss of IF in our flow system using laser-induced fluorescence for measuring IF number densities. We related the production of F-atoms to the residence time of CF_4 in the microwave discharge and found a yield of about 0.3 F-atoms per CF_4 molecule under typical operating conditions. We identified flow conditions that produce complete reaction of CF_3I in the injector and showed that a negligible amount of IF is destroyed in the injector under these conditions. Some loss of IF in the main flow tube was found at low flow velocities; however, this loss appears to be negligible at higher velocities and permits us to operate in a regime where IF number densities may be directly related to the amount of CF_3I flowing into the injector. We also found that operation of the injector using excess CF_3I results in the deposition of an optically opaque thin film on the reactor walls. This requires us to operate in excess F-atoms and eliminates the need to measure absolute F-atom number densities.

2.3 Absolute Photon Emission Rate Measurements

2.3.1 General Procedure

The analysis of IF(B) excitation by active nitrogen requires the determination of absolute IF(B) photon-emission rates. The following paragraphs detail how we calibrate our system for such measurements.

The observed signal is related to the true volume emission rate through

$$I_{obs} = I_{true} \frac{\Omega}{4\pi} \eta_\lambda T_\lambda V \qquad (16)$$

where $\frac{\Omega}{4\pi}$ is the effective solid angle subtended by the detection system, η_λ is the quantum efficiency of the photomultiplier at the wavelength of interest, T_λ is the transmission of the optical system (e.g. mirror reflectivities and grating efficiency) and V is the observed volume of luminous gas in the reactor. The wavelength dependence of the product $\frac{\Omega}{4\pi} \eta_\lambda T_\lambda V$ is given by the relative monochromator response function R_λ. Absolute values of that product are obtained in a calibration experiment using the O/NO air afterglow at one or several specific wavelengths. Absolute values at wavelengths other than those chosen for calibration experiments are obtained by scaling with R_λ.

The relative spectral response of the monochromator was calibrated between 200 and 800 nm using standard quartz-halogen and D_2 continuum lamps (Optronic Laboratories Inc.). Additional confirmation of the calibration between 400 and 800 nm is obtained by scanning the air afterglow spectrum and comparing observed relative signal levels with the relative intensities given by Fontijn et al. (Ref. 33). The absolute spectral response of the detection system is measured at 580 nm using the O/NO air afterglow as described in the following subsection.

When atomic oxygen and nitric oxide are mixed, a continuum emission extending from 375 nm to beyond 3000 nm is observed (Refs. 33-41). The intensity of this emission is directly proportional to the product of the number densities of atomic oxygen and nitric oxide, and independent of pressure of bath gas, at least at pressures above about 0.2 torr. Thus, the volume-emission rate of the air afterglow is given by

$$I_{true} = k_\lambda [O][NO] \Delta\lambda \qquad (17)$$

where k_λ is the air afterglow rate coefficient in units of cm^3 $molecule^{-1}$ s^{-1} nm^{-1} and $\Delta\lambda$ is the monochromator band width. Literature values for this rate coefficient span a range of more than a factor of two (Refs. 33-39), but recent studies (Ref. 38) indicate that the original work of Fontijn et al. (Ref. 33) is probably correct at wavelengths shorter than ≈ 800 nm. We use a value of 1.25×10^{-19} cm^3 $molecule^{-1}$ s^{-1} nm^{-1} at λ = 580 nm. Combining Eqs. (16) and (17) gives the observed air afterglow intensity:

$$I_\lambda^{O/NO} = k_\lambda [O][NO] \Delta\lambda \frac{\Omega}{4\pi} \eta_\lambda T_\lambda V \quad . \tag{18}$$

Air afterglow calibration experiments give a calibration factor,

$$\kappa_\lambda = \frac{I_\lambda^{O/NO}}{[O][NO]} = k_\lambda \Delta\lambda \frac{\Omega}{4\pi} \eta_\lambda T_\lambda V \ , \tag{19}$$

the determination of which will be described in the next subsection.

Absolute number densities of emitters are obtained by dividing absolute volume emission rates by known transition probabilities. The air afterglow calibration factor, κ_λ, and the moderately well established value of the air afterglow rate constant, k_λ, are used to convert observed emission intensities to volume emission rates:

$$I_{true} = \frac{I_{obs} k_{\lambda_c} \Delta\lambda_c R_{\lambda_c}}{\kappa_{\lambda_c} R_{\lambda_{obs}}} \tag{20}$$

where λ_c represents the wavelength of the calibration experiments and λ_{obs} is the wavelength of the transition of interest. I_{obs} must be the total integrated band intensity. In this work we usually measured emission intensities in terms of peak intensities. A calibration factor consisting of the ratio of the integrated band intensity to the product of the spectrometer band width and the peak intensity was determined for cases in which total intensities were needed. In calibration experiments, the band areas were integrated numerically using spectral scans which were greatly expanded along the wavelength axis.

A series of calibration experiments taken over a period of time established the calibration factor, κ_{580}, to ± 10%. An additional uncertainty of ± 25% exists in the absolute value of the air-afterglow rate constant k_{580}. Further uncertainties in the determination of the absolute photon-emission rate for IF(B) come in through the relative monochromator response function (10%), IF(B) band transition probabilities (10%), and minor uncertainties in the calibration factors to convert observed peak heights to band areas.

2.3.2 Air-Afterglow Calibration Procedure

In air-afterglow calibration experiments, the intensity at the calibration wavelength is measured when known quantities of both atomic oxygen and nitric oxide are added to the reactor. Known quantities of atomic oxygen are prepared by titration of nitrogen atoms with excess nitric oxide:

$$N + NO \rightarrow N_2 + O \qquad (21)$$

($k_{21} = 3.5 \times 10^{-11}$ cm^3 molecule^{-1} s^{-1}) (Refs. 42-44).

In the absence of added nitric oxide, N-atom recombination produces chemiluminescence from the nitrogen first-positive bands, the intensity of which is proportional to the square of the N-atom number density. The kinetic processes are described below.

$$N + N + M \rightarrow N_2(B^3\Pi_g) \qquad (22)$$

$$N_2(B\ ^3\Pi_g) \rightarrow N_2(A^3\Sigma_u^+) + h\nu \quad \text{(first-positive bands)}. \qquad (23)$$

Upon addition of NO the first-positive emission intensity decreases until such point as the quantity of NO added balances the amount of N-atoms initially in the flow. At this point, the end point of the NO titration, all N initially in the reactor has been quantitatively converted to O, and no emission is observed in the reactor. As NO is further added to the reactor, the air-afterglow emission begins to be observed, and the intensity of the emission varies linearly with the amount of NO added. Such a titration plot is shown in Fig. 10. The equation describing the change in the air-afterglow intensity as a function of added NO for NO additions beyond the titration end point is

$$I_{O/NO} = \kappa[O][NO] = \kappa[N]_o\left([NO]_o - [N]_o\right) \qquad (24)$$

where κ is the constant of proportionality relating the air-afterglow intensity to the product [O][NO], $[N]_o$ is the number density of N-atoms initially in the reactor prior to NO addition, and $[NO]_o$ refers to the NO number density which would obtain in the absence of reaction (21). The factor κ then is determined to be the ratio of the square of the slope to the intercept of the line describing the change in air-afterglow intensity with [NO].

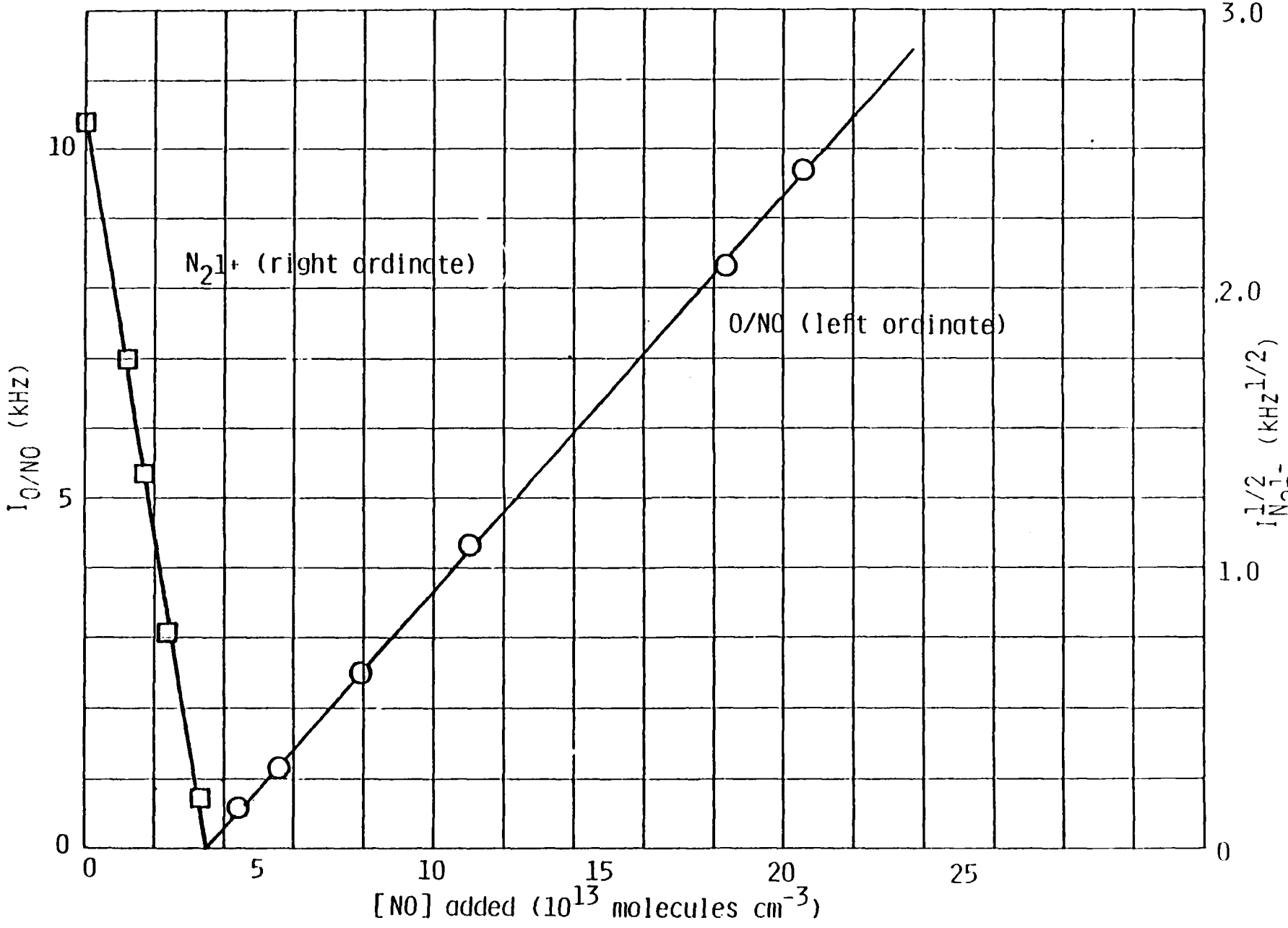

Fig. 10 Variation in emission at 580 ± 5 nm as a function of added [NO].

Two major complications can lead to problems in using the above technique to calibrate the apparatus for absolute photon-emission rates or for [O] measurements. If the initial N-atom number density is greater than about 10^{14} atoms cm^{-3}, some O_2 spectral features from O-atom recombination will begin to be observable above the air-afterglow continuum, and can lead to incorrect air-afterglow intensity determinations (Refs. 45-46). A more serious problem, however, lies in the slow removal of O-atoms in a three-body recombination with NO. The important reactions are

$$O + NO + M \rightarrow NO_2 + M \qquad (25)$$

($k_{25} = 7 \times 10^{-32}$ cm^6 $molecule^{-2}$ s^{-1} for M = Ar) (Ref. 47)

and

$$O + NO_2 \rightarrow NO + O_2 \quad (k_{26} = 9.5 \times 10^{-12} \text{ cm}^3 \text{ molecule}^{-1} \text{ s}^{-1}) \text{ (Ref. 47).} \qquad (26)$$

Reaction (26) is fast, and essentially acts to maintain a constant NO number density and to double the effective rate at which O is removed in reaction (25). This effect becomes a problem at higher pressures (> 1.5 torr), longer mixing times (> 30 ms) and large NO concentrations (> 10^{14} molecules cm^{-3}).

Unfortunately, it is just these adverse conditions which give the best signal-to-noise in the calibration experiments. The calibrations for the experiments described in this report were corrected when necessary for the effects of removal of O in reactions (25) and (26). Conditions were such that the corrections never amounted to more than 5% however.

3. THE EXCITATION OF IF(B $^3\Pi_{0^+}$) BY N_2(A $^3\Sigma_u^+$)

Three types of measurements fully characterize the excitation of IF(B $^3\Pi_{0^+}$) by N_2(A $^3\Sigma_u^+$). Spectral scans under a variety of conditions characterized the distribution of IF(B) vibrational levels excited in the energy-transfer reaction. Measurements of IF(B) intensities as a function of IF number density in the presence of known number densities of N_2(A) determined the rate coefficient for the excitation of IF(B) by N_2(A). Finally the rate coefficient for N_2(A) removal by IF was determined by monitoring the disappearance of N_2(A) as a function of added IF number density.

3.1 Vibrational Distributions from N_2(A) Excitation

When IF is added to a flow of N_2(A) metastables, the IF(B $^3\Pi_{0^+} \rightarrow X^1\Sigma^+$) system appears prominently between 440 and 640 nm. Figure 11 shows a typical spectrum. Relative populations of the B-state vibrational levels were determined by dividing the response-corrected intensity of a given band by the appropriate Einstein emission-rate coefficient (see Appendix A). In initial experiments, the band intensities were determined by planimetry. Later in the program we used a spectral fitting routine which determined the best set of populations in a least-squares sense which gave a synthetic spectrum most nearly reproducing the experimental spectrum (Ref. 48). Typical fits for runs at 0.5 and 5 torr (primarily argon) are shown in Figs. 12 and 13. Comparison of the spectra in Figs. 12 and 13 clearly shows evidence of vibrational relaxation of the IF(B) at the higher pressure. Figure 14 compares the vibrational distributions determined in three runs at three different pressures. Clearly the vibrational distribution is relaxed at the higher pressures. Figure 15 shows that nitrogen is more efficient at relaxing IF(B) vibration than is argon, and that CF_4 is even more efficient. The data of Fig. 15 all were taken at a constant total pressure but with varying mole fractions of N_2 and CF_4 in Ar. Figure 16 shows how the vibrational population distribution varies with pressure over the range of 0.5 to 9 torr. The increase in population of the lower vibrational levels and the concomitant decrease in population of the upper vibrational levels demonstrate, graphically, the extent of vibrational relaxation.

A modified Stern-Volmer analysis of the data in Fig. 16 allows us to estimate vibrational relaxation coefficients. The analysis assumes that

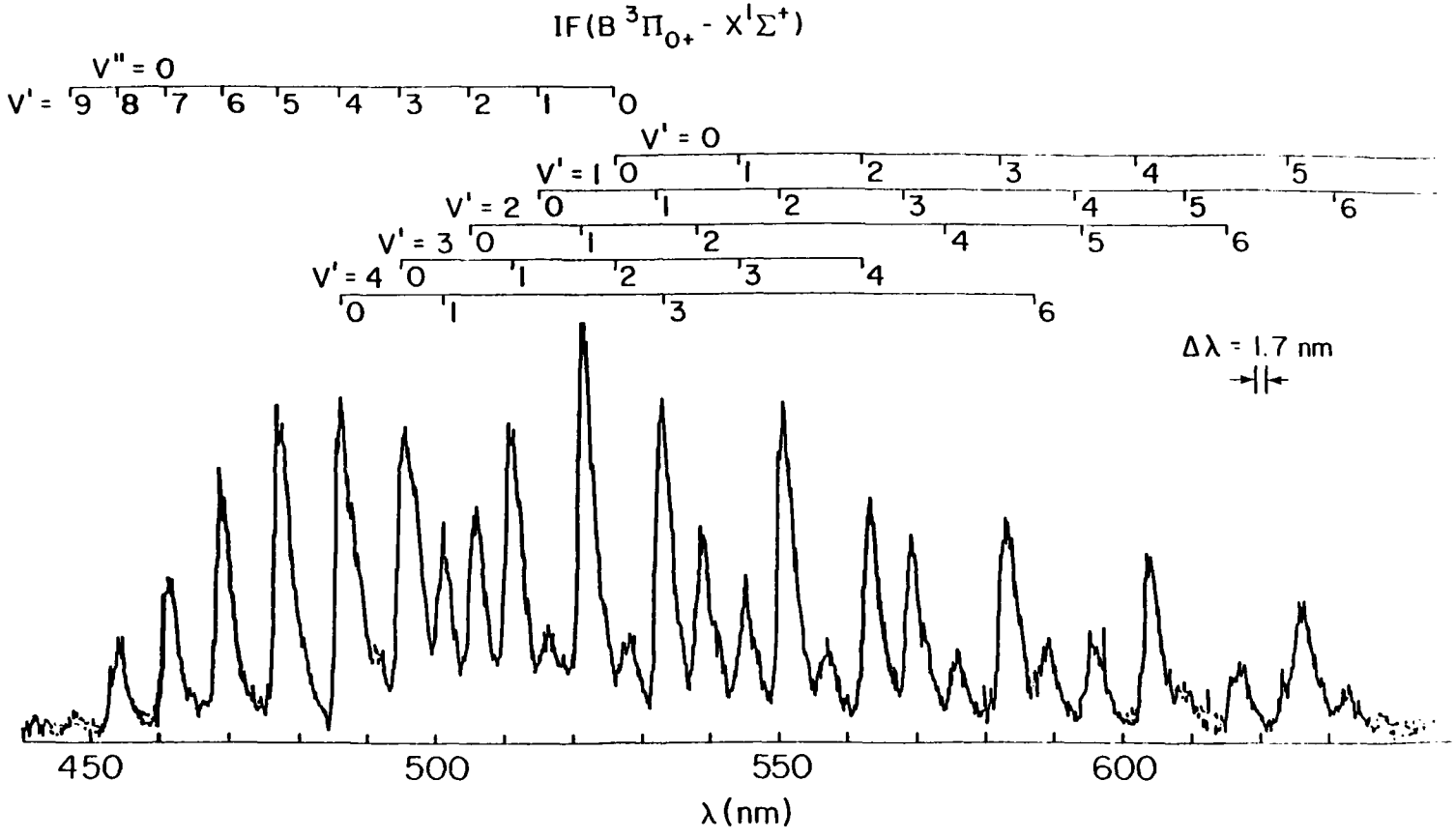

Fig. 11 Spectrum of IF(B $^3\Pi_{0+}$) excited in the energy-transfer reaction between N_2(A $^3\Sigma_u^+$) and IF(X $^1\Sigma_g^+$).

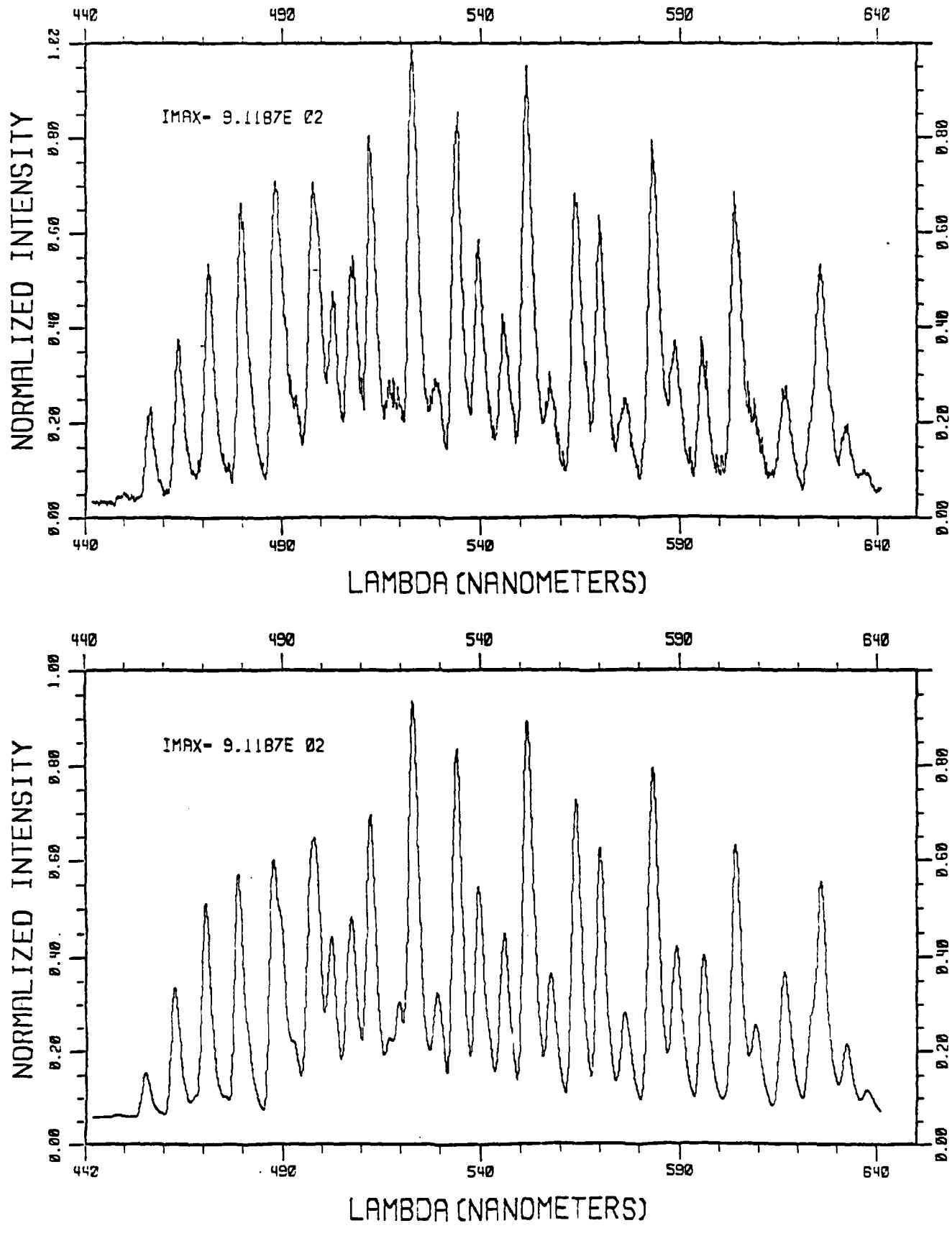

Fig. 12 **Experimental (top) and computed (bottom) IF(B) spectra from $N_2(A)$ excitation of IF at 0.5 torr.**

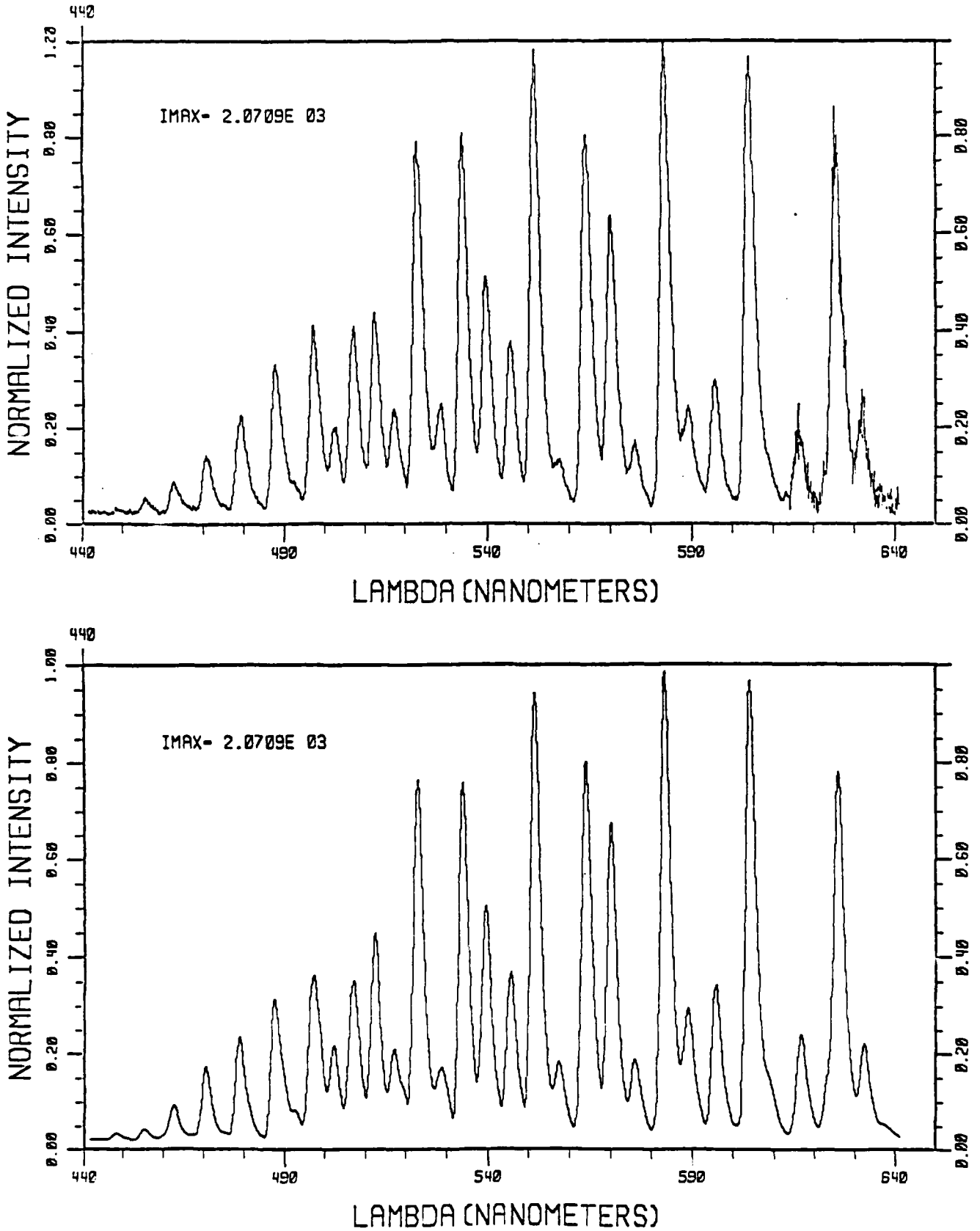

Fig. 13 **Experimental (top) and computed (bottom) IF(B) spectrum from $N_2(A)$ excitation of IF at 5 torr.**

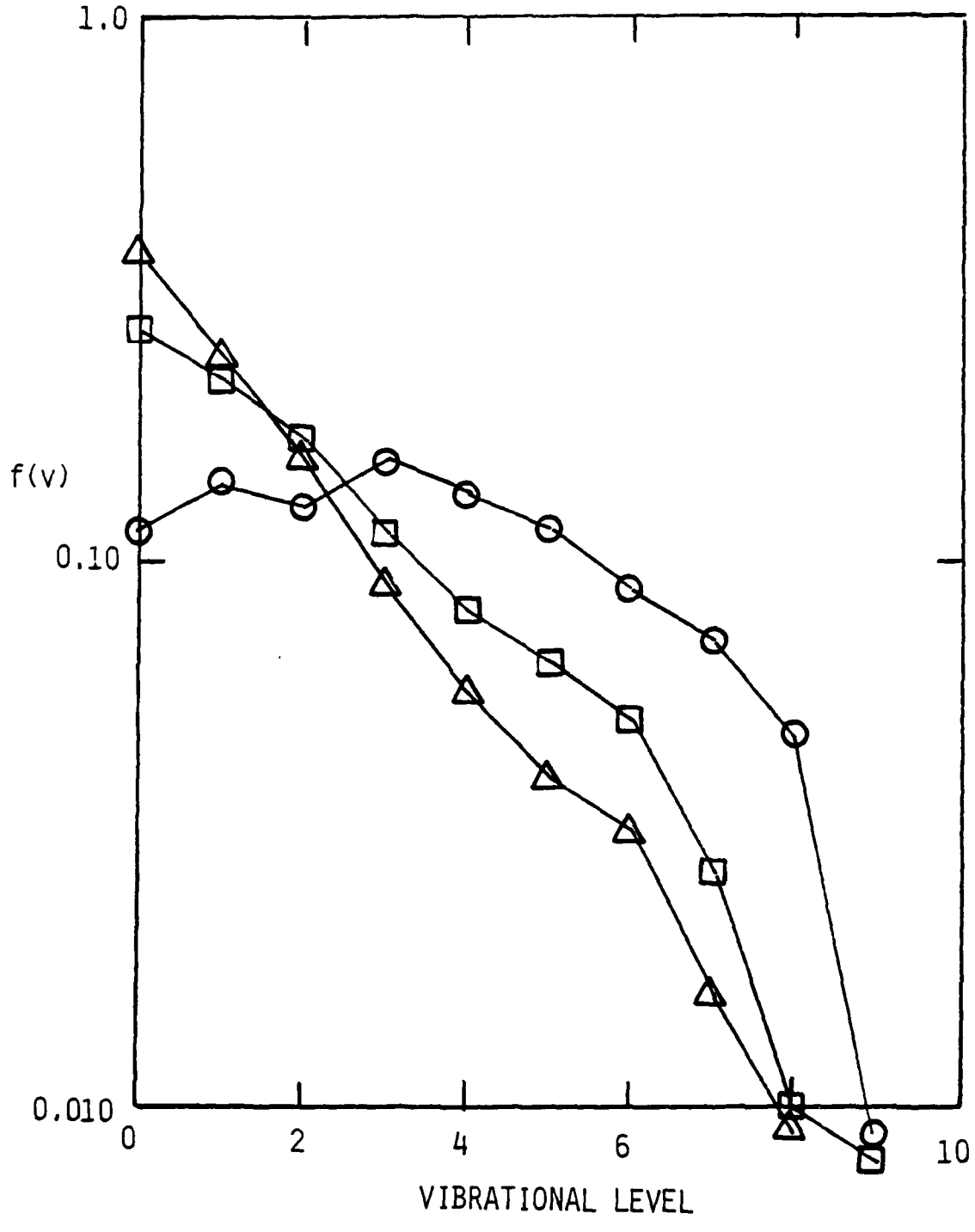

Fig. 14 Vibrational distribution of IF(B) excited in the $N_2(A)$ + IF reaction at 0.5 (○), 5 (□), and 9 (△) torr.

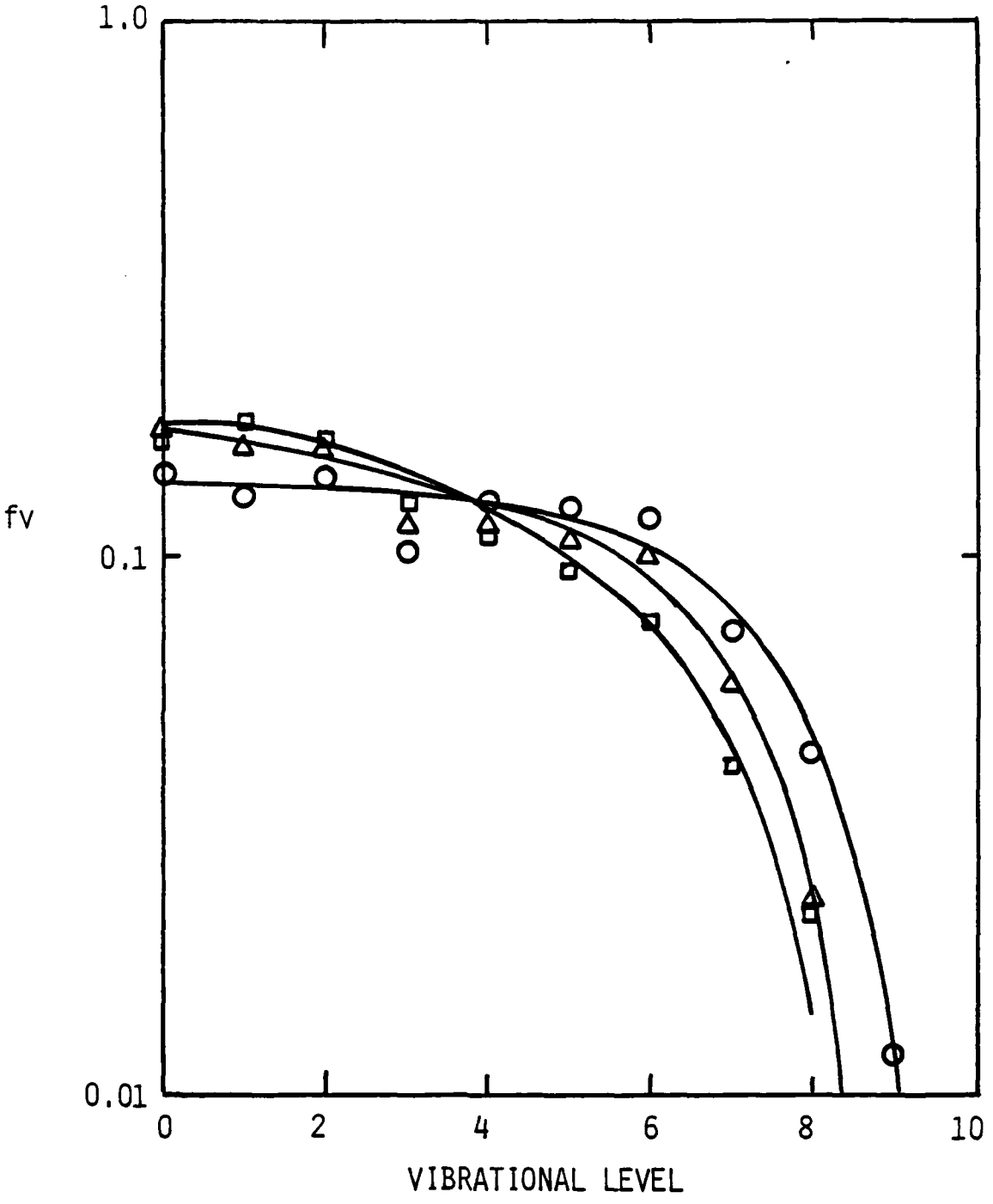

Fig. 15 Vibrational distributions of IF(B) excited by the $N_2(A)$ + IF reaction at 1 torr of argon with 2.6% N_2(○), 17% N_2(△), and 17% N_2-2% CF_4(□).

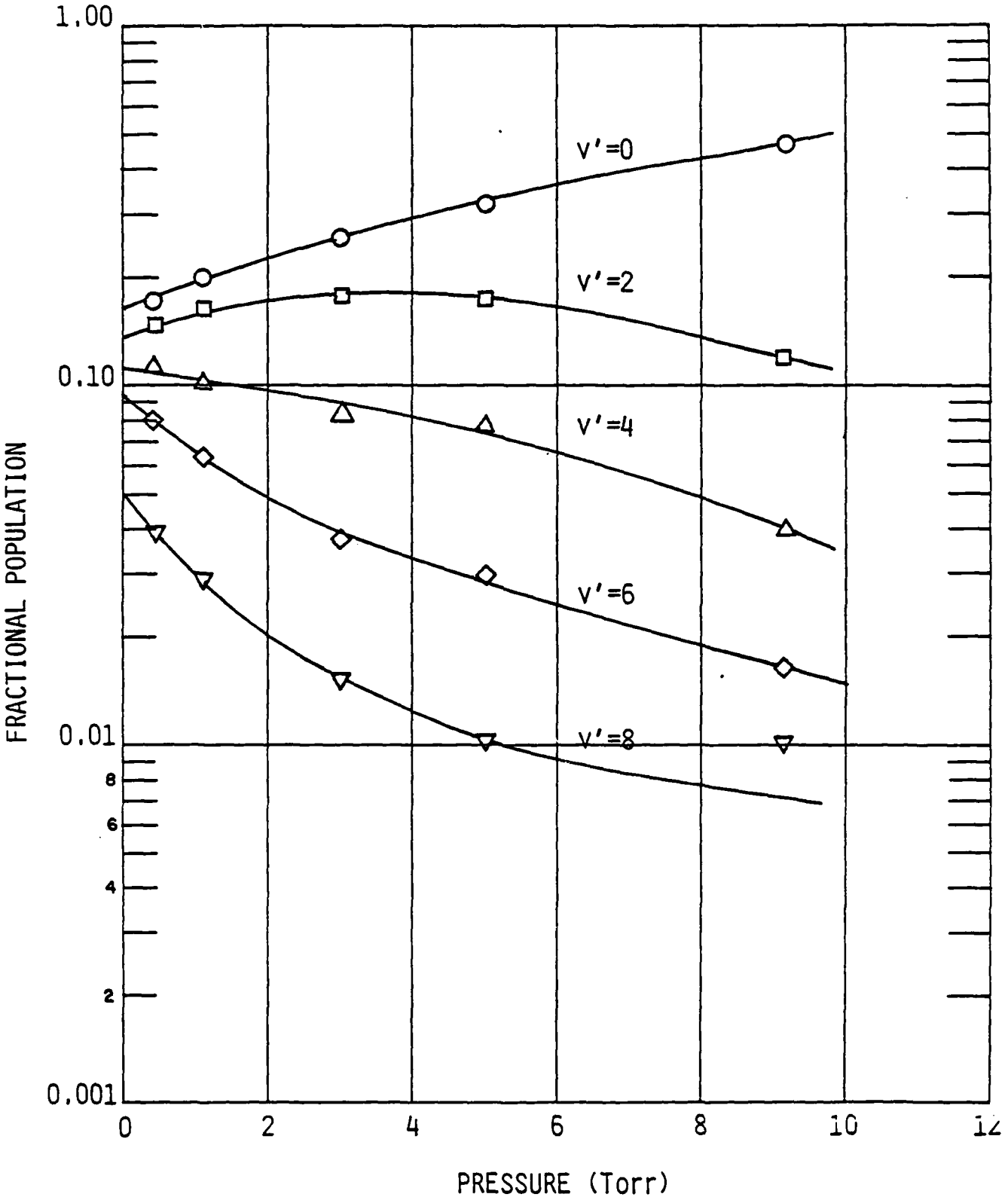

Fig. 16 IF($B^3\Pi_0^+$) populations from $N_2(A^3\Sigma_u^+$ v'=0) + IF(X).

electronic quenching is negligible, that vibrational relaxation proceeds only a single quantum at a time, and that the gas composition is constant. Our mixture is approximately 80% argon and 20% helium and nitrogen, with minor amounts of CF_4 added for this series of experiments to relax the $N_2(A)$ vibrational distribution to $v' = 0$.

Because radiation is so rapid in the reactor, IF(B) is in steady state in the observation region. Thus, in the absence of vibrational relaxation, we have

$$R_v = N_v^o A_v \tag{27}$$

where R_v is the rate of formation of IF(B) in vibrational level v, N_v^o is the population of that level, and A_v is the radiative decay rate. When vibrational relaxation is included, the Eq.(27) becomes:

$$R_v + k_{v+1,v} N_{v+1} P = (A_v + k_{v,v-1} P) N_v \tag{28}$$

where $k_{v,v-1}$ represents the vibrational relaxation rate out of level v; $k_{v+1,v}$, the vibrational relaxation rate coefficient into level v; and P is the gas pressure. If we now sum Eqs. (27) and (28) over all levels above level v, subtract the resultant sums of Eq. (27) from Eq. (28), and divide through by the quantity $N_v A_v$, we obtain the working equation for the vibrational-relaxation analysis:

$$\frac{N_v^o}{N_v} + \sum_{m=1}^{m_{max}} \left(\frac{N_{v+m}^o - N_{v+m}}{N_v} \right) = 1 + \frac{k_{v,v-1} P}{A_v} \tag{29}$$

Figure 17 shows some typical plots of the data analyzed according to Eq. (29). Least-squares fits to the data for each vibrational level indicate that the vibrational relaxation rate coefficients range from 2.6 to 4 x 10^{-12} cm^3 $molecules^{-1}$ s^{-1} for vibrational levels 3-8. Levels 1 and 2 appear to relax a bit more slowly with rate coefficients of 0.6 and 1.6 x 10^{-12} cm^3 $molecule^{-1}$ s^{-1}, respectively. Table 1 summarizes the vibrational-relaxation-rate measurements. Experiments at the Air Force Weapons Laboratories (Ref. 49) have

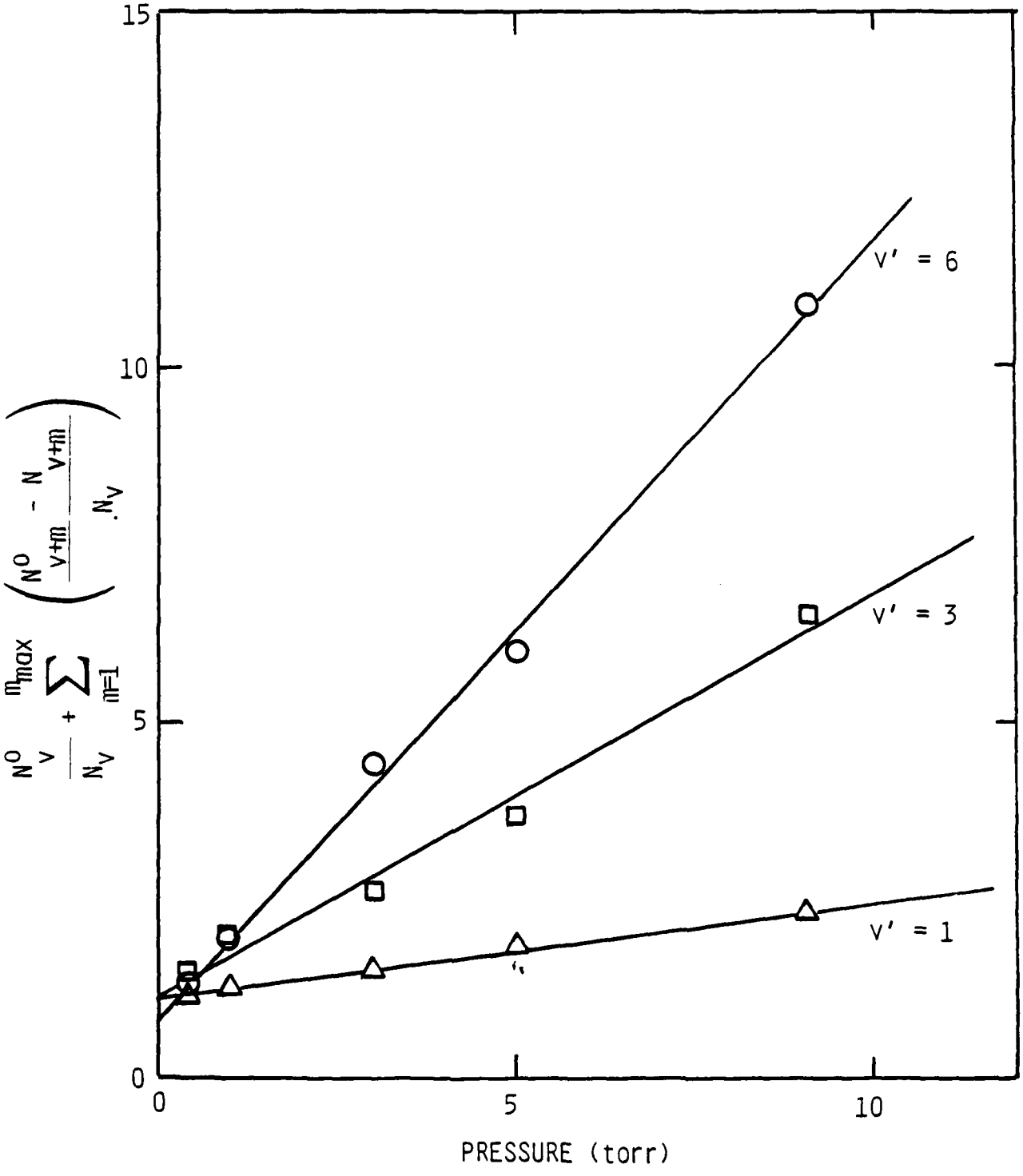

Fig. 17 Stern-Volmer plots for IF(B) vibrational relaxation in 80/20, Ar/N_2·He mixtures.

TABLE 1

RATE COEFFICIENTS FOR VIBRATIONAL RELAXATION OF IF($B^3\Pi_{0^+}$) BY AN 80/20 Ar/He-N_2 MIXTURE

v'	$k^a_{v,v-1}$
1	0.6 ± 0.1
2	1.6 ± 0.2
3	2.6 ± 0.2
4	3.5 ± 0.3
5	2.6 ± 0.1
6	4.1 ± 0.1
7	4.0 ± 0.2
8	2.9 ± 0.1

[a] Units of 10^{-12} cm^3 $molecule^{-1}$ s^{-1}

indicated that the rate coefficients for vibrational relaxation of IF(B;v'=3) by helium, nitrogen and argon are 5.7, 3.9, and 1.2 x 10^{-12} cm^3 $molecule^{-1}$ s^{-1}, respectively. From these data we calculate a vibrational relaxation rate coefficient for an 80/20 Ar/N_2-He mixture (with an average rate coefficient for the He-N_2 component of 5 x 10^{-12} cm^3 $molecule^{-1}$ s^{-1}) of 2.0 x 10^{-12} cm^3 $molecule^{-1}$ s^{-1}. This agrees excellently with our measured value of 2.6 x 10^{-12} cm^3 $molecule^{-1}$ s^{-1} given the 30-40% uncertainty in the AFWL data, and our own experimental uncertainties which must be of comparable size. The AFWL experiments also indicate that the rate coefficients for relaxation of vibrational level 1 by He, Ne, and N_2 are about a factor of three smaller than the corresponding rate coefficients for vibrational level 3. This agrees moderately well with the factor of four reduction observed in our experiments.

3.2 Rate Coefficients for the Excitation of IF(B $^3\Pi_{0^+}$) by N_2(A $^3\Sigma_u^+$)

Knowledge of the B-state vibrational distribution, and measurements of the change in intensity of various bands as a function of IF number density for otherwise constant conditions, *determines* the rate coefficient for excitation of IF by collisions with N_2(A). The differential equation describing the rate of change in the IF(B) number density with time is

$$\frac{d[IF^*]}{dt} = k_{ex}[IF][N_2(A)] - k_{rad}[IF^*] \quad . \tag{30}$$

(We have ignored electronic quenching of the IF(B) state by the various species in the reactor.) Because the IF(B) radiative-decay rate is quite large, IF(B) is in steady state in the observation volume. Thus, the B state emission intensity is

$$I_{IF^*} = k_{rad}[IF^*] = k_{ex}[IF][N_2(A)] = k_{ex}[IF] \frac{I_{N_2(A)}}{A_{N_2(A)}} \tag{31}$$

where $I_{N_2(A)}$ and $A_{N_2(A)}$ are the intensity and transition probability of N_2(A) in the observation volume. This expression can be rearranged to give

$$\frac{I_{IF^*}}{I_{N_2(A)}} = \frac{k_{ex}[IF]}{A_{N_2(A)}} \quad . \tag{32}$$

Equation (32) shows that the ratio of the intensity of IF(B) to that for $N_2(A)$ should vary linearly with IF number density. Figure 18 shows that this is indeed the case for a number of different IF(B) vibrational levels.

The experimental runs monitored only the intensities of the peak heights of the Vegard-Kaplan or IF(B) bands. Planimetry or numerical integration determined the ratio of band areas to peak heights which were the required correction factors in analyzing the raw data. Dividing the integrated band areas of a given v',v" band by branching ratios determined from our IF(B) Einstein-coefficient calculations (Appendix A) gave the total emission intensity out of a given vibrational level of the IF(B) electronic state. Dividing this IF(B;v') intensity by the fraction of the total IF(B) population in a given v' state gave the total fluorescence from all vibrational levels of the IF(B $^3\Pi_{0^+}$) state. Shemansky's (Ref. 50) Einstein coefficients, appropriately weighted to account for the different lifetimes of the degenerate levels of the $N_2(A)$ state, were used to convert the Vegard-Kaplan emission intensities to $N_2(A)$ number densities. A number of different runs at 1 torr total pressure showed that the total rate coefficient for IF(B) excitation into all vibrational levels in the energy-transfer reaction between $N_2(A)$ and IF(X) is $(8.3 \pm 0.10) \times 10^{-11}$ cm^3 molecule^{-1} s^{-1}. This value is independent of the observed band, the transit times from the injector to the observation volume (less than ≈10 ms), and the initial F-atom number density.

A few excitation-rate-coefficient measurements at higher pressures indicated a decrease in the excitation rate coefficient with increasing pressure. The drop was about a factor of two between one and five torr. Interpreting these results is not so straight forward, however. An over estimate in the IF number density will lead to an apparent reduction in the excitation-rate coefficient. This situation is likely to arise because the higher pressures are achieved by throttling the pumping system, which results in reducing the bulk flow velocity and an accompanying increase in the transit time from the injector to the observation region. Our laser-induced fluorescence studies indicated some fall off in the IF number density reaching the observation region at longer transit times, but constant pressure. The laser-induced fluorescence monitor is unsuitable at higher pressures, because the IF fluorescence distribution changes within the band pass of our detection system as the higher

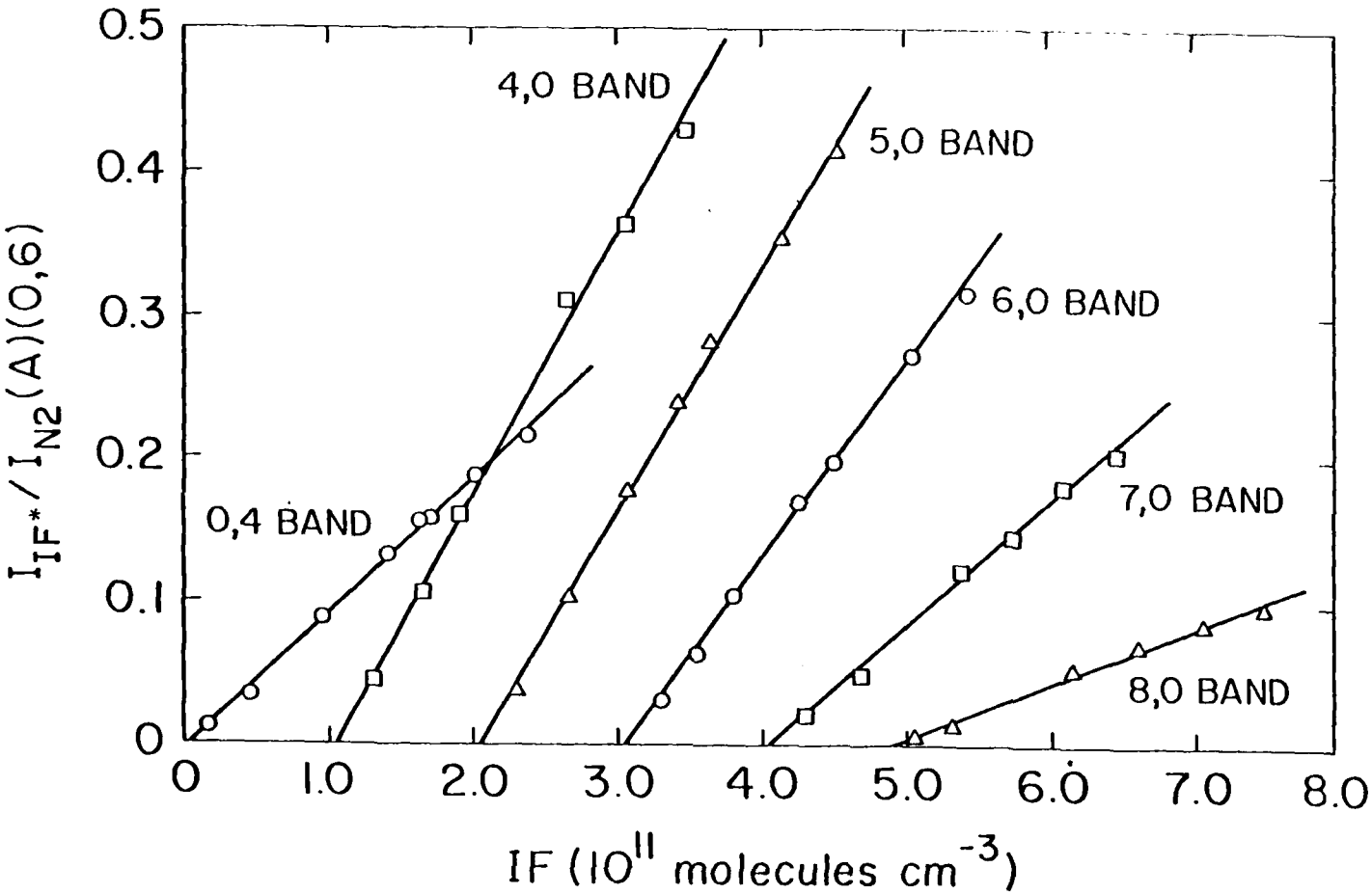

Fig. 18 Variation in the ratio of IF(B $^3\Pi_{0+}$) intensity to that for the 0,6 Vegard-Kaplan band as a function of IF number density. Abscissa offsets applied for clarity.

pressures relax the IF vibrational distribution. Thus, a calibration made at low pressure and short residence time cannot be used in measurements at high pressure and long residence time. A solution to this problem would be to use the IF(B→X), (v',v") = (0,0) transition for the laser-induced fluorescence studies. Our laser lacks sufficient energy to pump that transition adequately, however.

An indication that we did indeed overestimate the IF number density in the reactor at the higher pressures comes from our observation that the effective quenching rate of $N_2(A)$ by IF is also reduced at higher pressures. The $N_2(A)$ quenching data at the higher pressures cannot be used to calibrate the IF number densities, however, because the reaction-time mixing correction is also pressure dependent, and therefore is not the same at the different pressures.

We conclude, therefore, that the reduction in apparent IF excitation rates at higher pressures results predominantly from IF losses on the reactor walls during the longer transit times from the injector to the detector which accompanied the high pressure studies. Any real electronic quenching in our system is only minor.

The ratio of total IF fluorescence intensity to $N_2(A)$ number density in the presence of 2% CF_4 added to the bath gas just downstream of the metastable discharge indicated a decrease of approximately 20% in the IF fluorescence from the intensities observed in the absence of CF_4. The CF_4 relaxes the $N_2(A)$ vibrational levels, so that in its presence, only $N_2(A)$ v' = 0 is in the reactor. Thus, the implication of this study is that the excitation-rate coefficient is slightly smaller for $N_2(A)$ v' = 0 than it is for higher levels of $N_2(A)$. We do not feel confident in this assertion, however, because adding the CF_4 also causes the IF(B) distribution to be vibrationally relaxed, and any errors in relative monochromator response function or IF(B) transition probabilities will be reflected in the total IF fluorescence intensity measurement. Thus we can state with confidence only that no dramatic changes occur when the $N_2(A)$ is vibrationally relaxed compared to conditions under which it is not.

3.3 Rate Coefficients for $N_2(A)$ Removal by IF and Other Molecules

The important kinetic processes in our reactor which involve $N_2(A)$ are:

$$N_2(A) + IF \rightarrow N_2(X) + IF^* \quad (33a)$$

$$\rightarrow \text{other products} \quad (33b)$$

$$N_2(A) + Q \rightarrow N_2(X) + Q' \quad (34)$$

$$N_2(A) + \text{wall} \rightarrow N_2(X) \quad (35)$$

where Q represents other quenchers. Given these reactions, the differential equation describing the variation in the $N_2(A)$ number density with time is

$$\frac{d[N_2(A)]}{dt} = - \{k_{33}[IF] + k_{34}[Q] + k_{35}\}[N_2(A)] \ . \quad (36)$$

Because the number densities of IF and any other significant quenchers in the reactor will be much greater than that for $N_2(A)$, they can be considered to be constant (the pseudo-first-order approximation) and the differential equation can be solved to give

$$\ell n \frac{[N_2(A)]_{(t)}}{[N_2(A)]_{(t=0)}} = - \{k_{33}[IF] + k_{34}[Q] + k_{35}\} t \ , \quad (37)$$

where the reaction time, t, in the flow reactor is given by the ratio of the distance between the injector and the detection region, z, and the bulk flow velocity, $\bar{v}$. For fixed z and $\bar{v}$ (fixed-injection-port analysis), measurements of the change in $N_2(A)$ number density as a function of reagent number density give decay constant Γ,

$$\Gamma = - \frac{d \ \ell n I_{N_2(A)}}{d[Q]} = k_{34}[Q]\bar{z}/v \ , \quad (38)$$

given that the $N_2(A)$ number density is directly proportional to the Vegard-Kaplan emission intensity. The desired rate coefficient is then the ratio of the slope of a plot of $\ell n \ I_{N_2(A)}$ versus [Q] (i.e., Γ) to the reaction time, $z/\bar{v}$.

The above analysis assumes perfect mixing at the injector, and neglects the fluid dynamic effects of the coupling of the radial density gradient of the $N_2(A)$ with a radial velocity profile. ($N_2(A)$ is destroyed with unit efficiency in collisions with the walls.) This effect has been thoroughly discussed in the literature (Refs. 51-58). The result, under appropriate conditions, is $d\ell nI_{VK}/d[IF] = - 0.62\ k_1 z/\tilde{v}$. These conditions are generally obtained in our experiments.

The correction for imperfect mixing must be made empirically by doing experiments at several different values of z. Then the effective mixing length, $z_{eff} = z-z_o$, is deduced by plotting decay constants, Γ, as a function of reaction time and extrapolating to zero reaction time.

We observed the decays in the log of the Vegard-Kaplan intensity as a function of the number densitites of IF, CF_3I, CF_4, and NF_3 for both vibrational levels 0 and 1 of $N_2(A)$ and SF_6 for vibrational level 1. We made careful measurements of the CF_3I quenching rate coefficient at three different mixing distances, and applied the mixing correction so obtained to the results of the other systems.

Figure 19 shows the results of adding CF_4 to $N_2(A)$ with a reaction time of about 90 ms. Vibrational level 1 decays only slightly, while vibrational level 0 actually increases. This shows that vibrational relaxation of v'=1 is feeding v'=0, and that electronic quenching is negligible. Our data suggest that the rate coefficient for vibrational relaxation of v'=1 to v'=0 is about 3×10^{-13} cm^3 $molecule^{-1}$ s^{-1}, with an uncertainty of about a factor of 2 because of the small decay range of the measurement. In other experiments we added relatively large flows of CF_4 with the nitrogen just downstream of the Ar^* discharge and could thereby convert all $N_2(A;v'>1)$ to $N_2(A;v'=0)$.

Figure 20 shows the decay in the (0,6) Vegard-Kaplan intensity as a function of CF_3I number density for three different reaction times. The slopes of the decays in Fig. 20 are plotted against reaction time in Fig. 21 to determine a mixing correction to the data. These results and some similar data for v'=1 indicate that CF_3I quenches $N_2(A)$ with rate coefficients of 2.0 and

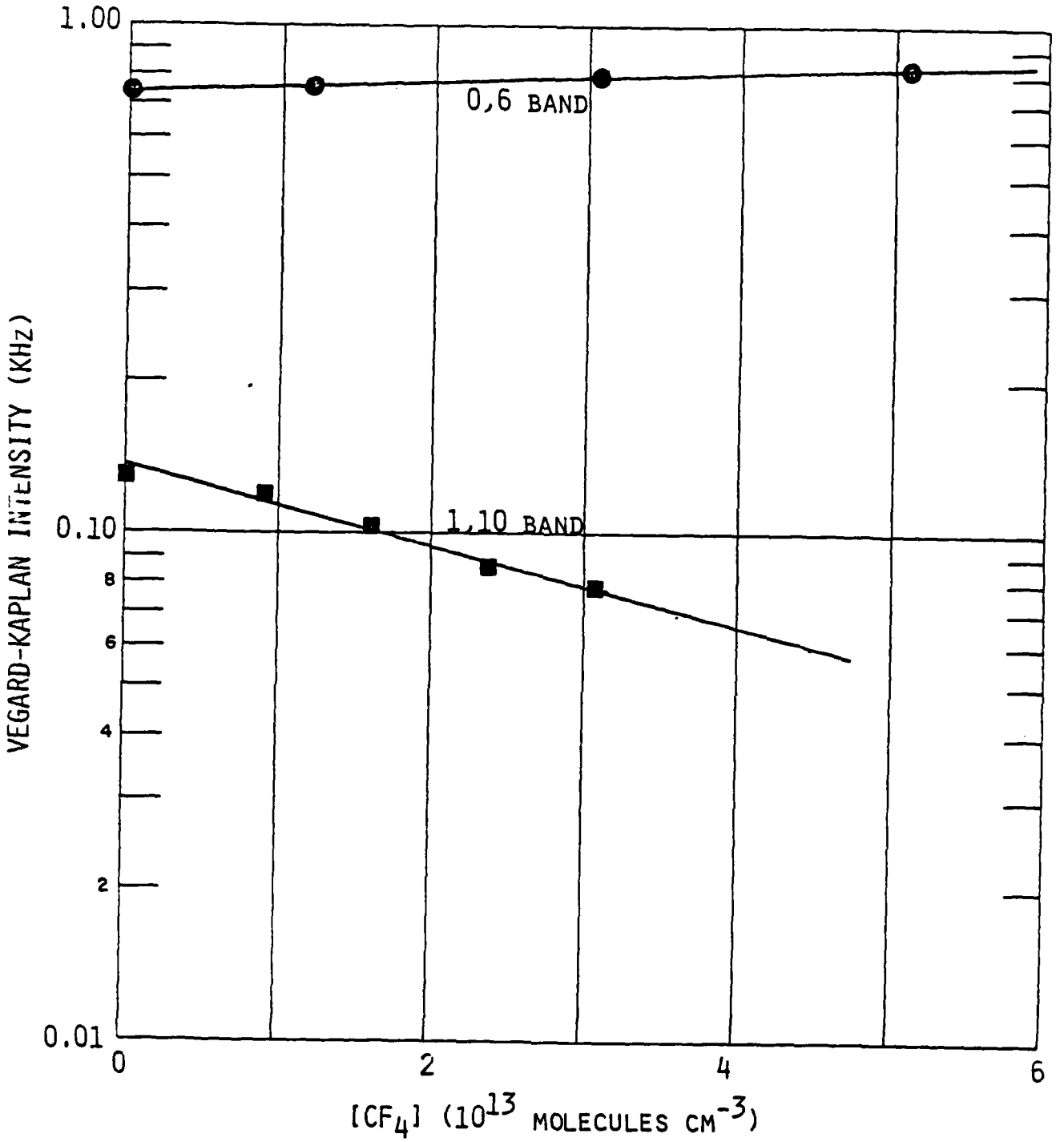

Fig. 19 Variation in Vegard-Kaplan intensity as a function of CF_4 number density. The data for the 0,6 band were taken at 7.1 torr while those for the 1,10 band were at 4.2 torr. The reaction times for both experiments were ≈ 90 ms.

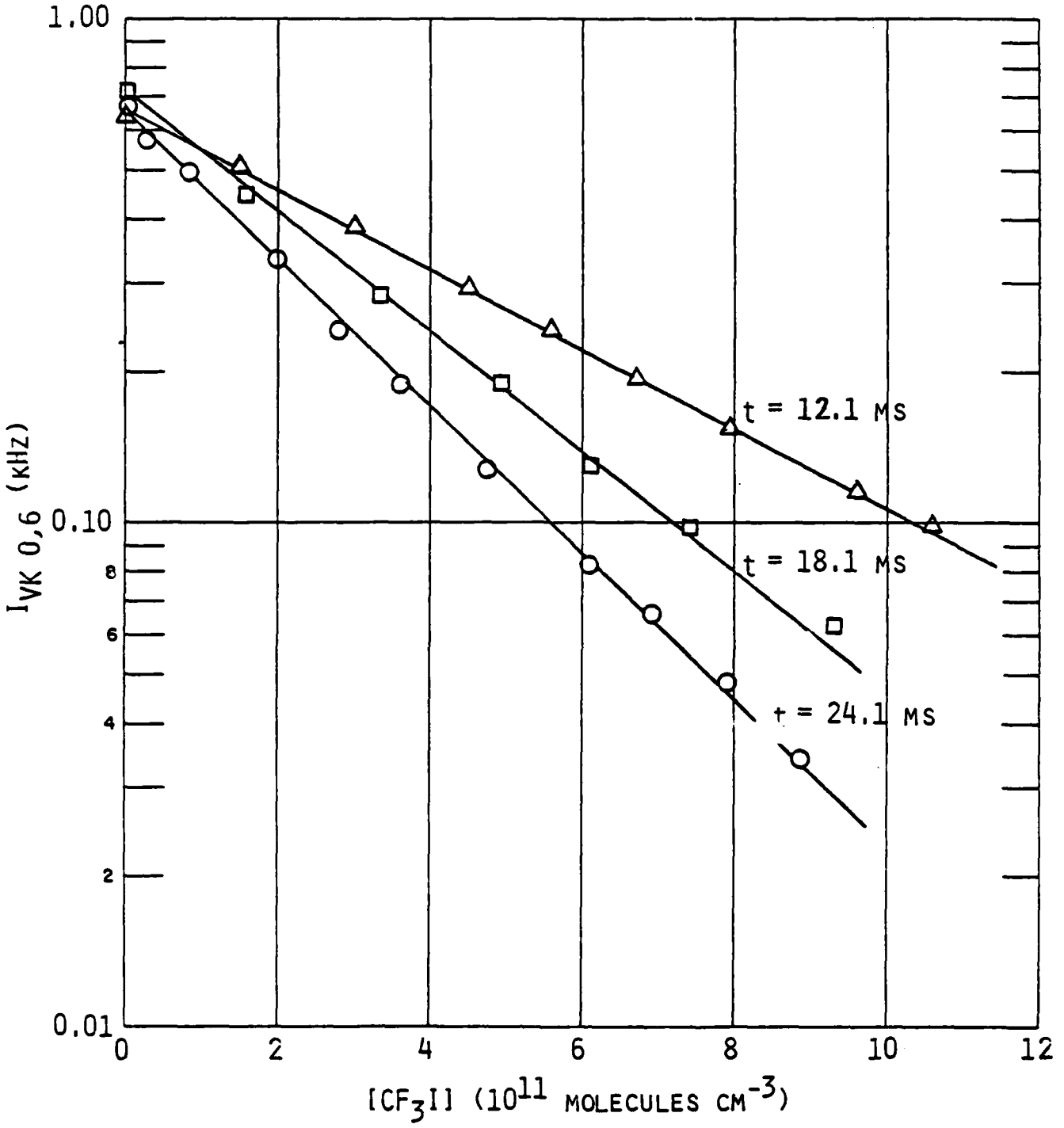

Fig. 20. The decay of the Vegard-Kaplan bands as a function of CF_3I number density for three different reaction times.

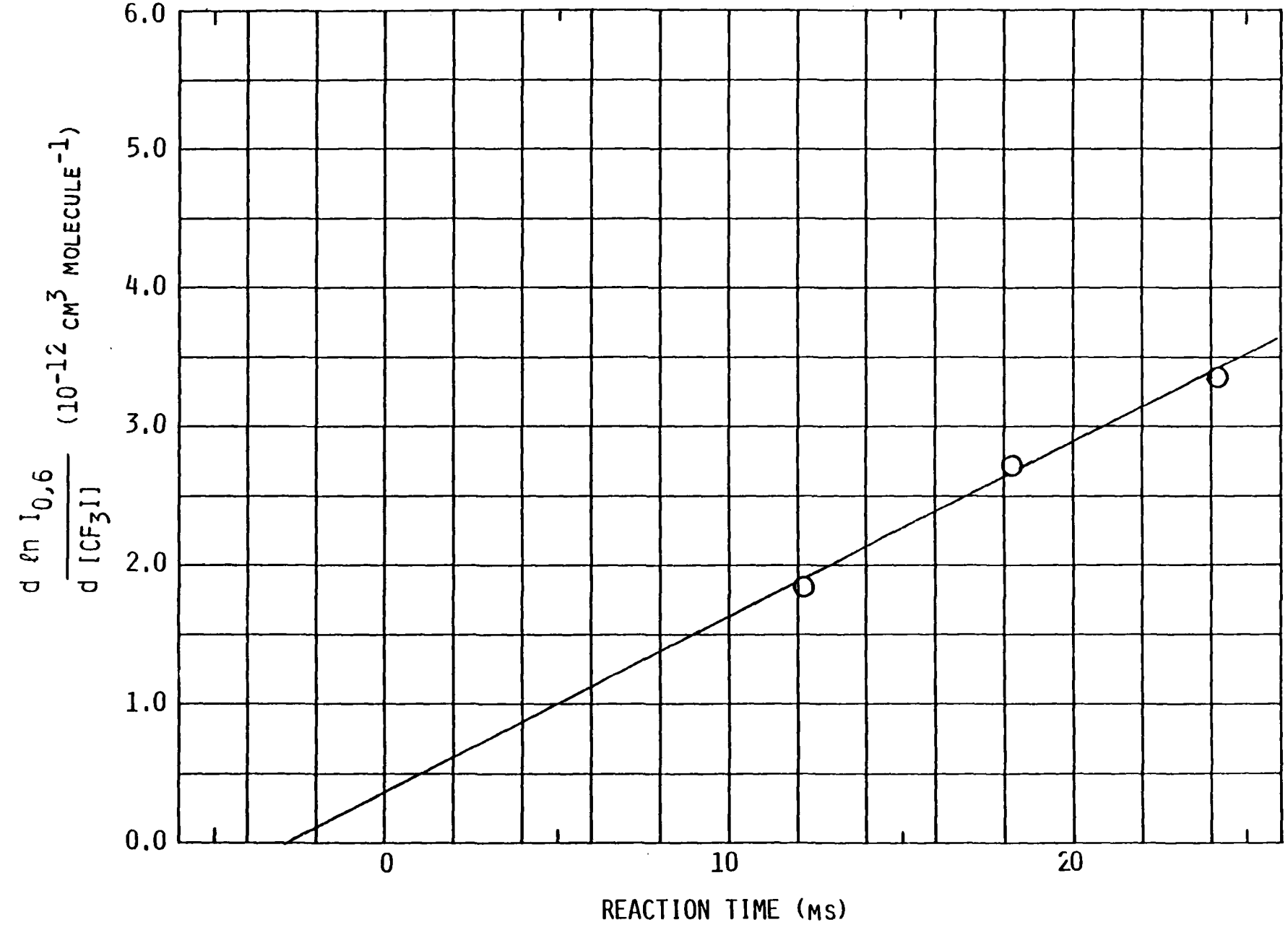

Fig. 21 Variation in Vegard-Kaplan decay rates with CF_3I as a function of reaction time.

2.1×10^{-10} cm^3 $molecule^{-1}$ s^{-1} for vibrational levels 0 and 1, respectively. Because the accuracy of these determinations is only about 15%, the difference in the coefficients for the two levels is not significant.

Figure 22 shows the decay of $N_2(A)$ as a function of IF number density. These data and some similar runs under different sets of conditions indicate that the rate coefficient for removal of $N_2(A)$ by IF is 1.9 and 2.0×10^{-10} cm^3 $molecule^{-1}$ s^{-1} for vibrational levels 0 and 1 of $N_2(A)$, respectively. Again the 5% difference between the coefficients for the two different levels is much smaller than the overall 15% uncertainty in the measurements.

Table 2 summarizes all quenching-rate coefficient determinations.

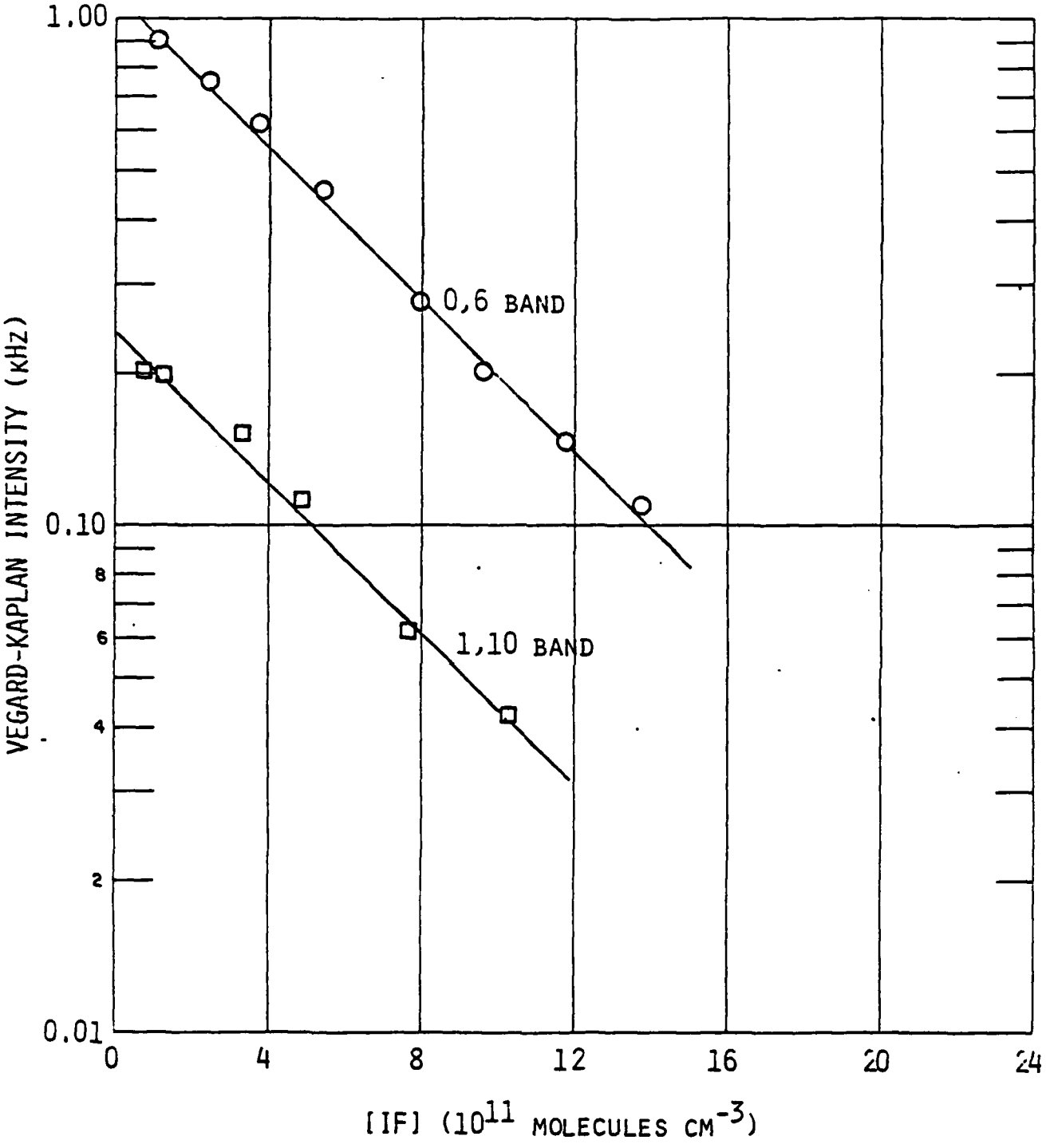

Fig. 22 Decay of the intensity of the Vegard-Kaplan bands as a function of IF number density.

TABLE 2

$N_2(A)$ RATE COEFFICIENT DETERMINATIONS

Reaction	Rate Coefficient (cm^3 $molecule^{-1}$ s^{-1})	
$N_2(A)_{v'=0,1} + IF \rightarrow IF(B\ ^3\Pi_{0^+}) + N_2(x)$	8.3×10^{-11}	
$N_2(A) + IF \rightarrow$ products	1.9×10^{-10}	$v'=0$
	2.0×10^{-10}	$v'=1$
$N_2(A) + CF_3I \rightarrow$ products	2.0×10^{-10}	$v'=0$
	2.1×10^{-10}	$v'=1$
$N_2(A)_{v'=1} + CF_4 \rightarrow N_2(A)_{v'=0} + CF_4$	3×10^{-13}	
$N_2(A)_{v'=0} + CF_4 \rightarrow N_2(x) + CF_4$	$< 10^{-14}$	
$N_2(A)_{v'=0,1} + NF_3 \rightarrow$ products	3×10^{-13}	$v'=0$
	9×10^{-13}	$v'=1$
$N_2(A)_{v'=1} + SF_6 \rightarrow N_2(A)_{v'=0} + SF_6$	1×10^{-14}	

4. IF(B) EXCITATION BY ACTIVE NITROGEN

4.1 Characterization of Active Nitrogen

We examined the spectrum from the products of an argon/nitrogen discharge under varying conditions of pressure, total flow rate, and nitrogen mole fraction. The $\Delta v = 2$, 3, 4, and 5 sequences of the N_2 First Positive ($B\ ^3\Pi_g - A\ ^3\Sigma_u^+$) bands comprise the visible portion of the spectrum (450 - 800 nm). The near ultraviolet (200-450 nm) spectrum consists of the $N(^2P-^4S)$ and the $N_2^+(B\ ^2\Sigma_u^+ - X\ ^2\Sigma_g^+)$ transitions as well as emission from several impurities, including $NO(A\ ^2\Sigma^+ - X\ ^2\Pi_{1/2,3/2})$ γ-bands and the $Na(4p^2P-3s^2S)$ transition. There are no N_2 Second Positive ($C\ ^3\Pi_u - B\ ^3\Pi_g$) bands present; however, there is a series of bands near 390 nm which we have not been able to identify but which we know are not the CN(B-X) bands commonly found in this region. The N_2 Lyman-Birge-Hopfield ($a\ ^1\Pi_g - X\ ^1\Sigma_g^+$) bands are prominent in the vacuum ultraviolet. All of these species, except $N(^2P-^4S)$, have radiative lifetimes which are much shorter than the 10 ms (nominal) transit time between the active nitrogen discharge and the detection region; hence they must be created by some energy transfer from some metastable carried downstream of the discharge. Probably the energy carrier that excites these nitrogen electronic states also plays some role in exciting the IF(B) state. Through these studies we hoped to gain some insight into the identity of the energy carrier.

Figure 23 shows the visible spectrum of active nitrogen recorded at 1 torr total pressure, 5000 μmole s^{-1} total flow rate, and 0.025 mole fraction of nitrogen in argon. The resolution of this spectrum is 1.67 nm. The open triangles in Fig. 24 summarize absolute populations of the $N_2(B)$ state vibrational levels 2-12 derived from the fitting of this spectrum. The populations range from approximately 10^7 molecules cm^{-3} in v=2 to 6×10^4 molecules cm^{-3} in v=12, decreasing smoothly over that range. The distribution is not Boltzmann. Increasing the pressure to 2 torr by throttling the pump at constant flow rate results in approximately a 50% decrease in the B-state vibrational populations. This distribution is shown as the filled triangles in Fig. 24.

At higher mole fractions of nitrogen ($X_{N_2} = 0.10$, 0.90), the relative B-state vibrational distribution does not change significantly; however, for

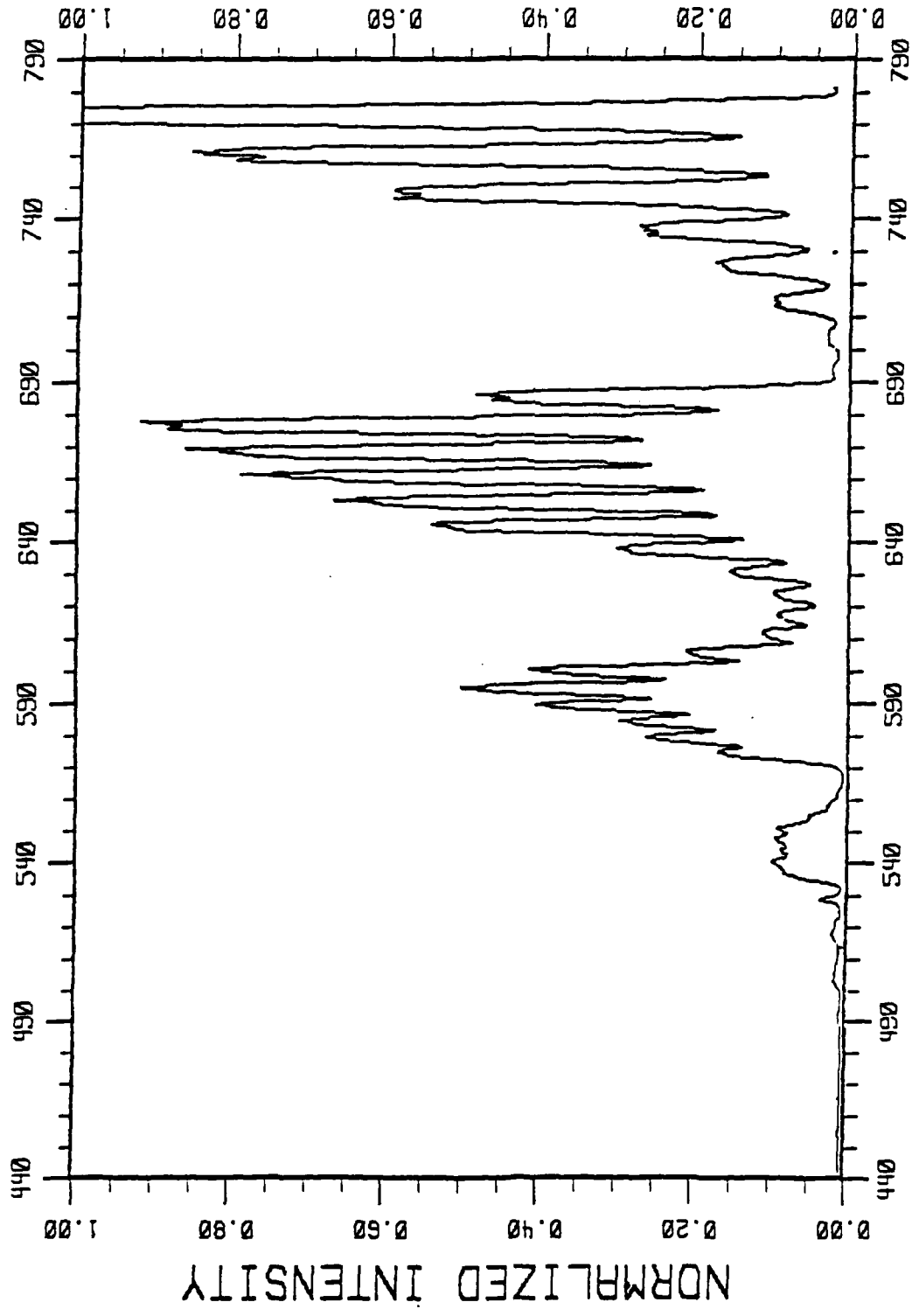

Fig. 23 $N_2(B-A)$ bands from active nitrogen for $X_{N_2} = 0.025$.

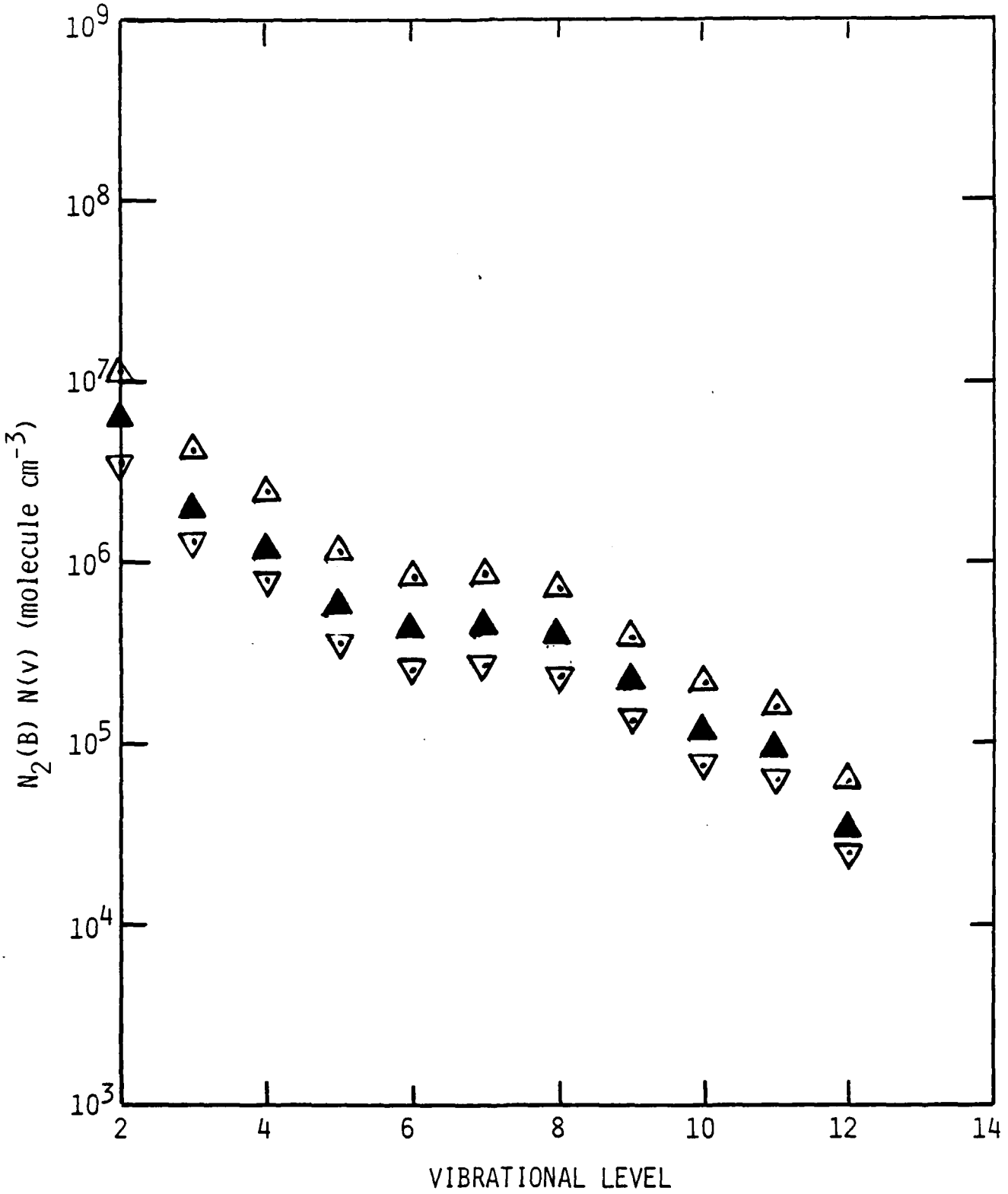

Fig. 24 $N_2(B)$ state vibrational populations at X_{N_2} = 0.025 for pressure and flow time of: △, 1 torr, 7.5 ms; ▲, 2 torr, 15 ms; ▽ 1 torr, 15 ms.

X_{N_2} = 0.90 the overall $N_2(B)$ number density is about half that for X_{N_2} = 0.025 and 0.10, which are about the same. This comparison may not be valid, since the discharge power had to be increased from 20W to 70W to sustain a discharge at a mole fraction of 0.90. At these higher mole fractions, increasing the pressure to 2 torr also does not change the vibrational distributions significantly but does decrease the absolute number densities to 36% and 13% of their original values for mole fractions of 0.10 and 0.90, respectively. This can be seen in Figs. 25 and 26 where the absolute populations are shown at 1 and 2 torr.

The total flow rate also has an effect on the B-state populations. Reducing the total flow rate to about 2500 μmole s^{-1} at 1 torr decreases the B-state populations to 31% and 17% of their original values for mole fractions of 0.025 and 0.10, respectively. The relative distributions remain unchanged from those at higher flow rates. This is also shown in Figs. 24 and 25.

Inserting a glass wool plug just downstream of the argon/nitrogen discharge removes all unstable constituents of active nitrogen except $N(^4S)$ from the gas stream (Ref. 59). Emission observed downstream from the plug must be due to species formed from N-atom recombination or the reaction of N-atoms with impurities. Spectra in the near-UV region show only NO γ-bands and no $N(^2P)$, while a spectrum in the visible region (Fig. 27) shows First Positive band emission characteristic of N-atom recombination on the A-state surface, followed by collisional coupling to the B-state manifold. The absolute vibrational populations, shown in Fig. 28, are bimodal with maxima at v=2 and v=11. The highest level populated is v=12, which lies just below the N_2 dissociation limit. The absolute N-atom number density in the viewing region was determined by doing an air afterglow calibration, as described earlier. The calibration showed the N-atom number density to be 3.6×10^{13} atoms cm^{-3}.

The results of these studies are summarized in Table 3 where the relative B-state populations, as well as the expected fluorescence quantum yields for First Positive emission, are given for each composition and pressure used. We have defined the fluorescence quantum yield as

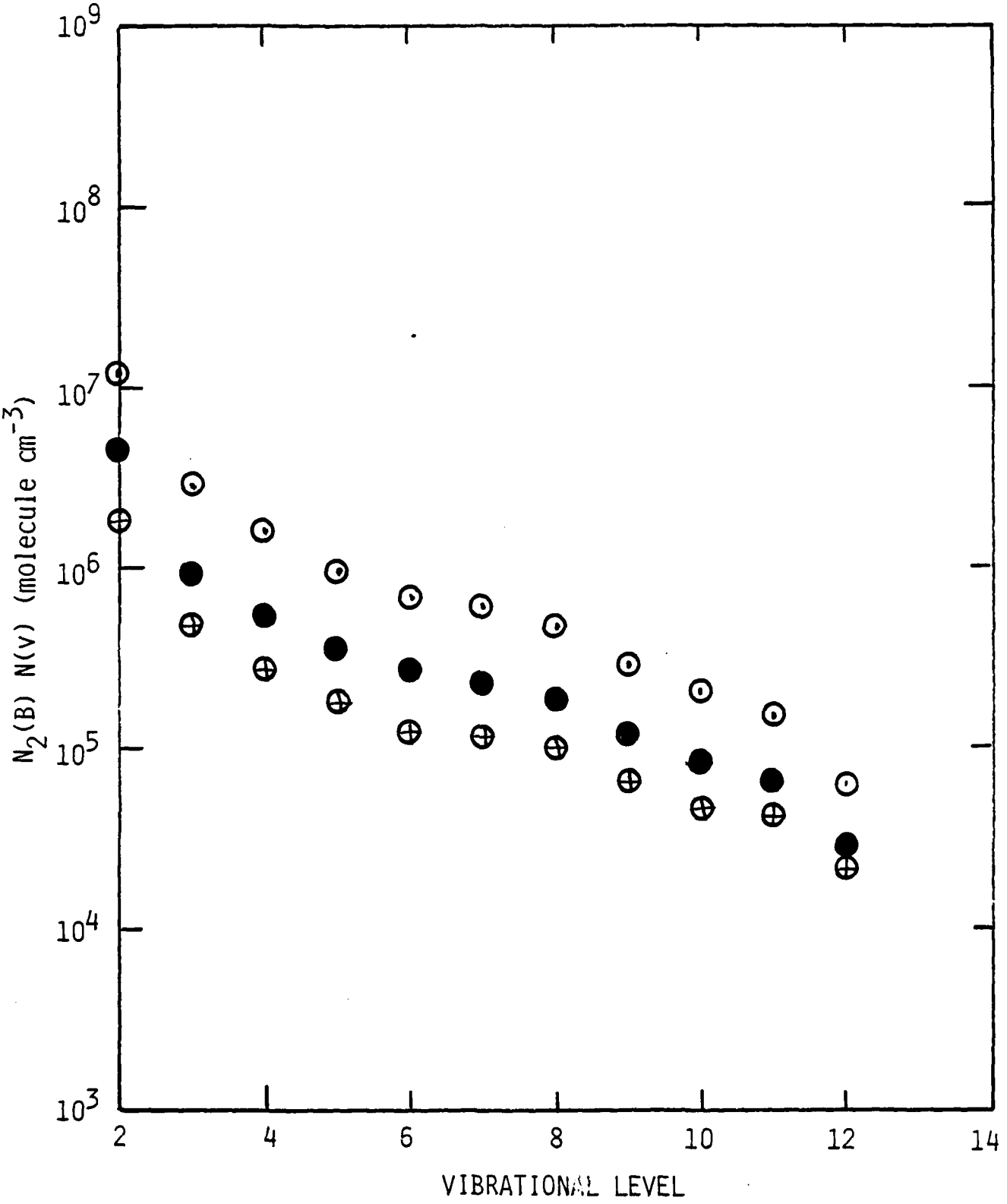

Fig. 25 $N_2(B)$ state vibrational populations at X_{N_2} = 0.10 for pressure and flow times of: ⊙, 1 torr, 6.9 ms; ●, 2 torr, 13.7 ms; ⊕, 1 torr, 13.6 ms.

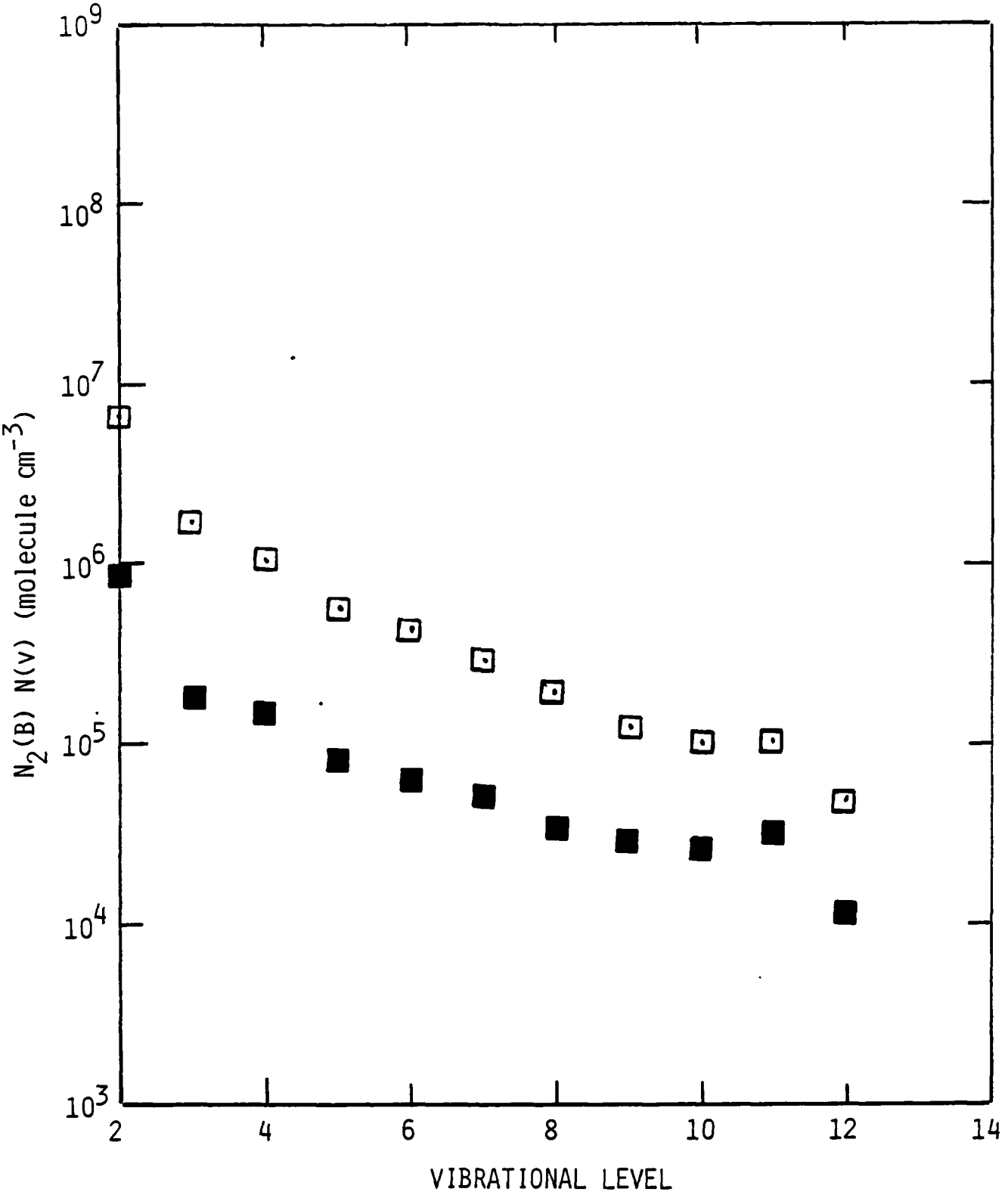

Fig. 26 $N_2(B)$ state vibrational populations at X_{N_2} = 0.90 for pressure and flow times of: ⊡, 1 torr, 8.8 ms; ■, 2 torr, 17.6 ms.

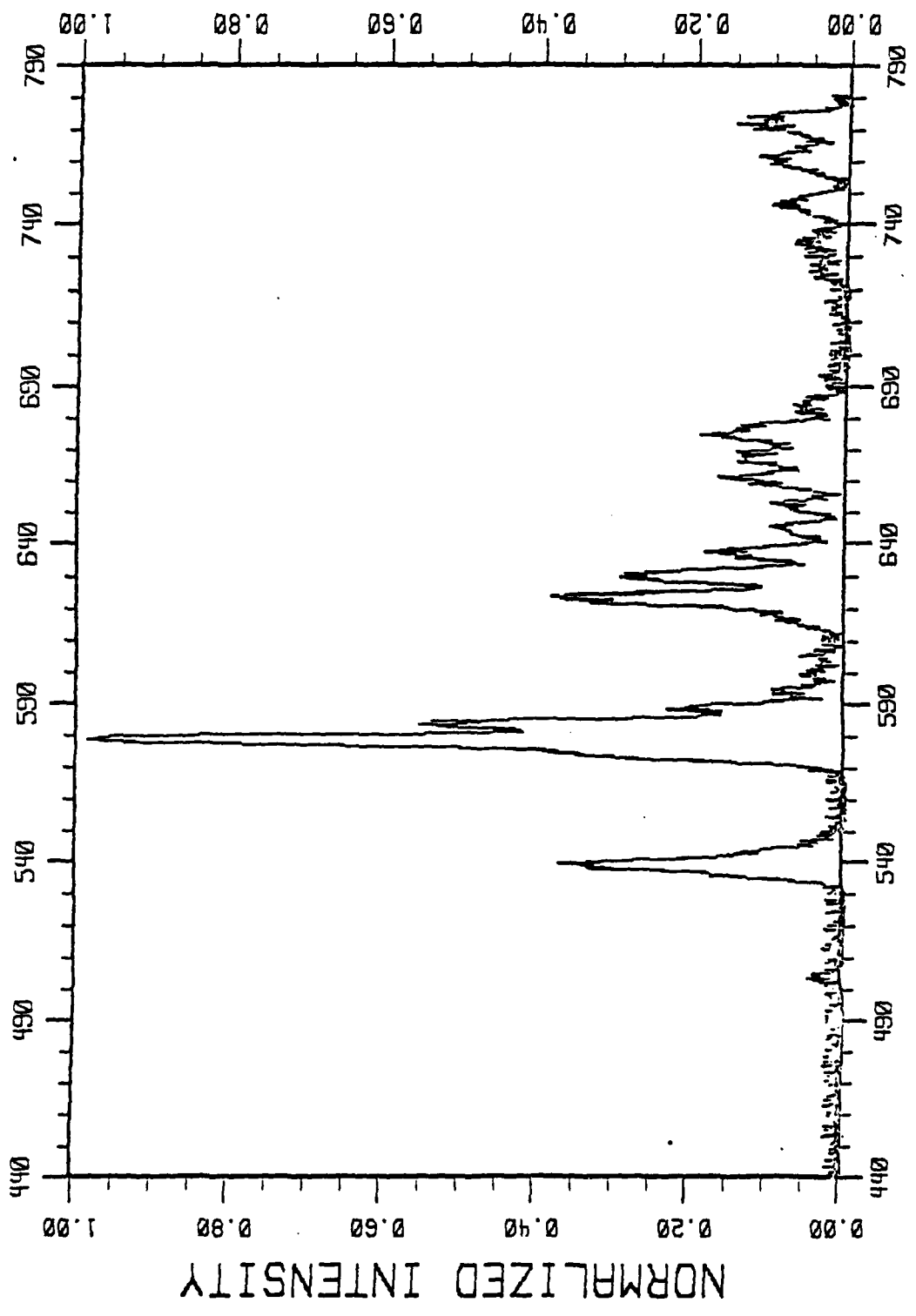

Fig.27. N_2(B-A) bands from active nitrogen with a glass wool plug downstream of the discharge.

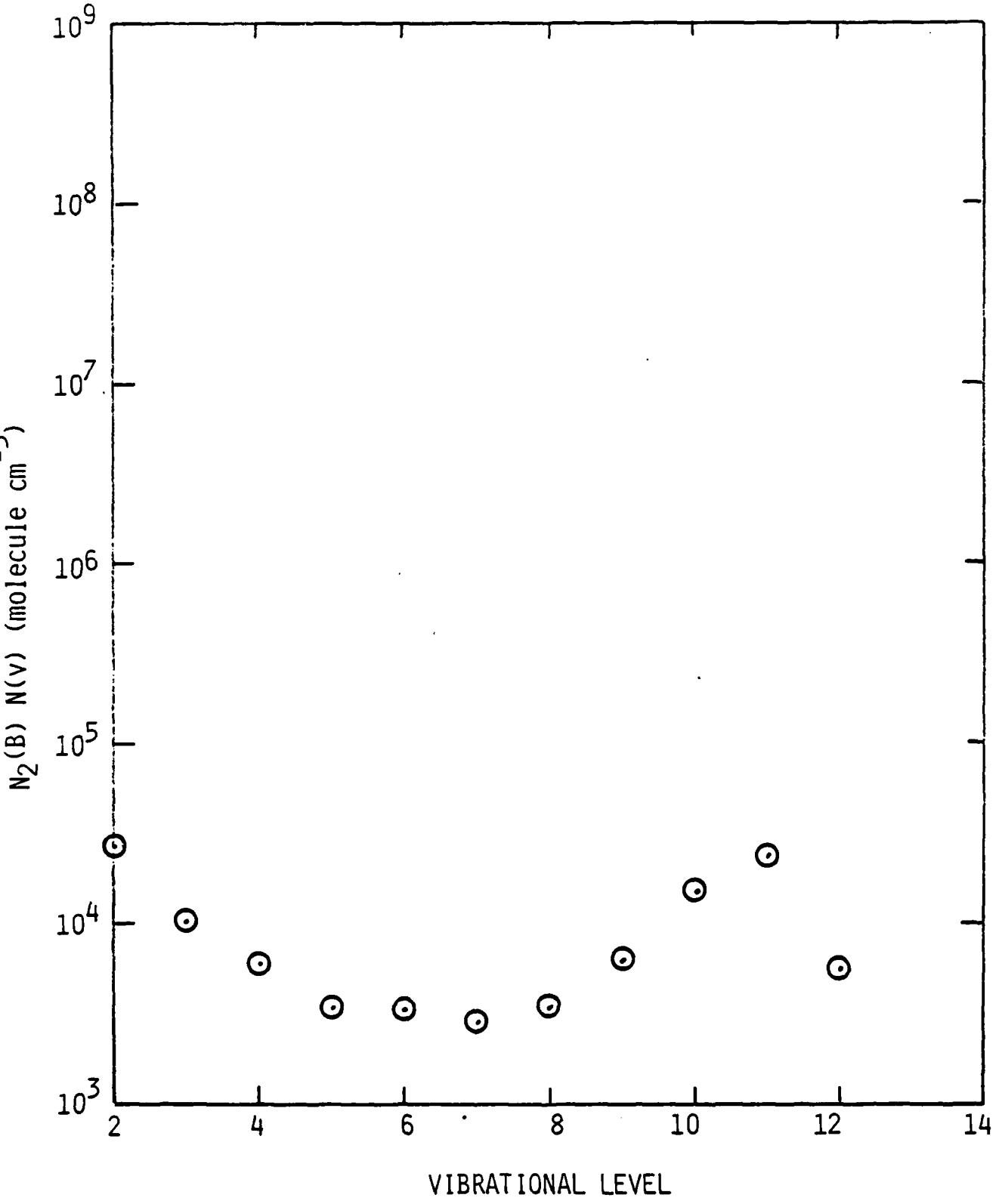

Fig. 28. $N_2(B)$ state vibrational populations determined in glass wool plug experiments.

TABLE 3

ACTIVE NITROGEN EXCITATION RESULTS

Mole Fraction Nitrogen	Pressure (torr)	τ_{flow} (ms)	ϕ_{fluor}	Relative $N_2(B)$	Relative $N_2(B)/\phi_{fluor}$	R_{ex}(IF) photon cm^{-3} s^{-1}/IF molecule
0.025	1	7.5	0.71	1.0	1.0	0.86
0.025	1	15	0.71	0.31	0.31	0.33
0.025	2	15	0.55	0.52	0.67	0.47
0.10	1	6.9	0.57	0.87	1.09	0.79
0.10	1	13.6	0.57	0.15	0.19	0.39
0.10	2	13.7	0.40	0.31	0.55	0.47
0.90	1	8.8	0.18	0.48	1.90	0.51
0.90	2	17.6	0.10	0.06	0.43	0.19
0.10*	1	15	0.57	0.005	0.006	0.05

*with glass wool plug

$$\phi_{fluor} = A + \frac{A}{k_{Ar}[Ar] + k_{N_2}[N_2]} \quad (39)$$

where the quenching rate coefficients, k_{Ar} = 1.6 x 10^{-12} cm^3 $molecule^{-1}$ s^{-1} and k_{N_2} = 2.7 x 10^{-11} cm^3 $molecule^{-1}$ s^{-1}, are taken from Young, Black, and Slanger (Ref. 60). The average transition probability for the bands, A, is taken to be 1.8 x 10^5 s^{-1} from Lofthus and Krupenie (Ref. 61). Because the radiative lifetime is short, $N_2(B)$ is in steady state in the viewing region. As can be seen from the fluorescence quantum yields, if the populations were adjusted to correct for quenching, it would not fully account for the differences in band intensity observed in varying pressure and would have no bearing on the changes with flow rate. Changes in the source mechanism must be occurring to produce these effects. The sharp reductions in B-state populations when the flow rate was reduced by 50% at constant pressure may give a measure of the lifetime of the energy carrier in our system; however, one must be careful in interpreting these results since the excited species spend approximately 50% more time in the discharge region and their production may be altered appreciably. Further experiments are required in which the gas flow velocity may be controlled independently of the flow in the discharge.

4.2 Excitation of IF(B)

When we added IF to active nitrogen, we observed IF(B-X) emission as well as emission from N_2(B-A) and CN(A $^2\Pi_{3/2,1/2}$ - X $^2\Sigma^+$). No IF(D'-A') emission was ever observed. The CN(A) state emission was also seen when only CF_3I was added to active nitrogen. It is probably formed from the reaction of some component of active N_2 with CF_3. Figure 29 shows the spectrum when IF is added to active nitrogen under the same conditions as Fig. 23. Adding IF does not change the $N_2(B)$ state vibrational distribution but does slightly decrease the overall population. The presence of CN(A-X) bands makes it very difficult to fit the entire spectrum accurately due to the large number of basis functions required and the great degree of overlap between basis functions. We were able to fit the IF(B) populations to within about 15% accuracy by fitting only over the region from 440-565 nm, where we could ignore CN(A) state emission. The overlapping $N_2(B)$ emission was fit by assuming the same relative vibrational level distribution as

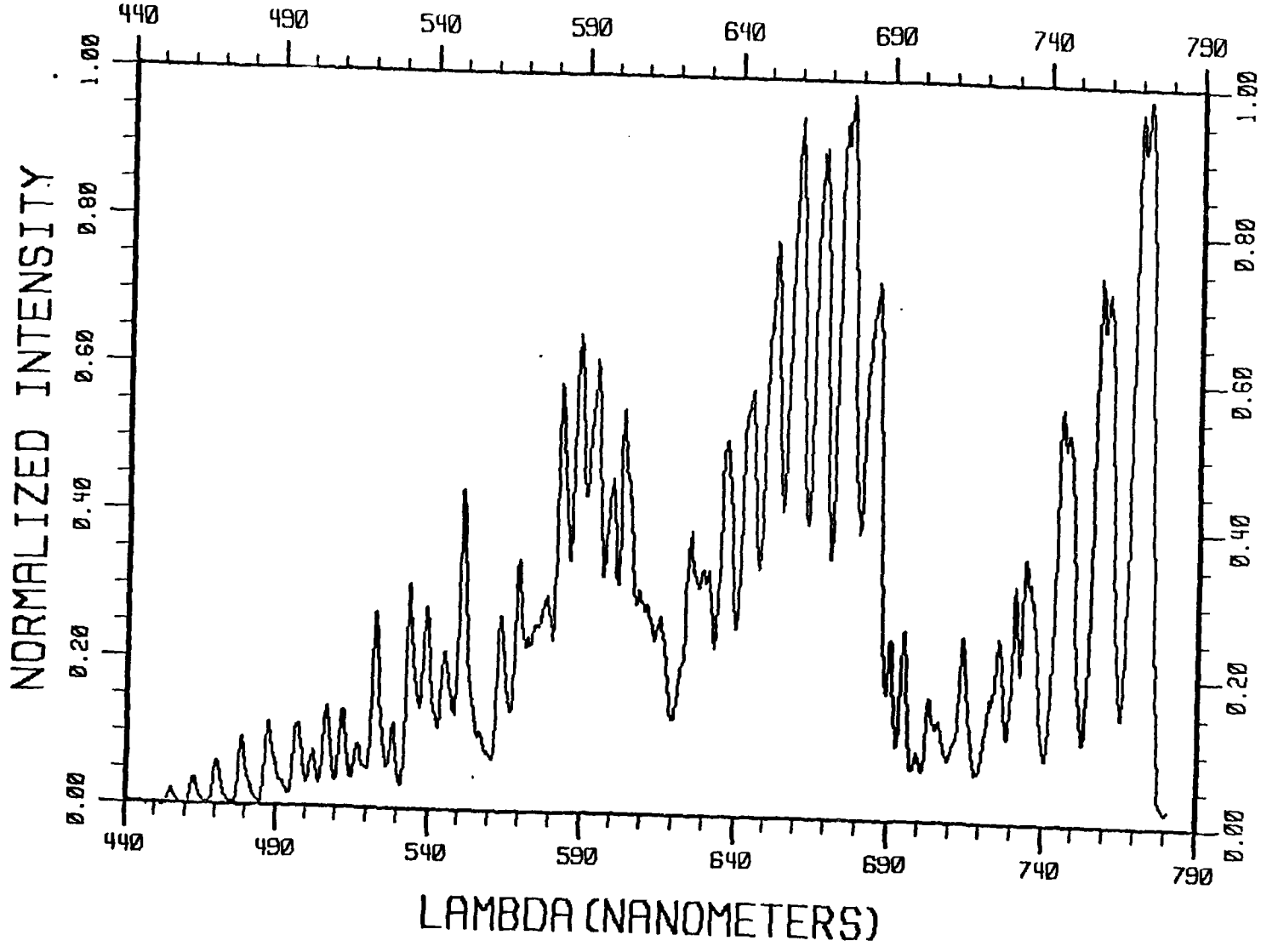

Fig. 29. IF excitation spectrum under conditions of Fig. 23.

obtained under identical conditions in the absence of IF, then scaling the First Positive system intensities to reproduce the observed emission intensity in the presence of IF. This assumption neglects $N_2(B)$ relaxation in the presence of IF.

IF(B) excitation rates and spectra were recorded at an instrumental solution of 1.67 nm under each of the conditions described above for active nitrogen. The relative B-state populations were independent of composition and flow rate, to within our fitting accuracy, but showed some evidence of relaxation at the higher pressure. The relative populations, averaged over composition and flow rate, are shown in Fig. 30 for pressures of 1 and 2 torr. The B-state distribution is significantly more relaxed in active nitrogen than for corresponding excitation by $N_2(A)$ under similar conditions of pressure and composition. This implies that there is a different excitation mechanism in this system.

Excitation spectra recorded when the glass wool plug was inserted in the active nitrogen flow were very weak. The CN(A-X) bands were comparable in intensity to the IF(B) emission. The $N_2(B)$ state distribution also became more relaxed when IF was added. These effects made it impossible to fit the spectrum. When comparable amounts of CF_3I were added, the $N_2(B)$ state distribution did not relax as it had with IF.

IF(B) state excitation rates were measured by recording the change in the emission intensity of a B-X vibronic band with added IF. This was then converted to a total B-state volume emission rate per IF molecule using the expression

$$k_F[N_2^*] = \frac{d[I^{pk}(v'v")]}{d[IF]} \cdot \frac{(A/P)}{B(v',v") \cdot f(v')} \cdot \frac{\beta}{R(\lambda)} = R_{ex} \qquad (40)$$

where (A/P) is the integrated-to-peak intensity ratio for the band observed, B(v',v") is the fluorescence branching ratio from the B-state level observed into that transition, f(v') is the fraction of the total population found in level v' from spectral fitting, $R(\lambda)$ is the relative response of the detection system at the observation wavelength, β is the absolute detector response calibration coefficient in photons cm^{-3} s^{-1} kHz^{-1} at the reference wavelength of

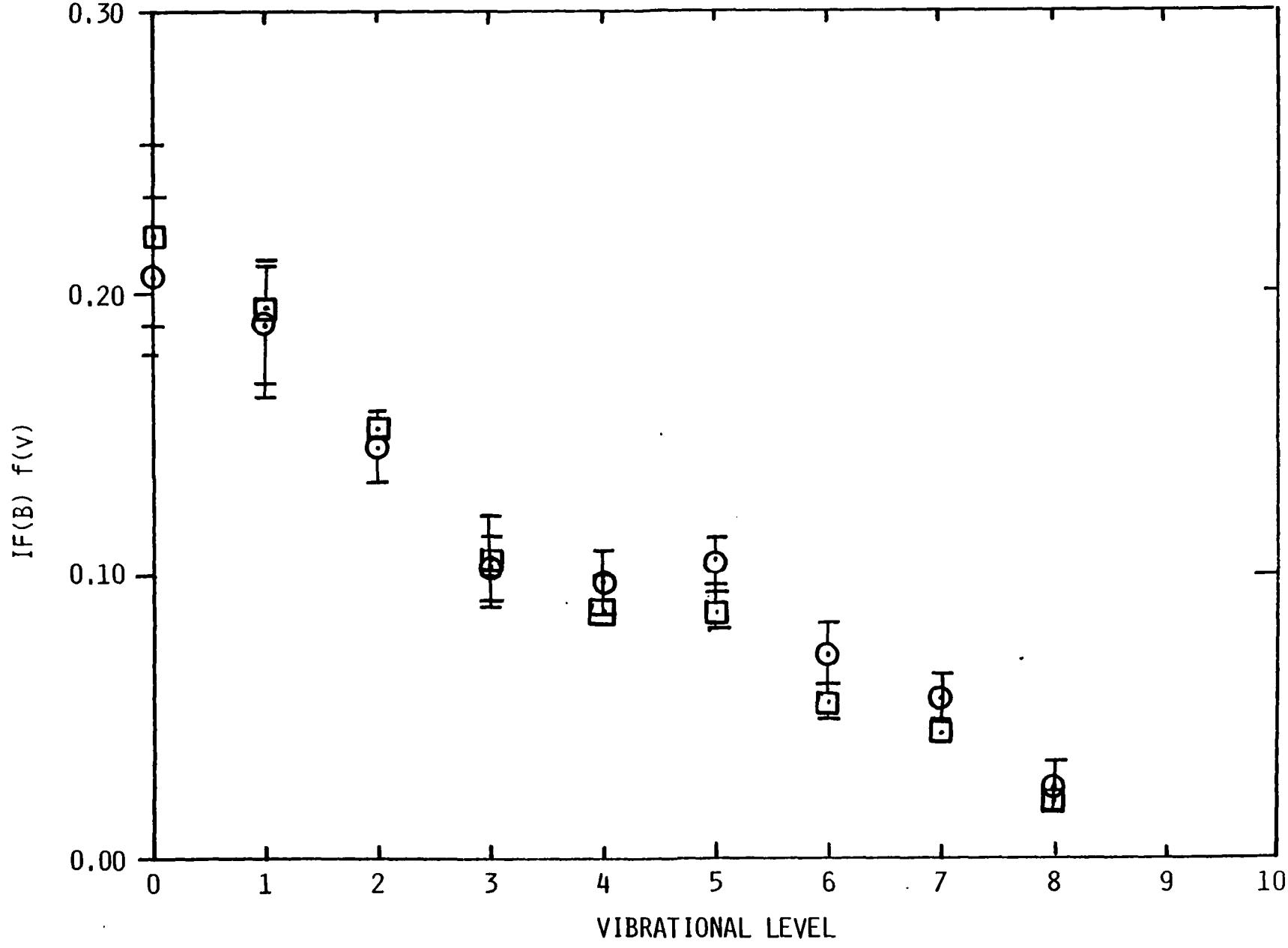

Fig.30. IF(B) average vibrational populations at 1 torr, ⊙, and at 2 torr, ⊡.

580 nm (i.e. $\beta = \frac{k_{\lambda c} \Delta_{\lambda c} R_{\lambda c}}{\kappa_{\lambda c}}$ from Eq. (20)), and $d[I^{pk}(v',v")]/d[IF]$ is the rate of change of the peak band intensity with added IF. Excitation rates could only be measured using the 6-0 and 5-0 $IF(B-X)_{vibrational}$ transitions because all others were overlapped by either other B-X transitions or by First Positive transitions. Values of R_{ex} determined using these bands usually agreed to within 7%. We estimate the overall uncertainty in the measurements to be about 35%.

A typical variation in IF(B) emission intensity for the 6-0 and 5-0 bands is shown in Fig. 31. In all of our experiments these plots are usually linear in IF number density up to about 1.3×10^{12} molecule cm^{-3} and then roll off due to depletion of F-atoms in the IF production step. The excitation rates measured for these various forms of active nitrogen are also given in Table 3. The rates vary from 0.13 to 0.86 photons cm^{-3} s^{-1}/IF molecule. These data show that the B-state excitation rates qualitatively follow the $N_2(B)$ populations but do not have any simple quantitative relationship. Electronic quenching of IF(B) at these pressures and compositions is negligible [$k_Q(Ar)$ and $k_Q(N_2) < 1 \times 10^{-14}$ cm^3 $molecule^{-1}$ s^{-1} (Ref. 49)], and no corrections to the excitation rates are necessary. Excitation rates measured using the glass wool plug are difficult to interpret since there are no relative populations available for these conditions. We have estimated a relative population for v=6 to be about 0.06, similar to what is observed under other conditions, and derive an excitation rate of 0.05 photons cm^{-3} s^{-1}/IF molecule with about a 50% level of uncertainty.

Our excitation rates are of the order of unity. If the excitation rate coefficient for the active species is gas kinetic ($\sim 10^{-10}$ cm^3 $molecule^{-1}$ s^{-1}) then the concentration of the exciting species must be $> 10^{10}$ molecule cm^{-3}. Table 4 lists estimates, based on photon-emission-rate measurements and other data, of the likely excited state species concentrations in active nitrogen for two different compositions at 1 torr. These estimates show that only $N(^2P)$, $N(^2D)$, and $N_2(v)$ exist in high enough concentrations to excite IF at the rates observed.

$N(^2D)$ is an unlikely precursor because its number density decreases dramatically with increases in nitrogen mole fraction. The IF excitation rates, on the other hand decreased only slightly.

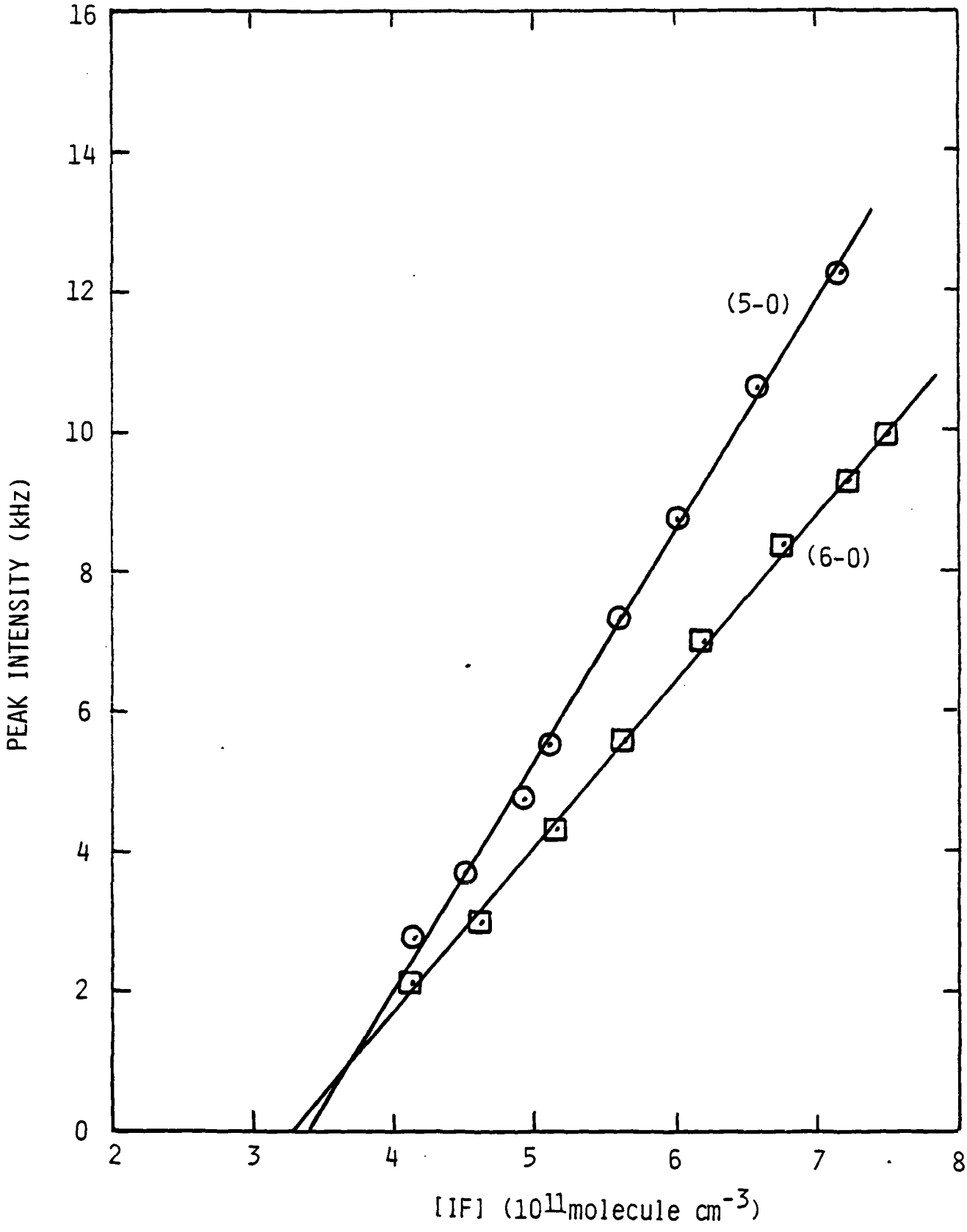

Fig. 31 Variation in IF(B) (6-0) band emission intensity with added IF at 1 torr and X_{N_2} = 0.025.

TABLE 4

ACTIVE NITROGEN CONSTITUENTS

Species	Band	Concentration (molecule cm^{-3}) 1% N_2	80% N_2	Comments
$N(^2D)$		1×10^{12}	1×10^{10}	Estimate: not likely precursor
$N(^2P)$	$(^2P-^4S)$	4×10^{10}	1×10^{10}	Further investigation; not likely precursor
$N_2(a\ ^1\Pi_g)$	(LBH)	5×10^6	none ($<10^6$)	Low conc.
$N_2(B\ ^3\Pi_g)$	(1^+)	8×10^6	6×10^6	Low conc.
$N_2(A\ ^3\Sigma_u^+)$	(V-K)	1×10^9	1×10^9	Low conc.
$N_2(v)$		2×10^{12}	2×10^{14}	Modeling of discharges; likely source

While none of our experimental observations can definitively rule out $N(^2P)$ as the percursor for IF(B) excitation, we think a more likely species is $N_2(X, v>>0)$. Extremely high levels of vibrational excitation can survive long into the afterglow because they will not be relaxed efficiently by N_2 or Ar. We feel that these levels are responsible for the excitation of N_2 electronic states in the afterglow as discussed in the previous subsection. The $N_2(B)$ emission intensity, when corrected for fluorescence quenching, should vary relative to the number density of the precursor state responsible for its excitation. Figure 32 shows that our measured IF excitation rates vary linearly with the corrected $N_2(B)$ fluorescence intensity, thus indicating that both species are likely to be excited by the same precursor. We used only the data for $X_{N_2} = 0.025$ and 0.10 in making this correlation, because those runs, unlike the $X_{N_2} = 0.90$ data, shared common discharge conditions. The precursor for the $N_2(B)$ emission cannot be (N^2P) because that state lacks sufficient energy to excite $N_2(B)$. Thus $N_2(X, v>>0)$, because it is the only remaining long-lived state in the reactor, appears to be the precursor state for IF(B) excitation. This excitation could be either direct, or indirect through an intermediary state of nitrogen which is excited from the $N_2(X, v>>0)$ precursor. At present we cannot probe the concentration of $N_2(X, v>>0)$ in our reactor, and can only infer its role as the precursor state.

Inserting the glass wool plug into the active nitrogen stream eliminates vibrationally excited N_2 and electronically excited species of N_2 and N-atoms, leaving only $N(^4S)$. The small residual IF excitation in this case is consistent with expected N_2^* number densities created by N-atom recombination.

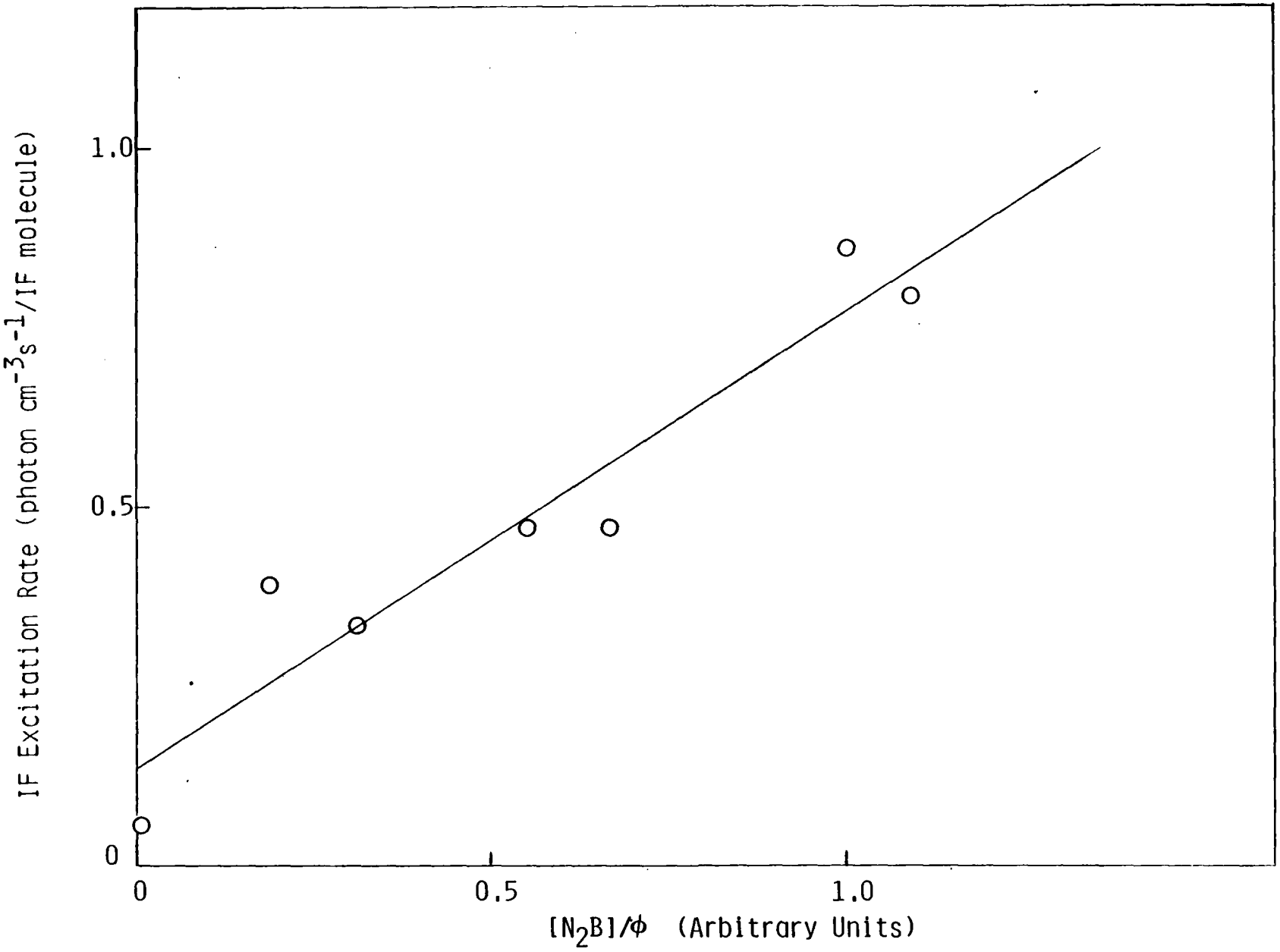

Fig. 32. Variation in IF(B) excitation rate with corrected N_2(B) fluorescence intensity.

5. PHOTON YIELDS

Given the energy-transfer reaction $N_2^* + Q \rightarrow Q^* + N_2$, we can compute the photon yield from Q^* as a function of the amount of Q in the system by studying the elementary kinetics of the energy-transfer reaction.

The photon yield, y, is defined as

$$y = \frac{\text{\# photons emitted by } Q^* \text{ per second}}{\text{\# quenchers, } Q, \text{ injected per second}} \tag{41}$$

This quantity is system specific, being a function both of geometry and initial number density of the donor species. Our particular system is a cylindrical flow reactor. In the subsequent discussion we assume only first order losses for the donor species, no electronic quenching of the fluorescing species, and that the fluorescing species is stable (i.e. it does not dissociate or disproportionate in collisions with the reactor walls or with other chemical species in the reactor).

The steady-state expression for the volumetric photon-emission rate in the reactor is

$$I = k_{ex}\,[Q][N_2^*] \tag{42}$$

where I has units of photons $cm^{-3}s^{-1}$, k_{ex} is the rate coefficient for excitation of Q^* in collisions with N_2^*, and N_2^* represents either active nitrogen or $N_2(A\ ^3\Sigma_u^+)$.

The yield is then the product of the volumetric photon-emission rate and the total reactor volume divided by the rate of injection of quenchers:

$$y = \frac{I\ V}{f_Q N_o} \tag{43}$$

where f_Q is the molar flow rate of quenchers and N_o is Avogadro's number. Combining the preceding two equations gives

$$y = \frac{k_{ex}[Q][N_2^*]\ V}{f_Q N_o} \tag{44}$$

For first-order losses of N_2^* we have

$$[N_2^*] = [N_2^*]^o \, e^{-K_\ell \, z/\bar{v}} \tag{45}$$

where $[N_2^*]^o$ is the initial number density of N_2^* at the injector, z is the distance down the flow reactor from the injector, $\bar{v}$ is the bulk flow velocity in the reactor and, K_ℓ is the first-order loss rate which will include quenching both by species in the reactor and by wall collisions.

For a cylindrical flow reactor with radius a, we have

$$y = \frac{k_{ex}[Q]\,[N_2^*]^o}{f_Q N_o} \int_0^\infty e^{-K_\ell \, z/\bar{v}} \, \pi a^2 dz \tag{46}$$

$$= \frac{\pi a^2 k_{ex}[Q][N_2^*]^o \, \bar{v}}{f_Q N_o K_\ell} \quad . \tag{47}$$

This expression can be simplified by noting that

$$[Q] = \frac{f_Q}{f_{Tot}} \, \frac{PN_o}{RT} \tag{48}$$

and

$$\bar{v} = \frac{f_{Tot} RT}{P \, \pi a^2} \tag{49}$$

where f_{Tot} is the total molar flow rate in the reactor and P,T and R are pressure, temperature and gas constant, respectively.

Thus,

$$y = \frac{k_{ex}[N_2^*]^o}{K_\ell} \quad . \tag{50}$$

For the case of IF excitation by $N_2(A)$, the loss rate is the sum of a diffusive loss term (wall quenching), k_{Diff}, and the total quenching rate of $N_2(A)$ by IF, $k_{TOT}[IF]$. The k_{Diff} is well established by the diffusion coefficient of $N_2(A)$ in argon (Ref. 62-64). Since we have measured k_{ex} and k_{TOT}, we can calculate

yields as a function of pressure, the initial number of density of the $N_2(A)$, the quencher number density, and the total gas flow rate in the reactor.

Figure 33 shows a plot of photon yields from the $N_2(A)$ plus IF interaction for several different sets of conditions. The major influences to the photon-yield calculation are the initial $N_2(A)$ number density, and the amount of IF injected into the reactor. Given additional $N_2(A)$ molecules, more IF photons can be excited. Once the IF has quenched all the vailable $N_2(A)$, however, adding more IF cannot increase the total number of photons emitted, but only can reduce the photon yield. We think a more useful figure to apply to this system is to calculate the maximum number of IF photons emitted per $N_2(A)$ molecule. Our results show that, in the absence of any other $N_2(A)$ loss processes, one can expect 4 IF photons for every 10 $N_2(A)$ molecules initially in the reactor.

For the excitation of IF by active nitrogen, we do not know the initial number density of the precursor responsible for IF excitation. We can, however, determine the product k_{ex} $[N_2^*]$. Measurements of the log of this product as a function of flow time down the reactor will give both K_ℓ and $k_{ex}[N_2^*]^o$. Thus we can again determine yields for this excitation reaction. As in the case of $N_2(A)$ yields, the active nitrogen yields we calculate are system specific and therefore are difficult to interpret.

Two sets of data for 2% nitrogen at a total pressure of 1 torr gave excitation rates for IF by active nitrogen of 0.86 and 0.33 s^{-1} for flow times from the discharge to the observation region of 7.5 and 14.9 ms, respectively. Assuming that the initial N_2^* number density exiting the discharge is the same for both sets of data, and that losses are first order, we compute a loss rate for the N_2^* of 129 s^{-1}. Extrapolating back to the discharge gives an initial IF excitation rate of 2.3 s^{-1} which results in a photon yield under those conditions of 0.018. This is an order of magnitude larger than the $N_2(A)$ + IF photon yield in our reactor under similar conditions of pressure, total flow rate, and nitrogen mole fraction. Thus discharge-excited N_2 in our reactor contained a greater concentration of precursors capable of exciting IF molecules to the B-state.

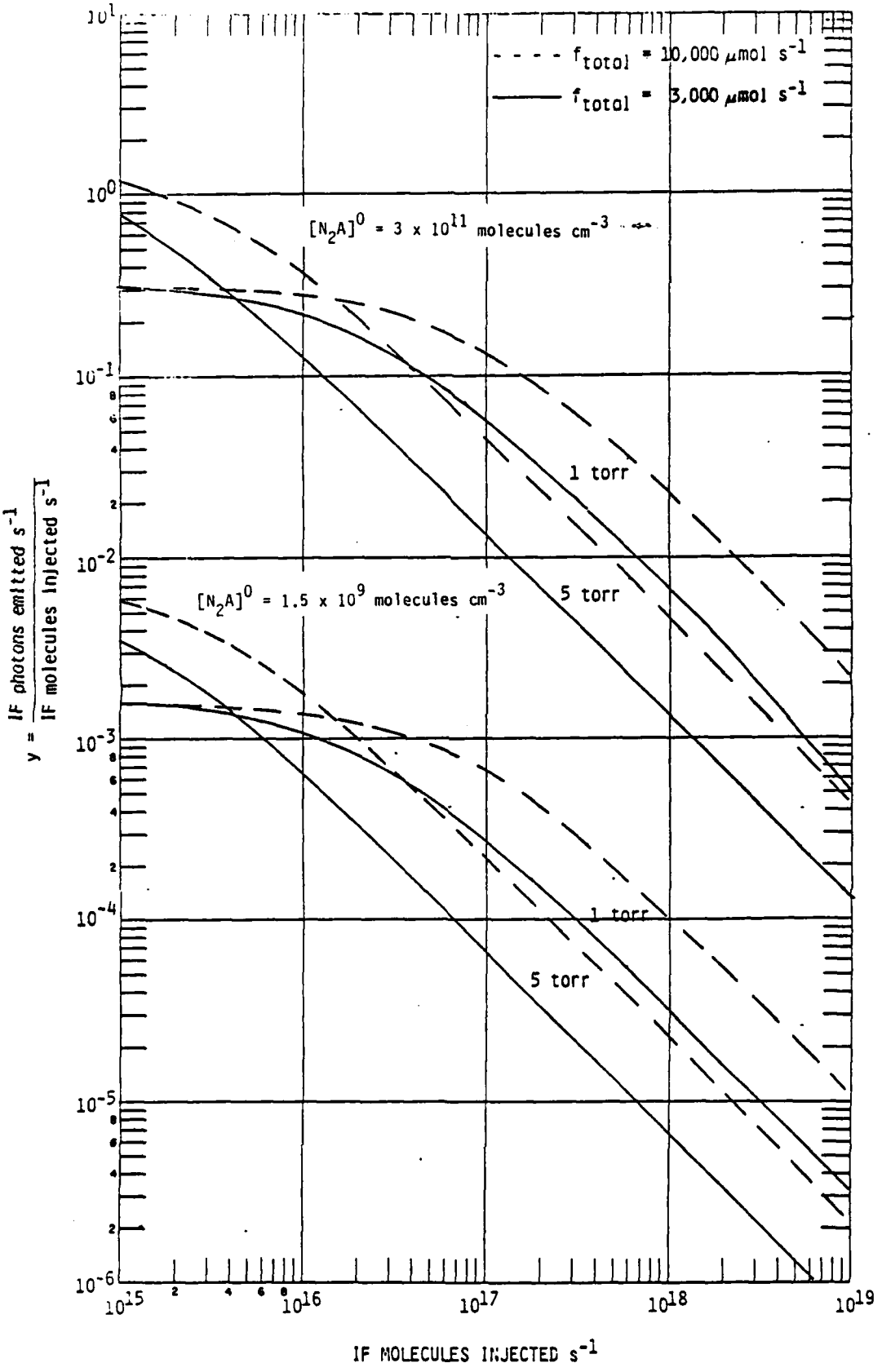

Fig. 33. Photon yields from $N_2(A)$ + IF reaction.

REFERENCES

1. Eden, J. G., Dlabal, M. L. and Hutchinson, S. B., "The Interhalogens IF and ICl as Visible Oscillators or Amplifiers," IEEE Journal of Quantum Electronics QE-17, 1085 (1981).

2. Clyne, M. A. A. and McDermid, I. S., "Quantum-resolved Dynamics of Excited States. Part 1.-Predissociation in the $B^3\Pi(0^+)$ State of BrF," J.C.S. Faraday II 74, 644 (1978).

3. Clyne, M. A. A. and McDermid, I. S., "Quantum-resolved Dynamics of Excited States. Part 2.-Stable Levels of the $B^3\Pi(0^+)$ State of BrF," J.C.S. Faraday II 74, 664 (1978).

4. Clyne, M. A. A. and McDermid, I. S., "Quantum-resolved Dynamics of Excited States. Part 3.-Collision-Free Lifetimes of BrF(B)," J.C.S. Faraday II 74, 1376 (1978).

5. Clyne, M. A. A. and McDermid, I. S., "Quantum-resolved Dynamics of Excited States. Part 4.-Radiative and Predissociative Lifetimes of IF $B^3\Pi(0^+)$," J.C.S. Faraday II 9, 1644 (1978).

6. Clyne, M. A. A., Heaven, M. C. and Martinez, E., "Quantum-resolved Dynamics of Excited States. Part 5.-The Long-lived $A^3\Pi(1_u)$ State of Br_2," J.C.S. Faraday II 76, 177-194 (1980).

7. Clyne, M. A. A. and Liddy, J. P., "Quantum-resolved Dynamics of Excited States. Part 6.-Radiative Lifetime and Collisional Deactivation Rates in BrF(B)," J.C.S. Faraday II 76, 1569-1585 (1980).

8a. Davis, S. J. and Hanko, L., "Optically Pumped Iodine Monofluoride $B^3\Pi(0^+) \rightarrow X^1\Sigma^+$ Laser," App. Phys. Lett. 37(8), 692 (1980).

8b. Davis, S. J., Hanko, L. and Shea, R. F., "Iodine Monofluoride $B^3\Pi(0^+) \rightarrow X^1\Sigma^+$ Lasing from Collisionally Pumped States," J. Chem. Phys. 78, 172 (1983).

9. Clyne, M. A. A., Coxon, J. A. and Townsend, L. W., "Formation of the $B^3\Pi(0^+)$ States of BrF and IF by Atom recombination in the Presence of Singlet ($^1\Delta_g$, $^1\Sigma_g^+$) Oxygen," J.C.S. Faraday II 68, 2134 (1972).

10. Whitefield, P. D., Shea, R. F. and Davis, S. J., "Singlet Molecular Oxygen Pumping of IF $B^3\Pi(0^+)$," J. Chem. Phys. 78, 6793 (1983).

11. S. J. Davis, private communication (1983).

12. Piper, L. G., Krech, R. H., and Taylor, R. L., "Generation of N_3 in the Thermal Decomposition of NaN_3," J. Chem. Phys. 71, 2099 (1979).

13. Kajimoto, O., Kawajiri, T. and Fueno, T., "Formation of Electronically Excited $NH_2(^2A_1, \nu_2 \leq 15)$ by the Reaction Between H and NH_3," Chem. Phys. Lett. 76, 375 (1980).

14. Clark, T. C. and Clyne, M. A. A., "Kinetics of Chemiluminescent Reactions of the Gaseous Azide Radical," Trans. Faraday Soc. 66, 877 (1970).

15. Pritt, A. T., Jr. and Coombe, R. D., "Azide Mechanisms for the Production of NCl Metastables," Int. J. Chem. Kinet. XII, 741 (1980).

16. Cheah, C. T. and Clyne, M.A.A., "Reactions Forming Electronically-excited Free Radicals," J.C.S. Faraday II 76, 1543 (1980).

17. Rawlins, W. T., Piper, L. G., Caledonia, G. E., and Green, B. D., "COCHISE Research," Physical Sciences Inc. Technical Report TR-298 Under Utah State Univ. Subcontract SC-80-028 (1981). Also published as Air Force Geophysics Laboratories Report, AFGL-TR-82-0305 (1982).

18. Piper, L. G., Caledonia, G. E., and Kennealy, J. P., "Rate Constants for Deactivation of $N_2(A\ ^3\Sigma_u^+\ v'=0,1)$ by O_2," J. Chem. Phys. 74, 2888 (1981).

19. Piper, L. G., Caledonia, G. E., and Kennealy, J. P., "Rate Constants for Deactivation of $N_2(A\ ^3\Sigma_u^+\ v'=0,1)$ by O," J. Chem. Phys. 75, 2847 (1981).

20. Piper, L. G., "The Excitation of $O(^1S)$ in the Electronic Energy Transfer Between $N_2(A\ ^3\Sigma_u^+)$ and O," J. Chem. Phys. 77, 2373 (1982).

21a. Piper, L. G., Murphy, H. C., and Rawlins, W. T., "Development of COCHISE UV Absorption System: Final Report," TR-292 (November 1981), AFGL-TR-81-0318, Air Force Geophysics Laboratory Report (1981).

21b. Rawlins, W. T. and Piper, L. G., "Effect of Excitation Mechanism on Linewidth Parameters of Conventional VUV Discharge Line Sources," Proc. Soc. Photo. Opt. Instr. Eng. 279, 58 (1981). Also presented at the Technical Symposium East '81 of the Society of Photo-Optical Instrumentation Engineers, Washington, D. C. (April, 1981).

22a Krech, R. H., Diebold, G. J. and McFadden, D. L., "Kinetics of the O + F_2 Reaction: A Case of Low Reactivity of Elemental Fluorine," J. Am. Chem. Soc. 99, 4605 (1977).

22b. Krech, R. H., "ESR Discharge - Flow Kinetics: the O + F_2 Reaction," Masters dissertation, Dept. of Chem., Boston College, 1976.

22c. Pak, S. J., Krech, R. H., McFadden, D. L. and MacLean, D. I., "EPR Discharge - Flow Kinetics: The H + ClF_3 Reaction," J. Chem. Phys. 62, 3419 (1975).

23. Kaufman, M. and Kolb, C. E., "Molecular Beam Analysis of the Reaction Between Atomic Fluorine and Carbon Tetrachloride," NR 092-531, 8 (1971).

24. Berg, H. C. and Kleppner, D., "Storage Technique for Atomic Hydrogen," Rev. Sci. Instrum. 33, 248 (1962).

25a. Setser, D. W., Stedman, D. H. and Coxon, J. A., "Chemical Applications of Metastable Argon Atoms. IV. Excitation and Relaxation of Triplet States of N_2," J. Chem. Phys. 53, 1004 (1970).

25b. Stedman, D. H. and Setser, D. W., "Chemical Applications of Metastable Argon Atoms II. A Clean System for the Formation of $N_2(A\ ^3\Sigma_u^+)$," Chem. Phys. Lett. 2, 542 (1968).

26. Sadeghi, N. and Setser, D. W., "Primary $N_2(B)$ Vibrational Distributions from Excitation-Transfer Reactions Between $Kr(^3P_2)$ or $Xe(^3P_2)$ Atoms and N_2," Chem. Phys. Lett. 82, 44 (1981).

27. Stedman, D. H. and Setser, D. W., "Chemical Applications of Metastable Rare Gas Atoms," Prog. React. Kinet. 6, 193 (1971).

28. Piper, L. G., Velazco, J. E., and Setser, D. W., "Quenching Cross-Sections for Electronic Energy Transfer Reactions between Metastable Argon Atoms and Noble Gases and Small Molecules," J. Chem. Phys. 59, 3323 (1973).

29. Appelman, E. H. and Clyne, M. A. A., "Reaction Kinetics of Ground-State Fluorine, F ^2P, Atoms Part 2 -- Reactions Forming Inorganic Fluorides, Studied Mass Spectrometrically," J. C. S. Faraday I 71, 2072 (1975).

30. Bozzelli, J. W. and Kaufman, M., "Kinetics and Mechanisms of the Reactions of Atomic Fluorine with CF_3I and $CC\ell_3Br$," J. Phys. Chem. 77, 1748 (1973).

31. Stein, L., Wanner, J., and Walther, H., "Laser-Induced Fluorescence Study of the Reactions of F-atoms with CH_3I and CF_3I," J. Chem. Phys. 72, 1128 (1980).

32. Kaufman, F., "Reactions of Oxygen Atoms," Prog. React. Kinet. 1, 1 (1961).

33. Fontijn, A., Meyer, C. B., and Schiff, H. I., "Absolute Quantum Yield Measurements of the NO - O Reaction and Its Use as a Standard for Chemiluminescent Reactions," J. Chem. Phys. 40, 64 (1964).

34. Vanpee, M., Hill, K. D., and Kineyko, W. R., "Absolute Rate Constant Measurements for the Radiative Combination of Atomic Oxygen with Nitric Oxide," AIAA J. 9, 135 (1971).

35. Golde, M. F., Roche, A. E., and Kaufman, F., "Absolute Rate Constant for the O + NO Chemiluminescence in the Near Infrared," J. Chem. Phys. 59, 3953 (1973).

36. Golomb, D. and Brown, J. H., "The Temperature Dependence of the NO - O Chemiluminous Recombination. The RMC Mechanism," J. Chem. Phys. 63, 5246 (1975).

37. Woolsey, G. A., Lee, P. H., and Slafer, W. D., "Measurement of the Rate Constant for NO - O Chemiluminescence Using a Calibrated Piston Source of Light," J. Chem. Phys. 67, 1220 (1977).

38. Sutoh, M., Morioka, Y., and Nakamura, M., "Absolute Rate Constant for the Chemiluminescent Reaction of Atomic Oxygen with Nitric Oxide," J. Chem. Phys. 72, 20 (1980).

39. Pravilov, A. M. and Smirnova, L. G., "Spectral Distribution of the Chemiluminescence Rate Constant in the O + CO(+M) and O + NO(+He) Reactions," Kinet. and Catal. 19 202 (1978).

40. Kaufman, F., "The Air Afterglow and Its use in the Study of Some Reactions of Atomic Oxygen," Proc. Roy. Soc. (London) A 247, 123 (1958).

41. Kaufman, F., "The Air Afterglow Revisited," Chemiluminescence and Bioluminescence, M. J. Cormier, D. M. Hercules, and J. Lee, eds. pp. 83-100 (1973).

42. Husain, D. and Slater, N. K. H., "Kinetic Study of Ground State Atomic Nitrogen, N(2 $^4S_{3/2}$) by Time-Resolved Atomic Resonance Fluorescence," JCS. Faraday II 76, 606 (1980).

43. Lee, J. H., Michael, J. V., Payne, W. A., and Stief, L. J., "Absolute Rate of the Reaction of N(^4S) with NO from 196-400 K with DF-RF and FP-RF Techniques," J. Chem. Phys. 69, 3069 (1978).

44. Clyne, M. A. A. and McDermid, I. S., "Mass Spectrometric Determinations of the Rates of Elementary Reactions of NO and NO_2 with Ground State N ^4S Atoms," JCS Faraday I 71, 2189 (1975).

45. Slanger, T. G., "Generation of O_2(c $^1\Sigma_u^-$, C $^3\Delta_u$, A $^3\Sigma_u^+$) from Oxygen Atom Recombination," J. Chem. Phys. 69, 4779 (1978).

46. L. G. Piper, unpublished results (1978).

47. Baulch, D. L., Drysdale, D. D., Horne, D. G., and Lloyd, A. C., Evaluated Kinetic Data for High Temperature Reactions. II. Homogeneous Gas Phase Reactions of the H_2 - N_2 - O_2 System. (Butterworths, London, 1973).

48. Lewis, P. F. and Green, B. D., "Computation of Electronic Spectra of Diatomic Molecules," Physical Sciences Inc. Report No. TR-413 (1984).

49. Wolf, P., Air Force Weapons Laboratory, private communication (1984).

50. Shemansky, D. E., "N_2 Vegard-Kaplan System in Absorption," J. Chem. Phys. 51, 689 (1969).

51. Ferguson, E. E., Fehsenfeld, F. C., and Schmeltekopf, A. L., "Flowing Afterglow Measurements of Ion-Neutral Reactions," Advances in Atomic and Molecular Physics V, edited by D. R. Bates, New York, Academic Press, (1970).

52. Bolden, R. C., Hemsworth, R. S., Shaw, M. J., and Twiddy, N. D., "Measurements of Thermal-Energy Ion-Neutral Reaction Rate Coefficients for Rare-Gas Ions," J. Phys. B 3, 45 (1970).

53. Farragher, A. L., "Ion-Molecule Reaction Rate Studies in a Flowing Afterglow System," Trans. Faraday Soc. 66, 1411 (1970).

54. Huggins, R. W. and Cahn, J. H., "Metastable Measurements in Flowing Helium Afterglow," J. Appl. Phys. 38, 180 (1967).

55. Walker, R. E., "Chemical Reaction and Diffusion in a Catalytic Tubular Reactor," Phys. Fluids 4, 1211 (1961).

56. Poirier, R. V. and Carr, R. W., "The Use of Tubular Flow Reactors for Kinetic Studies Over Extended Pressure Ranges," J. Phys. Chem. 75, 1593 (1971).

57. Cher, M. and Hollingsworth, C. S., "Chemiluminescent Reactions of Excited Helium with Nitrogen and Oxygen," Adv. Chem. Ser. 80, 118 (1969).

58. Kolts, J. H. and Setser, D. W., "Decay Rates of Ar(4s, $^3P_2$), Ar(4s, $^3P_0$) Kr(5s, $^3P_2$), and Xe(6s, $^3P_2$) Atoms in Argon," J. Chem. Phys. 68, 4848 (1978).

59. Morgan, J. E., Phillips, L. F., and Schiff, H. I., "Studies of Vibrationally Excited Nitrogen Using Mass Spectrometric and Calorimeter-Probe Techniques," Disc. Faraday Soc. 33, 118 (1962).

60. Young, R. A., Black, G. and Slanger, T. G., "Vacuum-Ultraviolet Photolysis of N_2O. II. Deactivation of $N_2(A\ ^3\Sigma_u^+)$ and $N_2(B\ ^3\Pi_g)$," J. Chem. Phys. 50, 303 (1969).

61. Lofthus, A. and Krupenie, P. H., "The Spectrum of Molecular Nitrogen," J. Phys. Chem. Ref. Data 6, 113 (1977).

62. Levron, D. and Phelps A.V., "Quenching of $N_2(A^3\Sigma^+_u$, v=0,1) by N_2, Ar, and H_2," J. Chem. Phys. 69, 2260 (1978).

63. Bromer, H.H. and Spieweck, F., "Lifetime and Diffusion Coefficient of the $A^3\Sigma_u^+$ State of N_2," Planet Sp. Sci. 15, 689(1967).

64. Zipf, E.C. Jr., Measurement of the Diffusion Coefficient and Radiative Lifetime of Nitrogen Molecules in the $A^3\Sigma_u^+$ State," J. Chem. Phys. 38, 2034 (1963).

APPENDIX

FRANCK-CONDON FACTORS AND ABSOLUTE TRANSITION PROBABILITIES FOR THE IF ($B^3\pi_{0^+} - X^1\Sigma^+$) TRANSITION

W.J. Marinelli and L.G. Piper

Air Force Contract No. F29601-83-C-0051
Air Force Weapons Laboratory
Kirtland AFB, NM 87117

Physical Sciences Inc.
Research Park, P.O. Box 3100
Andover, MA 01810

ABSTRACT

Improved spectroscopic constants have been used to calculate RKR potentials and Franck-Condon factors for the IF($B^3\pi_{0^+} - X^1\Sigma^+$) transition. The Franck-Condon factors are generally in good agreement with previously calculated values but differ by as much as 30% for transitions from higher levels of the B-state. Several experimentally measured relative transition moment functions have been evaluated and the best scaled so that the total transition probability calculated for each B-state vibrational level, A(v'), matches measured values. The scaled function was then used to calculate individual transition probabilities, A(v',v"), for the vibronic transitions.

1. INTRODUCTION

There is a renewed interest in the spectroscopy and kinetics of iodine monofluoride (IF), primarily as the lasing species in a chemical laser. Davis and Hanko and Davis, Hanko, and Shea have observed lasing on the B-X transition from several B-state rotational and vibrational levels by optically pumping the IF B-state (Refs. A-1, A-2). Dlabal and Eden used electrical discharges in $NF_3/CF_3I/He$ mixtures to induce lasing action on the D'-A' transition (Ref. A-3). There are now several research groups working to find efficient chemical pumping agents for either the D' or the B-states.

The IF ($B^3\pi_{0+} - X^1\Sigma^+$) transition was initially observed by Durie in an I_2-F_2 flame (Refs. A-4, A-5). He assigned the spectrum and produced the first spectroscopic constants. Clyne, Coxon, and Townsend observed a similar but more extensive band system in I-atom/F-atom/singlet oxygen mixtures (Ref. A-6). The ground state rotational constants were refined by Tiemann, Hoeft, and Törring who measured the pure rotational spectrum (Ref. A-7). Birks, Gabelnick, and Johnston observed chemiluminescence originating from both the B-X and A-X transitions in the reaction of I_2 with F_2, calculated Franck-Condon factors for the B-X transition, and measured the variation in the B-X relative electronic transition moment with r-centroid (Ref. A-9). Clyne and McDermid (Ref. A-10) recalculated the Franck-Condon factors for the B-X transition using spectral parameters derived from Coxon's (Ref. A-11) reinterpretation of Durie's data (Ref. A-5). They also observed laser-induced fluorescence from the transition (Ref. A-12), and measured the radiative lifetimes and apparent transition moments for B-state vibrational levels 0-9 (Ref. A-13). More recently Trautmann, Trickl, and Wanner and Trickl and Wanner have reported improved spectroscopic constants for both the B-and X-states, (Refs. A-14, A-15). Trickl and Wanner have also measured the

variation in the relative transition moment for the B-X transition over a wider range of vibrational levels (Ref. A-16).

In our studies of electronic energy transfer from $N_2(A^3\Sigma_u^+)$ and active nitrogen to the $IF(B^3\pi_{0^+})$ state, we found that there is still some confusion regarding the variation in the $IF(B^3\pi_{0^+} - X^1\Sigma^+)$ transition moment with r-centroid, and that recent measurements of the spectroscopic constants for both the X-and B-states made possible a more accurate determination of the Franck-Condon factors for the transition. It is now also possible to calculate absolute transition probabilities for the B-X system using information currently available in the literature. We have performed a new evaluation of the Franck-Condon factors and calculated transition probabilities as part of our present measurement program. These data are very useful for those engaged in kinetic studies of IF and for those who wish to model the B-X chemical laser system.

2. METHODS AND RESULTS

The determination of transition probabilities for the $IF(B^3\pi_{0^+} - X^1\Sigma^+)$ transition starts with the calculation of accurate RKR potentials for both the X-and B-states. A Numerov-Cooley routine is used to obtain numerical eigenfunctions and eigenvalues for each of the potentials and the necessary overlap integrals are computed to provide Franck-Condon factors and r-centroids for the B-X transition. The transition probabilities are then calculated using these Franck-Condon factors, the appropriate transition frequencies and molecular constants, and a scaled transition moment function. The scaling for the transition moment function is chosen so that the total transition probability for each B-state vibrational level agrees with the transition probability determined for that level from radiative lifetime measurements. The details of these procedures are discussed in the following sections

AD-A162 085 KINETICS OF IODINE MONOFLUORIDE EXCITATION BY ENERGETIC NITROGEN(U) PHYSICAL SCIENCES INC ANDOVER MA L G PIPER ET AL. OCT 85 PSI-051/TR-460 AFWL-TR-84-156 2/2

UNCLASSIFIED F29601-83-C-0051 F/G 7/4 NL

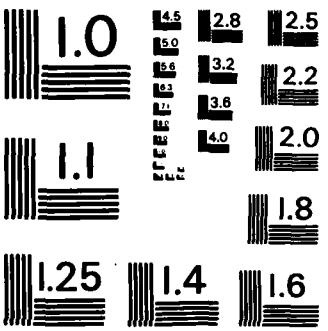

MICROCOPY RESOLUTION TEST CHART
NATIONAL BUREAU OF STANDARDS-1963-A

2.1 RKR Potentials

The RKR potentials for the X and B-states were calculated using a fast quadrature method developed by Tellinghuisen (Ref. A-17). Dunham expansions of the form

$$G(v) = T_e + \sum_{\ell=1}^{L} C_\ell \, (v + 1/2)^\ell \qquad (1)$$

and

$$B(v) = \sum_{p=0}^{P} C_p \, (v + 1/2)^p \qquad (2)$$

were used to generate the vibrational and rotational term values, respectively. Expansion parameters determined by Trickl and Wanner were used to give vibrational term values for both the X and B-states (Ref. A-15). The rotational constants of Durie were used in the X-state calculation, while those of Tiemann, Hoeft, and Törring were used for the B-state, (Refs. A-5, A-7). These parameters accurately reproduce the vibronic band origins to within 0.02 cm^{-1} for a range of transitions comprising $v' \leq 11$ and $v'' \leq 17$. They are summarized in Table A-1. The vibrational term values and classical turning points calculated for both electronic states are given in Table A-2.

2.2 Eigenfunctions and Franck-Condon Factors

Numerical eigenfunctions for vibrational levels up to 11 in the B-state and 17 in the X-state were calculated at 0.001 Å intervals using a Numerov-Cooley routine to solve the radial Schrödinger equation (Ref. A-18). Evaluations of the overlap integrals used to obtain Franck-Condon factors and r-centroids were done using Simpson's rule. The routines used 1000 uniformly spaced values of the potentials spanning a range of internuclear distance from 1.63 to 2.63Å. The potential arrays were constructed from the RKR turning points using a 7 term interpolation polynomial. The attractive and repulsive

TABLE A-1

DUNHAM EXPANSION PARAMETERS USED TO CALCULATE RKR POTENTIALS FOR THE IF B- AND X-STATES. SEE TEXT FOR REFERENCES.

Term	IF($X^1\Sigma^+$)		IF($B^3\Pi_{0+}$)	
	C_ℓ (cm^{-1})	C_p (cm^{-1})	C_ℓ (cm^{-1})	C_p (cm^{-1})
1	610.22649	0.2797108	411.2759	0.22721
2	-3.12534	-1.8734(-3)	-2.85844	-1.398(-3)
3	-2.6139(-3)	-2.7(-6)	-6.2411(-2)	-8.2(-5)
4	-5.8379(-5)		--	
5			--	
6			-1.8331(-5)	
7			--	
8			--	
9			-1.0956(-8)	
10			--	
11			--	
12			9.255(-12)	
13			--	
14			--	
15			-3.8574(15)	

TABLE A-2

TERM VALUES AND CLASSICAL TURNING POINTS CALCULATED BY RKR INVERSION USING THE EXPANSION PARAMETERS IN TABLE A-1

Vibrational Level	IF($X^1\Sigma^+$)			IF($B^3\Pi_{0^+}$)		
	$E(cm^{-1})$	$r_-(Å)$	$r_+(Å)$	$E(cm^{-1})$	$r_-(Å)$	$r_+(Å)$
0	304.332	1.8549	1.9708	204.916	2.0517	2.1930
1	908.299	1.8181	2.0197	610.272	2.0064	2.2527
2	1505.990	1.7943	2.0557	1009.345	1.9772	2.2972
3	2097.386	1.7759	2.0866	1401.739	1.9548	2.3361
4	2682.469	1.7606	2.1144	1787.011	1.9363	2.3720
5	3261.216	1.7474	2.1403	2164.615	1.9206	2.4064
6	3833.605	1.7357	2.1648	2533.882	1.9069	2.4399
7	4399.611	1.7252	2.1883	2893.609	1.8948	2.4733
8	4959.209	1.7156	2.2110	3242.523	1.8836	2.5070
9	5512.373	1.7068	2.2330	3578.471	1.8731	2.5419
10	6059.074	1.6987	2.2546	3898.045	1.8625	2.5790
11	6599.282	1.6911	2.2757	4193.911	1.8501	2.6214
12	7132.966	1.6840	2.2966			
13	7660.094	1.6773	2.3171	r_e = 2.1190		
14	8180.632	1.6710	2.3375			
15	8694.544	1.6650	2.3577			
16	9201.794	1.6593	2.3778			
17	9702.344	1.6539	2.3979			
	r_e = 1.9098					

regions of the potentials which fall outside the range of the classical turning points were evaluated by fitting the four closest turning points to the expressions

$$V(r) = D_e - c/r^d \tag{3}$$

for the attractive part and

$$V(r) = a/r^{12} + b \tag{4}$$

for the repulsive part. In these expressions, D_e is the dissociation energy and a, b, c, and d are adjustable parameters.

The computer routines and their inputs were verified by testing the eigenfunctions for proper normalization and orthogonality and by comparing the calculated eigenvalues with those used to calculate the RKR potentials. The normalization and orthogonality of the eigenfunctions for each potential were tested by doing the overlap integrals for each eigenfunction of the potential with itself and with all of the other eigenfunctions of that potential. The diagonal elements in the resulting overlap integral arrays, which correspond to the overlap of each eigenfunction with itself, were unity to within 1 part in 10^7. The off-diagonal elements in the arrays were not greater than 1.0×10^{-20}. Eigenvalues for the X-state calculated using the Numerov-Cooley routine agreed with those used in the RKR routine to within 0.03 cm^{-1} for the first 11 levels and were different by no more than 8 cm^{-1} for levels up to 17. A similar comparison for the B-state showed agreement to within 0.2 cm^{-1} for the first 5 levels and a maximum deviation of 2.3 cm^{-1} for levels up to 11.

2.3 Transition Moment and Transition Probabilities

The relative transition moment function spanning the widest range of B-state vibrational levels is given by Trickl and Wanner (Ref. A-16). Their

analysis of IF(B-X) fluorescence from the reaction of F-atoms with I_2, ICl, and IBr yielded the function

$$|R_e(v',v")|^2 \propto r(v',v") - r_0(v'), \tag{5}$$

with

$$r_0(v') = r(v',0) - (1 + 3.434 \times 10^{-5}\ v'^5)[r(v',0) - 1.859\ \text{Å}] \tag{6}$$

for $v' \leq 8$. We have modified their relative transition moment function to include a scaling parameter β such that the function becomes

$$|R_e(v',v")|^2 = \beta\ \{r(v',v") - r_0(v')\}. \tag{7}$$

We can write the expression for the total transition probability for a given vibrational level as

$$A(v') = \sum_{v"} A(v',v") = (64\pi^4/3h)\ \beta \sum_{v"} \omega^3\ |R_e(v',v")|^2\ |\langle q'|q"\rangle|^2\ , \tag{8}$$

where ω is the transition frequency in cm^{-1} and $|\langle q'|q"\rangle|^2$ is the Franck-Condon factor for the transition.

If all the transition frequencies and Franck-Condon factors from a given vibrational level are known, then a value of β can be chosen so that expression (8) produces the measured transition probability for that level. Our calculated Franck-Condon factors and the spectral parameters given above allow us to meet this criterion for levels 0-5 of the IF B-state. Using the measured transition probabilities of Clyne and McDermid for transitions from IF B-state levels 0-9 (Ref. A-13), we have done a least-squares fit for the parameter β that minimizes the differences between the measured and calculated probabilities for levels 0-5. The calculated and measured probabilities are given in Table A-3 and Fig. A-1. The calculated probabilities agree with those measured by Clyne and McDermid to within 7% for levels 0-5 and are nearly a linear function of vibrational level (Ref. A-13). A linear least-squares fit to the calculated probabilities, shown in Fig. A-1, allows

TABLE A-3

COMPARISON OF MEASURED AND FITTED TOTAL TRANSITION RATES FOR LEVELS 0-9 OF IF(B)

Vibrational Level	Measured A(v')[a]	Fitted A(v')[a,b]
0	1.44±0.10	1.54
1	1.49±0.07	1.48
2	1.42±0.12	1.43
3	1.45±0.06	1.38
4	1.34±0.11	1.34
5	1.23±0.06	1.27
6	1.21±0.06	1.22
7	1.16±0.05	1.17
8	1.16±0.07	1.12
9	1.14±0.12	1.07

[a] $10^5 s^{-1}$;
[b] Levels 6-9 extrapolated from calculated values for levels 0-5.

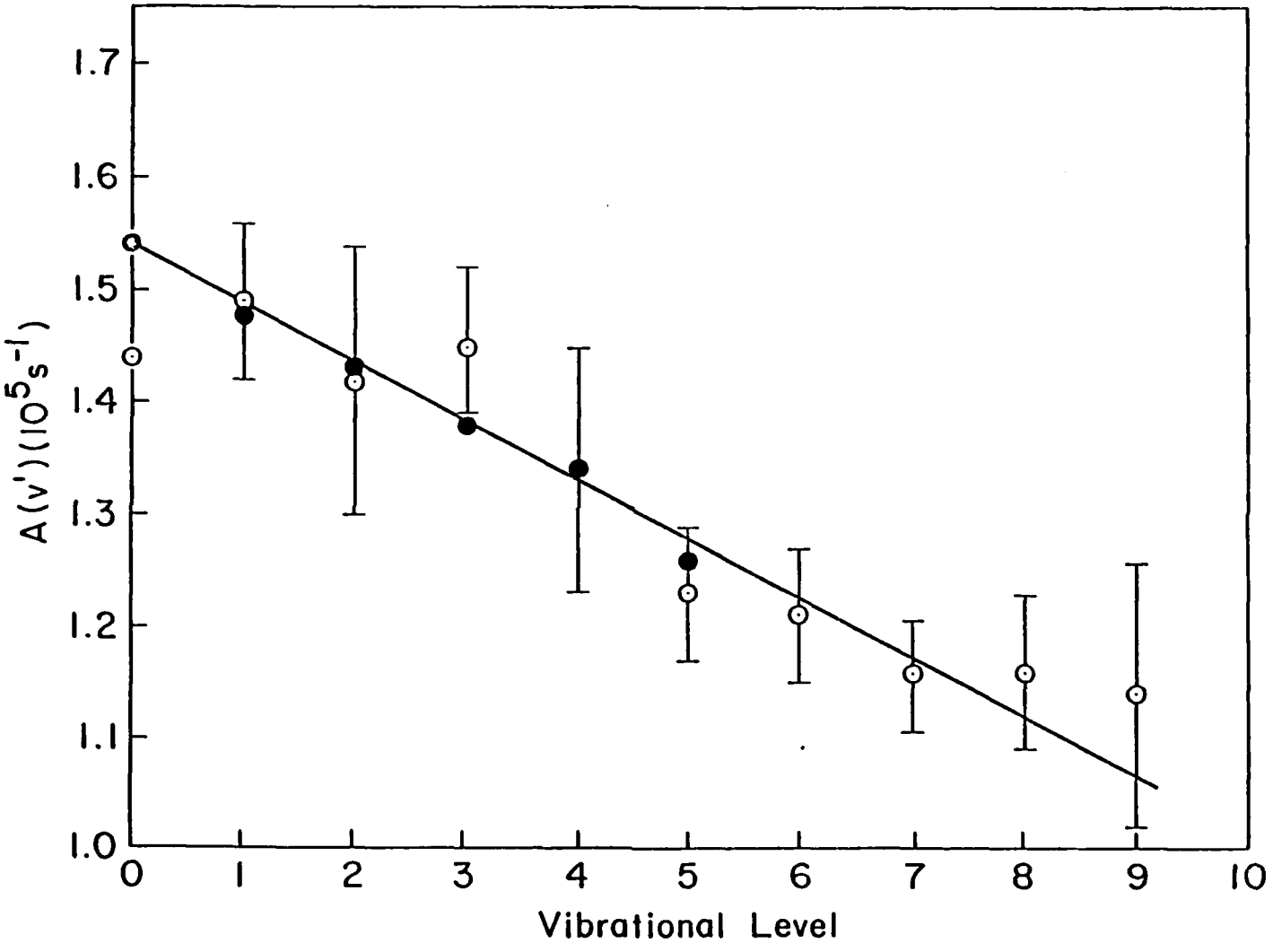

Fig. A-1. Measured total transition rates (Ref. 13), ◯; fitted total transition rates, ●; and linear least squares fit to fitted data, solid line, for IF(B) levels 0-9.

an extension of the calculated values for comparison with the full range of of the measured data. In the extrapolated region the agreement with the measured values is also quite good. We have included the extrapolated values in Table A-3.

The relative transition moment function of Trickl and Wanner (Ref. A-16) can now be put on an absolute basis using the fitted value of β and is given as

$$|R_e(v',v")|^2 = 0.445 \cdot [\, r(v',v") - r_0(v')], \qquad (9)$$

where the units are Debye^2 and $r_0(v')$ has its previously defined value. Using the absolute transition moment function, our calculated Franck-Condon factors, and the known transition frequencies for the B-X transition, we can calculate transition probabilities for all transitions of interest. These probabilities, as well as the corresponding Franck-Condon factors and r-centroids, are given in Table A-4 for transitions from B-state levels 0-9 to X-state levels 0-17.

3. DISCUSSION

Vibrational term values calculated for the X-state differ by as much as 1.3 cm^{-1} from those of Clyne and McDermid (Ref. A-13) and 13 cm^{-1} from those of Gabelnick (Ref. A-8), whose results are summarized in Reference A-9. The corresponding classical turning points for these levels change by as much as 0.002 Å and 0.003 Å, respectively. The term values calculated for the B-state using the new constants differ by 1 cm^{-1} from Clyne and McDermid and 3.2 cm^{-1} for Gabelnick. Classical turning points calculated from these term values differ by as much as 0.003 Å and 0.007 Å, respectively. These changes are a direct result of the use of improved vibrational and rotational parameters. This improved accuracy enables us to compute the Franck-Condon factors to X-state level 17. The shifts in the potentials are not sufficient to

TABLE A-4

FRANCK-CONDON FACTORS, R-CENTROIDS, AND TRANSITION PROBABILITIES FOR IF(B,0-9) TO IF(X,0-17). THE FIGURES IN BRACKETS ARE EXTRAPOLATED VALUES FROM FIG. A-1. EXPONENTS ARE IN PARENTHESES.

v' \ v"	0	1	2	3	4	5	6	7	8	9
0	4.952(-3) 2.007 6.97(2)	2.995(-2) 2.031 4.44(3)	8.638(-2) 2.055 1.32(4)	1.578(-1) 2.080 2.47(4)	2.046(-1) 2.106 3.22(4)	1.998(-1) 2.132 3.12(4)	1.522(-1) 2.158 2.33(4)	9.245(-2) 2.186 1.39(4)	4.546(-2) 2.215 6.62(3)	1.826(-2) 2.245 2.56(3)
1	2.288(-2) 1.991 3.06(3)	9.102(-2) 2.015 1.31(4)	1.498(-1) 2.038 2.25(4)	1.189(-1) 2.062 1.83(4)	3.166(-2) 2.085 4.90(3)	2.453(-3) 2.126 4.03(2)	6.417(-2) 2.142 1.01(4)	1.395(-1) 2.168 2.13(4)	1 564(-1) 2.195 2.33(4)	1.176(-1) 2.224 1.71(4)
2	5.505(-2) 1.975 6.88(3)	1.335(-1) 1.998 1.83(4)	9.772(-2) 2.021 1.41(4)	7.626(-3) 2.041 1.13(3)	2.983(-2) 2.073 4.68(3)	9.656(-2) 2.096 1.52(4)	6.666(-2) 2.119 1.04(4)	3.853(-3) 2.134 5.69(2)	2.771(-2) 2.180 4.28(3)	1.078(-1) 2.205 1.61(4)
3	9.227(-2) 1.960 1.08(4)	1.211(-1) 1.983 1.58(4)	1.764(-2) 2.004 2.44(3)	2.635(-2) 2.032 3.97(3)	8.467(-2) 2.054 1.30(4)	2.732(-2) 2.075 4.20(3)	8.289(-3) 2.111 1.35(3)	7.490(-2) 2.130 1.18(4)	6.828(-2) 2.154 1.05(4)	6.351(-3) 2.171 9.26(2)
4	1.216(-1) 1.946 1.33(4)	6.966(-2) 1.968 8.64(3)	3.761(-3) 1.998 5.39(2)	7.479(-2) 2.015 1.09(4)	2.889(-2) 2.036 4.35(3)	1.146(-2) 2.067 1.84(3)	7.009(-2) 2.087 1.11(4)	2.675(-2) 2.108 4.19(3)	7.428(-3) 2.148 1.21(3)	7.069(-2) 2.165 1.10(4)
5	1.348(-1) 1.931 1.38(4)	2.051(-2) 1.953 2.44(3)	4.066(-2) 1.978 5.52(3)	5.445(-2) 1.999 7.85(3)	1.526(-3) 2.035 2.50(2)	6.046(-2) 2.047 9.58(3)	2.194(-2) 2.067 3.47(3)	1.380(-2) 2.100 2.28(3)	6.392(-2) 2.120 1.03(4)	1.672(-2) 2.139 2.60(3)
6	1.314(-1) 1.918 1.32(4)	2.471(-4) 1.934 2.76(1)	6.787(-2) 1.963 9.20(3)	1.034(-2) 1.981 1.47(3)	3.745(-2) 2.010 5.90(3)	3.727(-2) 2.029 5.96(3)	5.475(-3) 2.061 9.33(2)	5.573(-2) 2.079 9.32(3)	9.825(-3) 2.096 1.59(3)	2.440(-2) 2.133 4.10(3)
7	1.163(-1) 1.904 1.17(4)	9.432(-3) 1.926 1.14(3)	5.943(-2) 1.950 8.29(3)	2.249(-3) 1.982 3.66(2)	5.430(-2) 1.994 8.73(3)	1.148(-3) 1.999 1.74(2)	4.402(-2) 2.040 7.56(3)	1.850(-2) 2.060 3.17(3)	1.662(-2) 2.091 2.93(3)	4.776(-2) 2.111 8.24(3)
8	9.543(-2) 1.891 9.64(3)	3.389(-2) 1.913 4.17(3)	3.042(-2) 1.938 4.39(3)	2.584(-2) 1.961 4.10(3)	2.927(-2) 1.979 4.82(3)	1.430)(-2) 2.008 2.55(3)	3.871(-2) 2.024 6.84(3)	2.391(-3) 2.060 4.54(2)	4.576(-2) 2.072 8.30(3)	3.351(-3) 2.085 5.80(2)
9	7.411(-2) 1.878 6.63(3)	5.910(-2) 1.900 6.73(3)	6.184(-3) 1.929 8.86(2)	4.648(-2) 1.948 7.17(3)	3.124(-3) 1.961 4.86(2)	3.961(-2) 1.992 6.90(3)	6.469(-3) 2.004 1.10(3)	3.158(-2) 2.036 5.77(3)	1.692(-2) 2.053 3.03(3)	1.671(-2) 2.085 3.10(3)

TABLE A-4 (Continued)

v' \ v''	10	11	12	13	14	15	16	17	$\sum$	$\tau_{v'}$
	6.027(-3)	1.642(-3)	3.708(-4)	6.956(-5)	1.086(-5)	1.413(-6)	1.535(-7)	1.403(-8)	1.000	
0	2.276	2.310	2.344	2.381	2.419	2.459	2.500	2.542	-	
	8.08(2)	2.10(2)	4.48(1)	7.92(0)	1.16(0)	1.39(-1)	1.40(-2)	1.17(-3)	1.54(5)	6.49(-6)
	6.514(-2)	2.781(-2)	9.389(-3)	2.546(-3)	5.607(-4)	1.011(-4)	1.497(-5)	1.839(-6)	1.000	
1	2.254	2.285	2.318	2.353	2.390	2.428	2.467	2.508	-	
	9.05(3)	3.69(3)	1.19(3)	3.04(2)	6.30(1)	1.06(1)	1.46(0)	1.65(-1)	1.48(5)	6.76(-6)
	1.462(-1)	1.189(-1)	6.754(-2)	2.864(-2)	9.398(-3)	2.440(-3)	5.089(-4)	8.588(-5)	1.000	
2	2.233	2.263	2.294	2.327	2.362	2.399	2.436	2.476	-	
	2.10(4)	1.64(4)	8.87(3)	3.57(3)	1.11(3)	2.71(2)	5.26(1)	8.24(0)	1.43(5)	6.99(-6)
	2.316(-2)	1.023(-1)	1.405(-1)	1.117(-1)	6.091(-2)	2.448(-2)	7.544(-3)	1.826(-3)	1.000	
3	2.218	2.243	2.272	2.303	2.336	2.371	2.408	2.446	-	
	3.48(3)	1.46(4)	1.91(4)	1.46(4)	7.52(3)	2.86(3)	8.25(2)	1.87(2)	1.38(5)	7.25(-6)
	5.957(-2)	2.804(-3)	3.165(-2)	1.104(-1)	1.363(-1)	9.938(-2)	4.986(-2)	1.842(-2)	0.993	
4	2.189	2.199	2.256	2.282	2.313	2.346	2.381	2.417	-	
	8.96(3)	3.88(2)	4.55(3)	1.50(4)	1.76(4)	1.22(4)	5.77(3)	1.99(3)	1.34(5)	7.46(-6)
	1.456(-2)	7.355(-2)	4.439(-2)	1.489(-6)	5.014(-2)	1.231(-1)	1.289(-1)	8.324(-2)	0.947	
5	2.180	2.201	2.225	3.298	2.294	2.323	2.356	2.390	-	
	2.34(3)	1.12(4)	6.48(3)	7.51(-1)	6.87(3)	1.59(4)	1.58(4)	9.57(3)	1.26(5)	7.94(-6)
	5.704(-2)	4.996(-3)	2.980(-2)	7.367(-2)	2.477(-2)	5.409(-3)	7.634(-2)	1.333(-1)	0.785	
6	2.153	2.165	2.214	2.237	2.261	2.317	2.335	2.366	-	
	9.24(3)	7.57(2)	4.66(3)	1.10(4)	3.49(3)	7.67(2)	9.96(3)	1.63(4)	[1.22(5)]	[8.20(-6)]
	8.182(-4)	4.001(-2)	4.266(-2)	5.655(-5)	5.015(-2)	6.368(-2)	6.828(-3)	2.438(-2)	0.598	
7	2.103	2.166	2.187	2.382	2.250	2.275	2.292	2.350	-	
	1.24(2)	6.73(3)	6.86(3)	1.27(1)	7.61(3)	9.15(3)	9.07(2)	3.24(3)	[1.16(5)]	[8.62(-6)]
	3.265(-2)	3.133(-2)	3.095(-3)	5.234(-2)	2.158(-2)	9.054(-3)	6.656(-2)	4.176(-2)	0.578	
8	2.124	2.143	2.194	2.200	2.220	2.269	2.288	2.313	-	
	5.89(3)	5.41(3)	5.60(2)	8.64(3)	3.37(3)	1.42(3)	9.71(3)	5.72(3)	[1.11(5)]	[9.01(-6)]
	3.463(-2)	1.167(-3)	4.404(-2)	1.114(-2)	1.955(-2)	5.133(-2)	3.667(-3)	3.162(-2)	0.497	
9	2.104	2.157	2.157	2.171	2.216	2.236	2.247	2.302	-	
	6.24(3)	2.27(2)	7.70(3)	1.82(3)	3.27(3)	8.06(3)	5.28(2)	4.59(3)	[1.06(5)]	[9.43(-6)]

affect significantly the Franck-Condon factors for transitions between levels with eigenfunctions having few nodes, but do result in large changes for transitions occuring between high levels in each manifold. For such transitions the present values differ by as much as 30% from previous results.

Extension of the Franck-Condon factor matrix to include X-state levels up to 17 gives us the full sum of the overlap integrals for B-state levels 0-4 and 95% of the sum for level 5. This procedure allows us to use these levels to determine the optimum value of β in the transition moment fitting routine. Previous calculations only determined the full overlap integral sum for levels 0 and 1, limiting the accuracy of any fit for the transition moment function (Refs. A-9, A-10).

There have been three determinations of the variation in the relative transition moment with r-centroid for the B-X transition. The initial measurements of Birks, Gabelnick, and Johnston (Ref. A-9) showed a variation in the relative transition moment for transitions from B-state levels 0-2 characterized by the expression

$$|R_e(v',v'')|^2 \propto r(v',v'') - 1.859 \text{ Å} . \qquad (10)$$

The function varies by about a factor of three over the corresponding range of r-centroids. Subsequently, Clyne and McDermid inferred from their lifetime measurements that the transition moment varied by only about 10% for transitions originating from B-state levels 0-9 (Ref. A-13). Recently Trickl and Wanner investigated the variation in the relative transition moment and reported a change with r-centroid previously given in expression (5) for transitions originating from B-state levels 0-8 (Ref. A-16). Their transition moment function gives values of the transition moment which agree with those of Birks and coworkers (Ref. A-9) where they overlap, and extends the range over which the transition moment is known.

We have determined that the apparent discrepancy between the transition moments of Clyne and McDermid (Ref. A-13) and other measurements is due to a misinterpretation of the lifetime data by those authors. In reporting their transition moment values, Clyne and McDermid actually calculated the average transition moment for all transitions originating from a given B-state vibrational level. This quantity is given by the expression

$$R_e(v') = \frac{3h}{64\pi^4} \frac{A(v')}{\bar{\omega}^{-3}(v')} \tag{11}$$

where

$$\bar{\omega}^{-3}(v') = \sum_{v''} \omega(v',v'')^3 \left|\langle q'|q''\rangle\right|^2. \tag{12}$$

This average transition moment does vary by only about 10% for levels 0-9; however, this interpretation neglects the fact that the transition moment may vary significantly within any given vibronic progression while having the same average value relative to other progressions in the system.

The data of Clyne and McDermid are consistent with other measurements of the relative transition moment if viewed more closely (Ref. A-13). The quantity $\bar{\omega}^{-3}(v')$, which is the Franck-Condon weighted average transition frequency for a vibronic progression, varies only slightly for progressions originating from B-state levels 0-9. Since B-X emission occurs almost entirely at the classical turning points, transition frequencies can be associated with the r-centroids for those transitions. A plot of transition frequency vs. r-centroid is approximately linear and the average transition frequencies of Clyne and McDermid and can be assigned corresponding r-centroids from this plot. When these r-centroids are used in the relative transition moment function of Birks, Gabelnick, and Johnston (Ref. A-9), this function gives both the same sign and magnitude of the variation in average transition moment observed

by Clyne and McDermid. Hence all of the data sets are consistent and we feel confident to use the more extensive relative transition moment function of Trickl and Wanner (Ref. A-16).

We have done a linear propagation of errors analysis for our computation of the transition probabilities. This analysis included a 10% uncertainty in the transition moment and a 5% uncertainty in the Franck-Condon factors. The total uncertainty in the transition probabilities is estimated to be 10% for strong transitions and as great as 30% for weaker transitions. We have used these transition probabilities in a linear least-squares spectral fitting routine. In Fig. A-2 we show the spectrum of IF(B-X) emission excited by energy transfer from $N_2(A)$ (light line) at 5 torr total pressure of Ar buffer. Some emission from NF($b'\Sigma^+ - X^3\Sigma^-$) lies under the 0-0 band. The least-squares fit to the spectrum is shown as the darkened line in the figure. The accuracy of the transition probabilities is demonstrated by the good fits to the long progressions orginating in v' = 0-2. Over the range of these progressions, the transition moment varies by approximatly a factor of 2, while the spectral fits match the observed spectra to within 15%. If the transition moment were invariant with r-centroid, a much larger error would be observed in the spectral fit.

While there have been no other determinations of transition probabilities for this system, the transition probabilities reported here are at least in qualitative agreement with the stimulated emission data reported by Davis, Hanko, and Shea (Ref. A-2). Our calculations would predict strong emission from the 1-8, 2-10, 3-11, 3-12, 4-0, and 5-11 bands, in agreement with their low pressure optical pumping experiments. We would also predict lasing on the 0-5 band relative to the 0-4 band when the probabilities are converted to stimulated emission coefficients. Clyne and McDermid showed that radiative lifetimes for

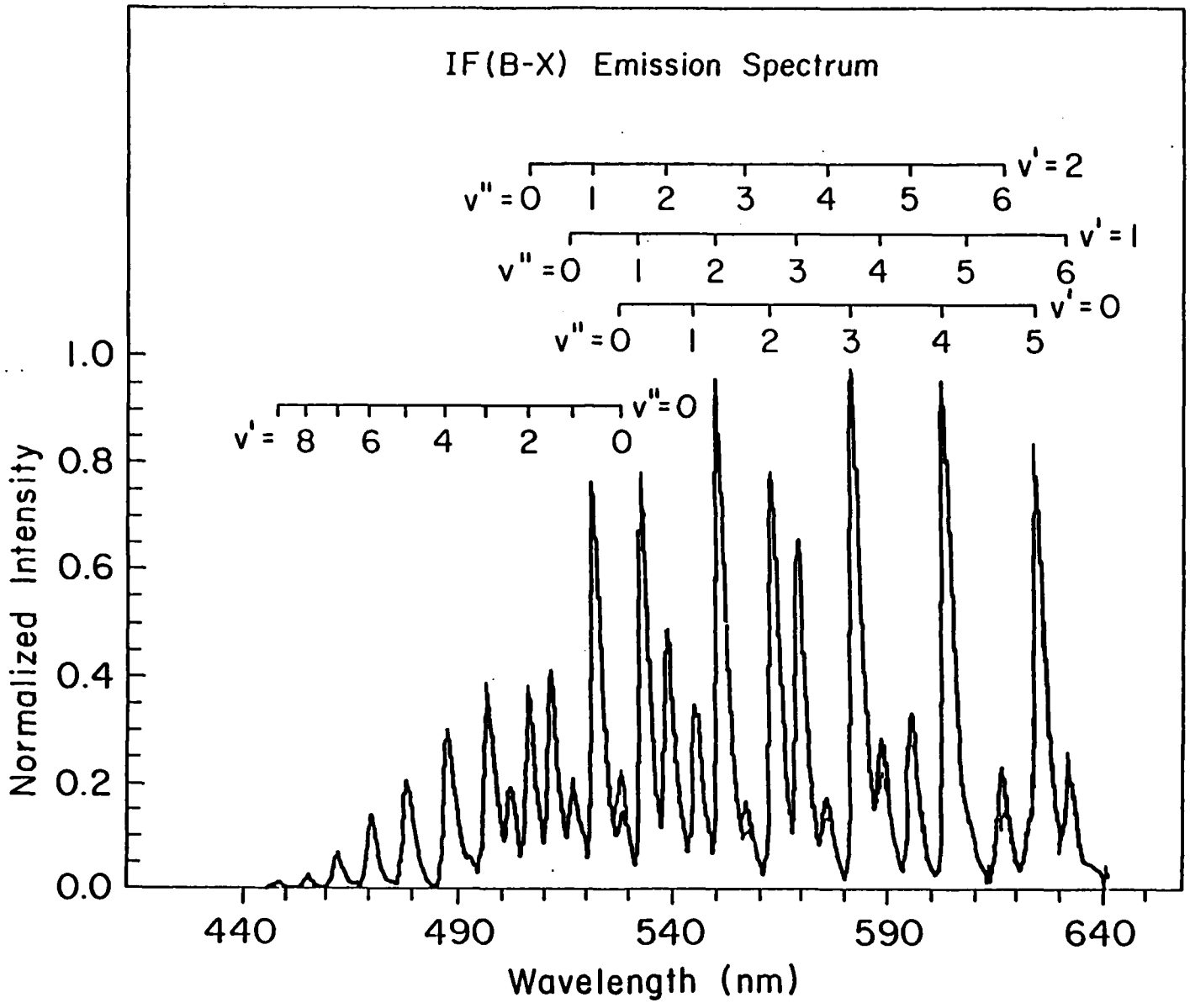

Fig. A-2. IF(B-X) emission spectrum excited by $N_2(A)$ energy transfer (light line) and least-squares fit to data using calculated transition probabilities (dark line).

$4 < J' < 50$ in each of B-state levels 0-8 are essentially equal (Ref. A-13). Work on Franck-Condon factors for I_2 have shown little variation with rotational quantum number except in highly rotationally excited species (Ref. A-19). Thus, we might expect to see little variation in these transition probabilities with rotational quantum number, aside from the usual Hönl-London line strength factor.

4. CONCLUSIONS

Franck-Condon factors for the IF(B-X) transition calculated using improved spectroscopic constants differ negligibly from previously calculated values for transitions originating from low levels of the B-state. For transitions originating from higher levels of the B-state, which are most affected by the use of improved spectroscopic constants, the newly calculated values differ by as much as 30% from prior results (Refs. A-9, A-10). We have resolved the discrepancy between previously reported variations in the relative transition moment by a reinterpretation of the results of Clyne and McDermid (Ref. A-13), resulting in 3 consistent sets of data. The relative transition moment function of Trickl and Wanner, (Ref. A-16), has been scaled so that calculated total transition probabilities match measured values in Reference A-13. Calculated probabilities for individual B-X transitions using the scaled function are consistent with observations of lasing on strong transitions originating from the outer turning point of the B-state potential.

REFERENCES

A-1 S.J. Davis and L. Hanko, "Optically Pumped Iodine Monofluoride $B^3\Pi(0^+) \rightarrow X^1\Sigma^+$ Laser," App. Phys. Lett. 37(8), 692 (1980).

A-2 S.J. Davis, L. Hanko, and R.F. Shea, "Iodine Monofluoride $B^3\Pi(0^+) \rightarrow X^1\Sigma^+$ Lasing from Collisionally Pumped States," J. Chem. Phys. 78, 172 (1983).

A-3 M.L. Dlabal and J.G. Eden, "On the Upper State Formation Kinetics and Line Tunability of the Iodine Monofluoride Discharge Laser," J. Appl. Phys. 53, 4503 (1982).

A-4 R.A. Durie, "The Visible Emission Spectra of Iodine and Bromine Monofluorides and Their Dissociation Energies," Proc. Roy. Soc. A207, 388 (1951).

A-5 R.A. Durie, "Electronic Emission Spectrum and Molecular Constants of Iodine Monofluoride," Can. J. Phys. 44, 337 (1966).

A-6 M.A.A. Clyne, J.A. Coxon, and L.W. Townsend, "Formation of the $B^3\Pi(0^+)$ States of BrF and IF by Atom recombination in the Presence of Singlet ($^1\Delta_g$, $^1\Sigma_g^+$) Oxygen," J.C.S. Faraday II 68, 2134 (1972).

A-7 A-E Tiemann, J. Hoeft, and T. Torring, "DAS Rotationsspektrum des IF," Z. Naturforsch 28a, 1405 (1973).

A-8 S.D. Gabelnick, PhD, Spectroscopic and Kinetic Studies of Iodine Monofluoride Chemiluminescence, Thesis, University of California, Berkeley and Lawrence Radiation Laboratory Report UCRL-18623.

A-9 J.W. Birks, S.D. Gabelnick, and H.S. Johnston, "Chemiluminescence of IF in the Gas Phase Reaction of I_2 with F_2," J. Mol. Spectrosc. 57, 23 (1975).

A-10. M.A.A. Clyne and I.S. McDermid, "$B^3\Pi(0^+)$ States of IF, ICl and IBr, Part 1. - Calculation of the RKR Turning Points and Franck-Condon Factors for the B-X Systems," J. Chem. Soc. Faraday II 72, 2242 (1976).

A-11. J.A. Coxon, "Dissociation Energies of Diatomic Halogen Fluorides," Chem. Phys. Lett. 33, 136 (1975).

A-12. M.A.A. Clyne and I.S. McDermid, "$B^3\Pi(0^+)$ States of IF, ICl and IBr, Part 2.-Observation and analysis of the Excitation Spectra of IF and ICl," J. Chem. Soc. Faraday II 72, 2252 (1976).

A-13. M.A.A. Clyne and I.S. McDermid, "Quantum-resolved Dynamics of Excited States. Part 4.-Radiative and Predissociative Lifetimes of IF $B^3\Pi(0^+)$," J.C.S. Faraday II 9, 1644 (1978).

A-14. M. Trautmann, T. Trickl, and J. Wanner, "Laser Spectroscopy of Iodine Monofluoride Produced in Situ in a Molecular Beam Experiment," Ber. Bunsenges, Phys. Chem. 86, 842 (1982).

A-15. T. Trickl and J. Wanner, "High-Resolution, Laser-Induced Fluorescence Spectroscopy of Nascent IF: Determination of X- and B-State Molecular Constants," J. Mol. Spectrosc. 104, 174 (1984).

A-16. T. Trickl and J. Wanner, "The Dynamics of the Reactions F+IX→IF+X(X=Cl, Br,I): A Laser-Induced Fluorescence Study," J. Chem. Phys. 78, 6091 (1983).

A-17. J. Tellinghuisen, "A Fast Quadrature Method for Computing Diatomic RKR Potential Curves," Comp. Phys. Comm. 6, 221 (1974).

A-18. J. Eccles and D. Malik, "Systems for the Numerical Solution of the Radial Schroedinger Equation," QCPE 13, 407 (1981).

A-19. J. D. Brown, G. Burns, and R. J. LeRoy, "Improved Spectroscopic Data Synthesis for $I_2(B^3\Pi Ou^+)$ and Predictions of J Dependence for $B(^3\Pi_{Ou}^+)$-$X(^1\Pi_g^+)$ Transition Intensities," Can. J. Phys. 51, 1664 (1973).

END

FILMED

1-86

DTIC